

University of Surrey  
Faculty of Engineering and Physical Sciences  
School of Sustainability, Civil and Environmental Engineering



# **How Moisture Affects Mechanical Properties and Failure Mechanisms Across Bamboo Species**

**Allan Ndubi Maugo**

6857626

A dissertation submitted in partial fulfilment of the requirements for the Degree of  
Master of Science in Msc Structural Engineering

August 2025

Word count: 19756

### **Declaration of Originality**

I confirm that the dissertation entitled 'How Moisture Affects Mechanical Properties and Failure Mechanisms Across Bamboo Species' for the partial fulfilment of the degree of MSc in Structural Engineering, has been composed by myself and has not been presented or accepted in any previous application for a degree. The work, of which this is a record, has been carried out by myself unless otherwise stated and where the work is mine, it reflects personal views and values. All quotations have been distinguished by quotation marks and all sources of information have been acknowledged by means of references including those of the internet.

Student's name: Allan Ndubi Maugo Date: 26/08/2025

## Abstract

This dissertation investigates how moisture content and specimen aspect ratio ( $L/D$ ) influence the mechanical properties and failure mechanisms of bamboo culms, focusing on *Guadua angustifolia* and *Dendrocalamus asper* tested in compression and bow-tie shear parallel to grain under oven-dry (<2%), ambient (9–12%), and wet (>30%) conditions at aspect ratios  $L/D = 1.0$  and  $2.0$ . A total of 108 specimens were prepared from full-length culms, conditioned, and tested under compression and shear, with digital image correlation to track strain localisation and an image-based sectional analysis to quantify fibre/matrix volume distributions. Moisture emerged as the dominant factor: strengths and stiffnesses peaked in oven-dry state and declined notably towards wet state, with typical reductions of 40–50% from oven-dry to wet in compression and 30–45% in shear, and increased ductility and post-peak softening at high moisture contents beyond the fibre saturation point. Species effects were pronounced: *D. asper* achieved higher compressive and shear capacities but failed in a more brittle manner, whereas *G. angustifolia* exhibited lower strengths but greater ductility, with crushing more prevalent at higher moisture content. Geometric effects varied across tests. Compression strengths were similar between short ( $L/D = 1.0$ ) and long ( $L/D = 2.0$ ) tubes, while shear strengths were consistently lower for longer tubes, underlining slenderness sensitivity in shear. The results expose limitations of ISO 22157 specimen protocols for design-representative capacities and support slenderness-aware testing, and species-specific grading to bridge laboratory data and structural design of bamboo culms.

## **Acknowledgements**

This dissertation has been shaped and strengthened by the support, guidance, and encouragement of many people, to whom I am profoundly grateful.

First and foremost, I wish to thank my supervisor, Dr Alireza Behnejad, for his insight, patience, and steady guidance at every stage of this research. I am equally thankful to Dr Dan Bompa, whose constructive feedback and thoughtful suggestions have been invaluable.

The experimental phase of this project could not have proceeded without the dedication of the Structures Laboratory team in the Department of Civil and Environmental Engineering at the University of Surrey. I am especially indebted to Thabang Ntanda and Dr Ge Cui for their technical expertise and unfailing assistance.

I gratefully acknowledge the financial support provided by the Department of Civil and Environmental Engineering, University of Surrey, which made this work possible.

To my friends and colleagues at the University of Surrey, thank you for your camaraderie, inspiration, and many moments of levity that sustained me throughout this journey.

Finally, my deepest gratitude goes to my family in Nairobi, Kenya. To my parents, whose love, encouragement, and unwavering belief in me have been my greatest source of strength. This achievement is as much yours as it is mine.

## Table of Contents

1. Introduction.....	12
1.1. Problem context and relevance.....	12
1.2. Rationale.....	18
1.3. Research objectives.....	20
1.4. Overview.....	20
2. Literature Review.....	23
2.1. Bamboo structure.....	23
2.2. Mechanical Properties of Bamboo Culms.....	28
2.3. Short and long tubes.....	30
2.4. Rule of mixtures.....	31
2.5. Bamboo species.....	33
2.6. Standards and codes.....	36
2.7. Summary.....	41
3. Methodology.....	43
3.1. Material procurement.....	43
3.2. Specimen preparation.....	43
3.3. Experimental setup.....	50
3.4. Section analysis.....	53
3.5. Limitations and rationale.....	56
4. Results.....	58
4.1. Sectional analysis.....	58
4.2. Physical properties.....	60

4.3. Mechanical properties.....	61
4.4. Compression.....	64
4.5. Shear.....	66
4.6. Stress stain curves.....	70
4.7. Failure modes.....	80
4.8. Summary.....	82
5. Discussion.....	84
5.1. MC sensitivity.....	84
5.2. Species mechanical performance.....	84
5.3. Geometric effects and sectional analysis.....	85
5.4. Section analysis.....	88
5.5. Failure mechanisms.....	90
5.6. Implications for structural applications.....	91
5.7. Limitations.....	92
5.8. Future research.....	93
6. Conclusions.....	96
6.1. Key findings.....	97
6.2. Implications.....	98
6.3. Contributions.....	99
6.4. Limitations.....	100
6.5. Recommendations.....	100
6.6. Remarks.....	101
References.....	103

## **Appendix**

Appendix A. Methodology.....	113
Appendix B. DIC analysis.....	115
Appendix C. Section analysis (Hutchison and Koepferl, 2024; Bompa, 2025).....	119
Appendix D. Elastic modulus, ISO 22157:2019 (ISO, 2019).....	120

## Table of Figures

Figure 1.1. Global temperature change of different bio-based construction materials considering the cradle-to-gate emission and subsequent biogenic carbon sequestration from replanting of 1 kg of each. Straw and bamboo allow for fast cooling of the atmosphere in the near term (cooling within a decade) due to short rotation periods, while sawn wood and glue-laminated (glulam) timber only reach negative temperature change starting from about 2040 onwards. (Göswein <i>et al.</i> , 2022).....	13
Figure 1.2. Vernacular structures across the tropical belt. From left to right (1) Mayans, Mexico (2) Kunas, Panama (3) Taironas and Muiscas, Colombia (4) Gamos, Ethiopia (6) Sumbese, Indonesia and (7) Lumad, The Phillipines. (Matos, 2022)....	14
Figure 1.3. (a - b)Traditional bahareque housing in El Salvador (Kaminski, Lawrence and Trujillo, 2016a). (c-d) Well maintained bahareque housing in Colombia (Kaminski, 2013).....	15
Figure 1.4. Modern bamboo construction. (a) Footbridge, Santa Fe de Antioquia, Colombia (Minke <i>et al.</i> , 2016). (b) Temple of no religion, Cartagena, Colombia . (c) ZERI pavilion, EXPO 2000 in Hanover, Germany (Minke <i>et al.</i> , 2016). (d) Jenny Garzon Pedestrian Bridge, Bogota, Colombia. (e) Tollgate, Pereira, Colombia (Minke <i>et al.</i> , 2016).....	16
Figure 1.5. Contemporary bamboo construction. (a) Kura Kura Badminton Court in Ubud, Bali (IBUKU, no date) (b) The Arc in Sibang, Bali (IBUKU, no date) (c) Hui pavilion in Foshan, China. Image © Siming Wu (Arch2o, 2021).....	18
Figure 1.6. Load testing of structures and members in bamboo projects. (a-b) The Arc, Bali, Indonesia ( <i>The Arc: bamboo as low-carbon structural material</i> , 2024). (c) Millennium Bridge at Green School, Bali, Indonesia ( <i>NEBgS Lecture Series #3 with Jörg Stamm _ Bamboo in the Future of Design: Long, light and strong</i> , 2024).....	19
Figure 2.1. Anatomy of a bamboo culm: (a) schematic view of a culm segment, © Sebastian Kaminski, David Trujillo and Andrew Lawrence, (b) section of culm wall showing grading of vascular bundles (Gottron, Harries and Xu, 2014).....	25

Figure 2.2. Vascular bundle types. (10) Type I - e.g. <i>Phyllostachys edulis</i> . (11) Type II - e.g. <i>Cephalostachyum pergaclile</i> . (12) Type III - e.g. <i>Oxytenanthera albociliata</i> . (13) Type IV – e.g. <i>Bambusa polymorpha</i> . (Grosser and Liese, 1971).....	27
Figure 3.1. Typical section of bamboo culm. To account for the oval shape of the culms, how diameters and thickness measurements were carried out were adjusted. For the outside diameter was equal to the average value of the measurements along the major axis and minor axis of the oval culm. In similar fashion the thickness was taken as the average value of the four measurements, two along each axis. These four thickness measurements also represented the shear planes in the bowtie test. 45	
Figure 3.3. DIC preparation for specimens. (a) Spray painting of specimens. (b) Application of speckle pattern. (c) Bamboo specimens with speckle pattern.....	49
Figure 3.2. Specimen preparation. (a) Full-length culms. (b) Segmenting of full-length culms into thirds. (c) Marking of cutting points along the length of thirds. (d) cutting of specimens using band-saw. (e) Labelling of specimens. (f) Sanding of specimens. (g) Cut specimens. (h) Weighing of specimens. (i) Measuring of specimen dimensions. (j) Oven-drying of specimens. (k) Soaked specimens.....	48
Figure 3.4. Typical experimental setup.....	50
Figure 3.5. Compression test setup. ISO setup diagram on the left and actual test setup on the right. D is outer diameter, $\delta$ is wall thickness, F is load, L is length of specimen, 1 is upper loading platen with spherical bearing, 2 is intermediate layer, 3 is bamboo specimen, 4 intermediate layer and 5 is lower loading platen (ISO, 2019). .....	51
Figure 3.6. Shear setup. ISO recommended setup on the left and actual experiment setup on the far right. $\delta$ is wall thickness, D is outer diameter, F is load, L is length of specimen, 1 is upper loading platen with spherical bearing, 2 is shear plate, 3 is bamboo specimen, 4 is lower loading platen, 5 is shear area, normally calculated from $\delta \times L$ .....	52
Figure 3.7. Alignment of shear plates. (a) Alignment of bottom plates. (b) Locating of centre of machine platen.....	53

Figure 3.8. Section analysis process. (a) Original image. (b) Isolated and enhanced image. (c) Equalised image. (d) Inverted binary image. (e) Noise-reduced image. (f) Detected external and internal contour. (g) Fitted ellipses used for calculating cross-section properties. (h) Fitted ellipses. (i) Tangential segments.....	54
Figure 4.1. Results of segmentation for both <i>D. asper</i> and <i>G. angustifolia</i> . The first segment was ignored when fitting the curves.....	59
Figure 4.2. Ambient-dry compression stress-strain curves.....	67
Figure 4.3. Wet compression stress-strain curves.....	69
Figure 4.4. Oven-dry compression stress-strain curves.....	71
Figure 4.5: Ambient-dry shear stress-strain curves.....	73
Figure 4.6. Wet shear stress-strain curves.....	75
Figure 4.7. Oven-dry shear stress-strain curves.....	77
Figure 4.8. Compression test failure modes. (a) Combined failure mode for an ambient-dry specimen (b) Splitting failure mode for an oven-dry specimen. The specimen was held together by the node. (c) Crushing failure mode (d) Splitting failure mode for an oven-dry specimen without node (e) Crushing failure mode for a wet specimen. Crushing occurred at the top and bottom.....	79
Figure 4.9. Shear test failure modes. (a-b) Splitting failure mode for an ambient-dry specimen. (b) Splitting failure mode for an oven-dry specimen. (c) Internal splitting. (d) Splitting failure mode where a quarter of the specimen was sheared off.....	80
Figure 1. Full experimental setup.....	114
Figure 2. Strains across a specimen undergoing compression.....	116
Figure 3. Strains across a specimen undergoing splitting and crushing failure.....	117
Figure 4. Strains across a specimen undergoing shear failure.....	118

## **Index of Tables**

Table 2.1. Average bamboo mechanical property values. (Vivas <i>et al.</i> , 2019).....	32
Table 2.2. Codes for bamboo structural design (Amede <i>et al.</i> , 2021).....	38
Table 2.3. Standards for bamboo structural design (Amede <i>et al.</i> , 2021).....	38
Table 3.1. Sample details.....	46
Table 4.1: Compression test results.....	62
Table 4.2: Shear test results.....	63

## 1. Introduction

### 1.1. Problem context and relevance

In recent years, bamboo has been likened to vegetal steel (Tropical Commons, 2018). Bamboo is a natural grass with a fast growth rate of 4–5 years and can achieve earth cooling effects within a decade (see Figure 1.1) as compared to timber's 40 years (Göswein *et al.*, 2022). Bamboo's harvest cycle takes a rapid 3–5 years, hence a managed bamboo plantation can sequester up to 1.7 times the same amount of carbon as Chinese fir trees (King *et al.*, 2021). Moreover, bamboo is a lightweight material and therefore has a high strength to weight ratio. Bamboo as a sustainable material targets to alleviate the construction industry's 37% contribution to global CO<sub>2</sub> emissions (UNEP, 2024), of which 11% is embodied carbon (WGBC, 2019). There has been progress in reducing the operational carbon (Röck *et al.*, 2020), but the World Green Building Council argues that the focus will soon shift to embodied carbon, especially with most of urbanisation set to take place in low-income countries for the next 50 years (UN-Habitat, 2022). Bamboo thrives predominantly across the Global South (A.N. Rao, V. Ramanatha Rao, and J.T. Williams, 1998), positioning itself as an accessible material whose advantages can be extensively leveraged in the built environment and climate crisis.

Bamboo is an incredibly versatile material with over 1,000 documented uses (Liese and Köhl, 2015). Of interest in this dissertation is bamboo as a structural material, specifically in its full culm (pole) state. Bamboo's use in construction is far from new; it has been employed for thousands of years by communities living where the plant grows naturally (see Figure 1.2). For example in Latin America, a rich bamboo housing culture (referred to as Guadua culture, named after the prevalent bamboo species *Guadua angustifolia* Kunth) has existed particularly in Colombia, Ecuador and El Salvador where it has been primarily reserved for inexpensive, owner-constructed housing. As a result, bamboo is often seen as a “poor man's wood”, valued mainly as a stopgap solution until better economic means permit more permanent alternatives such as masonry or concrete (Gutiérrez, 2000). However, in such regions, bamboo has proven as a robust material, combating steep slopes,

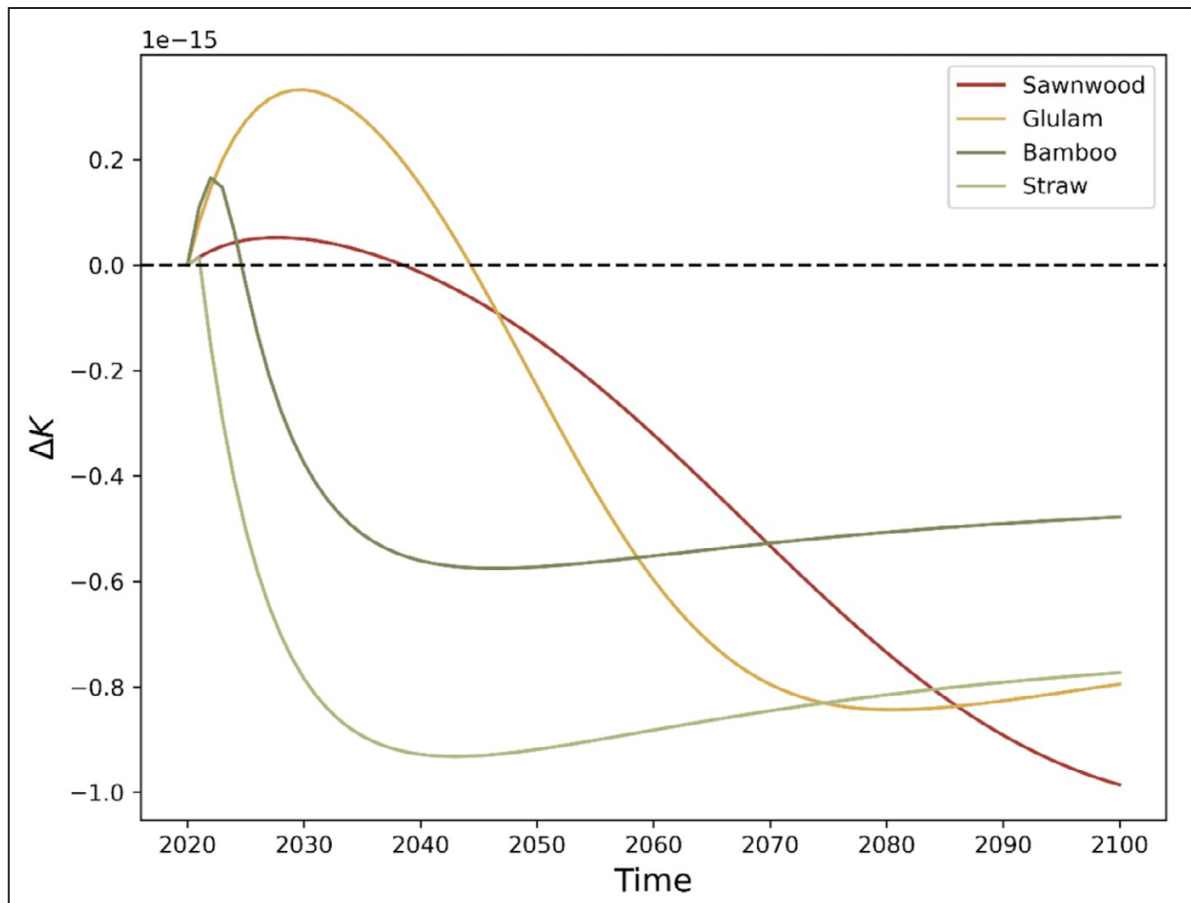


*Figure 1.1. Global temperature change of different bio-based construction materials considering the cradle-to-gate emission and subsequent biogenic carbon sequestration from replanting of 1 kg of each. Straw and bamboo allow for fast cooling of the atmosphere in the near term (cooling within a decade) due to short rotation periods, while sawn wood and glue-laminated (glulam) timber only reach negative temperature change starting from about 2040 onwards. (Göswein et al., 2022)*

swampy coastal grounds and earthquakes (Gutiérrez, 2000, 2004; Lopez, Bommer and Mendez, 2004).

Gutierrez (2000) with the help of Alexander (2002) explains that bamboo construction in Latin America is two-pronged: unselfconscious (traditional *bahareque*) and self-conscious (*bahareque*). *Bahareque* refers to a building technique similar to wattle-and-daub, consisting of a structure formed from interwoven sticks, reeds, or bamboo,

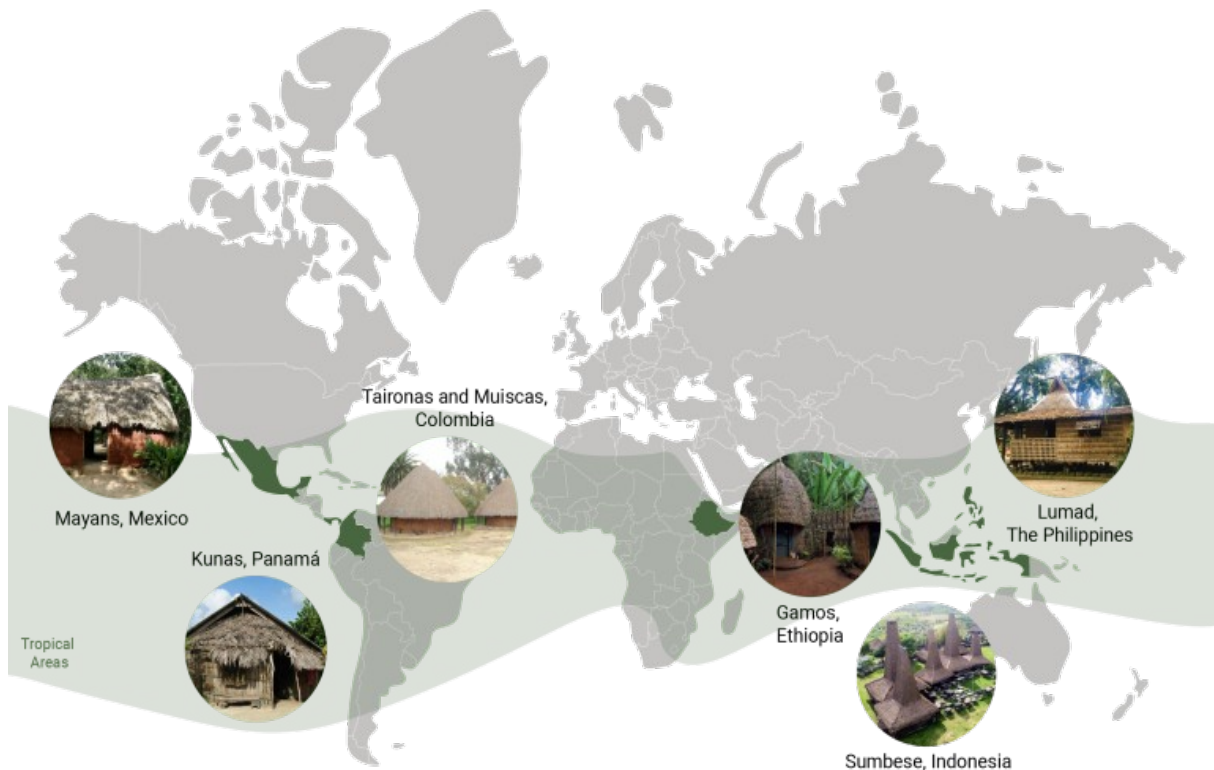


*Figure 1.2. Vernacular structures across the tropical belt. From left to right (1) Mayans, Mexico (2) Kunas, Panama (3) Taironas and Muiscas, Colombia (4) Gamos, Ethiopia (6) Sumbese, Indonesia and (7) Lumad, The Phillipines. (Matos, 2022)*

which is then covered with a mixture of mud, clay, or loam, often reinforced with straw. The first type of bamboo construction is an intuitive, unreflective practice found in vernacular structures, in which builders rely on time-honoured construction methods, repeating solutions that have worked for generations with little alteration. A few examples of vernacular structures have been illustrated in Figure 1.2. The second type of bamboo construction is a deliberate, self-aware approach employed by architects or engineers. Unselfconscious construction predominates in rural areas of El Salvador and Colombia, whereas selfconscious construction is characteristic of their urban areas. Without discounting the other, they both boast sound structural performance despite the harsh conditions of the region, even so far as resisting earthquakes (Gutiérrez, 2000). Bamboo's seismic performance is tied to its lightweight properties and ability to absorb energy at its joints (Kaminski, Lawrence and Trujillo, 2016b).



*Figure 1.3. (a - b) Traditional bahareque housing in El Salvador (Kaminski, Lawrence and Trujillo, 2016a). (c-d) Well maintained bahareque housing in Colombia (Kaminski, 2013).*

In modern construction (Figure 1.4), bamboo appears mainly in low rise buildings and pedestrian bridges (Correal, 2016). Pioneers of modern bamboo construction, such as Simón Vélez and Jörg Stamm, are often referred to as master builders. This designation reflects the integrated demands of design, engineering, and construction inherent to working with bamboo. Simón Vélez pioneered use of mortar filled joints in bamboo for his structures, a breakthrough that increased the load-bearing capacity of bamboo joints and span ranges of bamboo members (Structural Bamboo, 2013). Simón Vélez mentions that in the early stages of modern bamboo construction, bamboo was used as a counter-cultural substitute for concrete or masonry (*Working With Bamboo in Architecture - Simón Vélez | 25 Years 25 Hours*, 2021). As the climate change agenda gained momentum, modern bamboo structures were reinterpreted as a sustainable initiative, not only for bamboo's low embodied carbon but also for the local jobs created by its cultivation, treatment and assembly.

Durability of bamboo culms which was a major concern was now addressed in modern construction through four simple rules: no contact with the ground, no contact with water and no direct sunlight, and decay (NEBgS Lecture Series #3 with Jörg

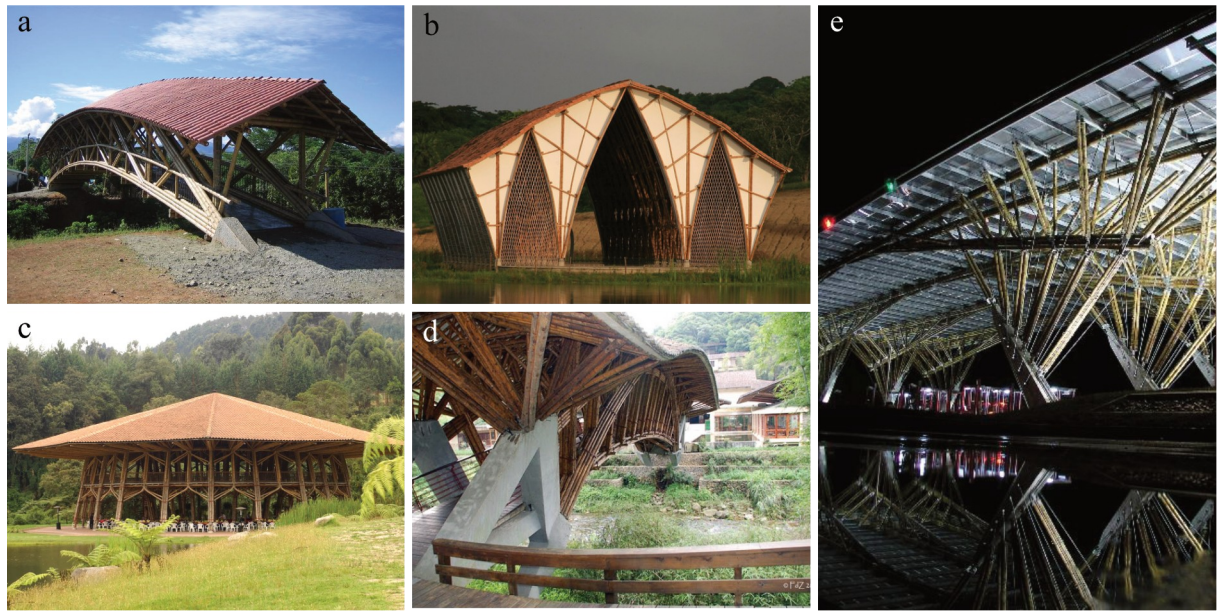


*Figure 1.4. Modern bamboo construction. (a) Footbridge, Santa Fe de Antioquia, Colombia (Minke et al., 2016). (b) Temple of no religion, Cartagena, Colombia . (c) ZERI pavilion, EXPO 2000 in Hanover, Germany (Minke et al., 2016). (d) Jenny Garzon Pedestrian Bridge, Bogota, Colombia. (e) Tollgate, Pereira, Colombia (Minke et al., 2016).*

*Stamm \_ Bamboo in the Future of Design: Long, light and strong, 2024).* Modern structures feature (1) a platform construction, with the bamboo structure seated on masonry or concrete, to protect from ground water (2) a roof overhang to protect from rain and sunlight and (3) treated bamboo poles in salts such as Borax (Correal, 2016).

In contemporary bamboo construction (see Figure 1.5), structures tend towards biophilic and parametrically generated forms serving functions such as beach resorts, pavilions, and yoga studios. Contemporary bamboo structures feature curved shells, arches and grids in which every culm contributes simultaneously to form and load-bearing action. To achieve such geometries, harvested culms are first sorted into naturally curved and straight batches. The curved culms define the flow line of the roof or facade, while straight culms are reserved for primary compression or tension members. An alternative to achieve curvature is the reb-reb technique which is used where natural curvature is insufficient (*The Arc: bamboo as low-carbon structural*

*material*, 2024). Short segments are cut, bent to the desired radius, and re-assembled inside a sleeve. The disadvantage of this technique is that part of the culm section is eaten away, diminishing the strength of the member. These complex contemporary structures are typically assembled on site prior to erection, enabling exceptionally rapid construction. Contemporary bamboo structures help redefine bamboo's image, elevating it beyond its traditional perception as the "poor man's wood."

With all these examples, we can see that bamboo is more than capable as a building material, handling various loading scenarios. However, bamboo's uptake as a construction material has been stifled by the lack thereof building standards and codes. Because variability in bamboo exists at every scale, developing universally applicable test protocols and design standards remains a challenge. Bamboo is inherently heterogenous. Its mechanical and physical properties vary: longitudinally (along the culm from base to tip), transversally (from inner diameter to outer diameter), between individual culms of the same species, and across different species altogether. India issued the first national bamboo code in 1975 (Amede *et al.*, 2021), yet an international bamboo standard did not appear until 2004 and a formal standard for the design of bamboo structures has not yet been established (Amede *et al.*, 2021). The intervening years have produced varied research whose methods and studies vary so widely that findings cannot be readily synthesised, built on, validated and refine one another. All this leads to an empirical approach to the design of bamboo structures as shown in Figure 1.6.

By contrast, concrete, masonry and steel have benefited from a century of harmonised research, standardised testing and iterative code development. The resulting breadth of knowledge creates a high entry barrier for full culm bamboo as a structural material. Thus stakeholders cannot put trust in a material that has not been fully standardised (Kaminski, 2013). However, as the world slowly moves towards sustainable options, it will serve as a catalyst for more documentation of structural design of bamboo.



*Figure 1.5. Contemporary bamboo construction. (a) Kura Kura Badminton Court in Ubud, Bali (IBUKU, no date) (b) The Arc in Sibang, Bali (IBUKU, no date) (c) Hui pavilion in Foshan, China. Image © Siming Wu (Arch2o, 2021)*

While the environmental imperatives and growing climate concerns have positioned bamboo as an increasingly attractive alternative to conventional materials, the construction industry's acceptance remains constrained by the absence of comprehensive, standardised knowledge frameworks that can provide the confidence necessary for widespread adoption in contemporary structural applications.

## **1.2. Rationale**

The utilisation of bamboo as a structural material presents considerable engineering potential due to its exceptional strength-to-weight ratio, renewable nature, and rapid growth characteristics. However, the absence of comprehensive design guidelines for bamboo components can result in premature failure, particularly through splitting and brittle fracture mechanisms. This limitation necessitates a thorough understanding of the mechanical behaviour of bamboo culms under varying environmental conditions, particularly the influence of moisture content on structural performance.

Current standards and research on bamboo mechanical testing employ short, stubby specimens with a length-to-diameter ( $L/D$ ) or aspect ratio of 1.0. While commonplace, this approach does not consider end effects in stub tubes that inflate strength values, leading to unconservative strength predictions for actual structural members. In contrast, slender tubes tend to fail via local buckling before the material's true compressive capacity is developed. The local buckling phenomena alters the failure mechanism from material strength-governed to stability-governed modes. This

geometric influence on failure is particularly important for bamboo due to its distinct longitudinal and transverse anisotropy. This geometric dependency creates a disconnect between laboratory test results and the actual behaviour of bamboo elements in structural applications, where inter-nodal lengths typically result in notably higher aspect ratios.

Moreover, for splitting tests, crack propagation and failure rates are affected by the specimen length; short specimens exhibit rapid crack propagation and failure, which can yield misleadingly low (overly conservative) assessments of splitting strength for design. The result is a lack of representativeness for real-world bamboo components, especially where internodal lengths and natural diaphragms considerably alter local stress distributions and buckling resistance.



*Figure 1.6. Load testing of structures and members in bamboo projects. (a-b) The Arc, Bali, Indonesia (The Arc: bamboo as low-carbon structural material, 2024). (c) Millennium Bridge at Green School, Bali, Indonesia (NEBgs Lecture Series #3 with Jörg Stamm \_ Bamboo in the Future of Design: Long, light and strong, 2024)*

The ductility characteristics of bamboo also demonstrate moisture dependency, with wet conditions potentially transforming brittle failure modes into more ductile responses. This transformation has implications for structural resilience and energy dissipation capacity.

Furthermore, the lack of reliable non-destructive grading methods presents a substantial barrier to bamboo's industrial adoption. While fibre distribution and packing density appear to correlate with structural performance, systematic methods for predicting mechanical properties through sectional analysis remain

underdeveloped. This limitation hinders quality control and standardisation efforts essential for bamboo's acceptance in mainstream construction.

### **1.3. Research objectives**

This research aims to investigate the mechanical response of *Guadua angustifolia* (*G. angustifolia*) and *Dendrocalamus asper* (*D. asper*) bamboo properties under varying moisture conditions. The primary objective is to characterise the mechanical behaviour of *G. angustifolia* and *D. asper* bamboo culms under compression and shear loading parallel to grain, across different moisture contents and slenderness ratios. Secondary objectives include:

1. To evaluate existing testing methods by introducing variable slenderness ratios in compression and shear testing, enabling better characterisation of buckling behaviour in full bamboo culms.
2. To investigate the influence of moisture content on the mechanical properties of both species across three distinct conditions: oven-dry (moisture content <2%), ambient equilibrium (9-11%), and saturated (>30%) states.
3. To conduct comparative analysis between *G. angustifolia* and *D. asper*, documenting species-specific mechanical properties and behaviour patterns.
4. To employ Digital Image Correlation (DIC) techniques to compare failure patterns and stain distribution in bamboo specimens, providing understanding of failure progression and mechanisms.
5. To investigate correlations between fibre packing density, sectional properties, and mechanical performance, developing potential non-destructive methods for bamboo quality assessment.

### **1.4. Overview**

This dissertation is divided into six chapters. Chapter 1 establishes the research foundation by presenting the contextual framework for bamboo as a sustainable construction material and documenting the motivation for this investigation. The

chapter examines bamboo's historical, modern and contemporary applications, identifies key knowledge gaps in current understanding, and articulates the research rationale. The research objectives are defined, providing direction for the subsequent investigation, while this overview outlines the dissertation's organisational structure and methodological approach.

Chapter 2 provides a literature review encompassing both the macrostructural and microstructural characteristics of bamboo culms. The chapter examines bamboo's hierarchical organisation from cellular level through whole culm properties, establishing the theoretical basis for understanding mechanical behaviour. Physical and mechanical properties are reviewed, with attention to moisture effects and species variations. An analysis of existing testing methodologies and standards is presented, highlighting limitations in current approaches and justifying the need for methodological refinements proposed in this research.

Chapter 3 details the experimental methodology, beginning with material selection and characterisation of the *G. angustifolia* and *D. asper* specimens. Sample preparation methods are described. The chapter presents detailed descriptions of testing arrangements for compression and shear investigations. The DIC setup and sectional analysis procedures, are also documented.

Chapter 4 presents the experimental findings across all testing configurations and moisture conditions. Results are organised by species, moisture content, and loading condition. Documentation of failure mechanisms and deformation patterns is provided, supported by DIC analysis. Also the fibre volume results obtained from the sectional analysis are presented.

Chapter 5 provides a discussion and interpretation of the experimental results, contextualising findings within the broader bamboo research landscape. The chapter examines correlations between moisture content, slenderness ratio, and mechanical performance, identifying relationships and trends. Species-specific behaviour patterns are analysed and compared. The discussion addresses implications for current testing standards and construction practices, while identifying areas where current methodologies may require refinement.

Chapter 6 synthesises the research contributions and presents conclusions addressing each research objective. The chapter summarises the main findings and their significance for bamboo construction practice, highlighting contributions to the field. Practical recommendations for testing protocols, design approaches, and future research directions are provided. The chapter concludes by outlining potential applications of the research findings and identifying priority areas for continued investigation.

## **2. Literature Review**

### **2.1. Bamboo structure**

Bamboo is classified as a giant grass, belonging to the *Poaceae* family (Liese and Köhl, 2015; Maria S. Vorontsova *et al.*, 2016), specifically the subfamily *Bambusoideae*. This botanical classification distinguishes it from woody trees, as bamboo does not produce secondary growth or increase in diameter with age, unlike trees which possess a vascular cambium (Liese, 1998; Liese and Köhl, 2015). Bamboos represent a single evolutionary radiation comprising 1,642 species, including 1,521 woody bamboos (Liese and Köhl, 2015). They exhibit considerable variability in habit, ranging from woody to herbaceous, and thrive across a broad range of global environments, predominantly in tropical to warm temperate ecosystems, with some diversity also found in cold temperate regions (Maria S. Vorontsova *et al.*, 2016). Bamboo is a rapidly growing and highly versatile plant, often reaching its full height within its first year (Liese and Weiner, 1996). Depending on the species and plantation, it can typically be harvested between 3 to 6 years of age (Liese and Weiner, 1996). This rapid growth cycle and high biomass yield contribute to bamboo's recognition as a potentially sustainable material with a low 'carbon footprint' and considerable social equity benefits.

Historically, bamboo has attracted human attention for centuries, leading to hundreds of applications across various fields. In civil engineering alone, it has been traditionally used as a structural material in low-rise houses, short-span foot bridges, long-span roofs, and construction platforms in regions with abundant bamboo resources (Arce, 1993). Its versatility extends to food, crafts, furniture, accessories, and clothing. Despite its long-standing use, developing bamboo as a modern construction material has been constrained by a lack of standardised design guidelines for its mechanical properties and structural adequacy (Chung and Yu, 2002).

### 2.1.1 Bamboo morphology

Understanding the anatomical structure of the bamboo culm is important to comprehending its physical and mechanical properties, as these are directly determined by the culm's structure and the properties of its constituent material (Liese, 1998). The bamboo culm, or stalk, is characterised by its hollow, segmented structure, with solid transverse diaphragms, known as 'nodes', separating the hollow 'internodal regions' along its height (Grosser and Liese, 1971). The bamboo culm is illustrated in Figure 2.1. The circular cross-section of a bamboo culm is primarily composed of unidirectional cellulosic fibres embedded within a parenchyma tissue matrix, oriented parallel to the culm's longitudinal axis (Grosser and Liese, 1971). In general, the culm wall thickness comprises approximately 52% parenchyma cells, 40% fibres, and 8% conducting elements (such as vessels and sieve tubes with companion cells) (Liese and Köhl, 2015).

Bamboo is recognised as a functionally graded material (Trujillo and López, 2016). This means that its composition and microstructure vary across its volume (radially, transversally and longitudinally), producing a corresponding change in its properties both mechanical and geometrical. A key aspect of this grading is the density of fibres, which increases notably from the inner culm wall to the outer culm wall (Grosser and Liese, 1971). The volume fraction of fibres can range from approximately 10–15% near the interior face to about 60% at the exterior face (Liese, 1998). About half of the fibres are concentrated in the outer third section of the culm wall. This increasing concentration of fibres towards the outer culm wall contributes to its resistance to its natural loadings, such as its own self-weight and lateral wind effects (Trujillo and López, 2016; Akinbade *et al.*, 2019).

The culm also exhibits variations along its length. The wall thickness is generally largest at the base of the culm and decreases with height (Arce, 1993). Concurrently, the size and quantity of vessels decrease with culm height, being progressively replaced by bamboo fibres. This natural optimisation results in relatively uniform engineering properties along the entire culm height (Amada *et al.*, 1996). However, it is noted that radial variations across the culm wall are typically more pronounced than longitudinal variations along the culm (Yu *et al.*, 2008). Therefore, bamboo is

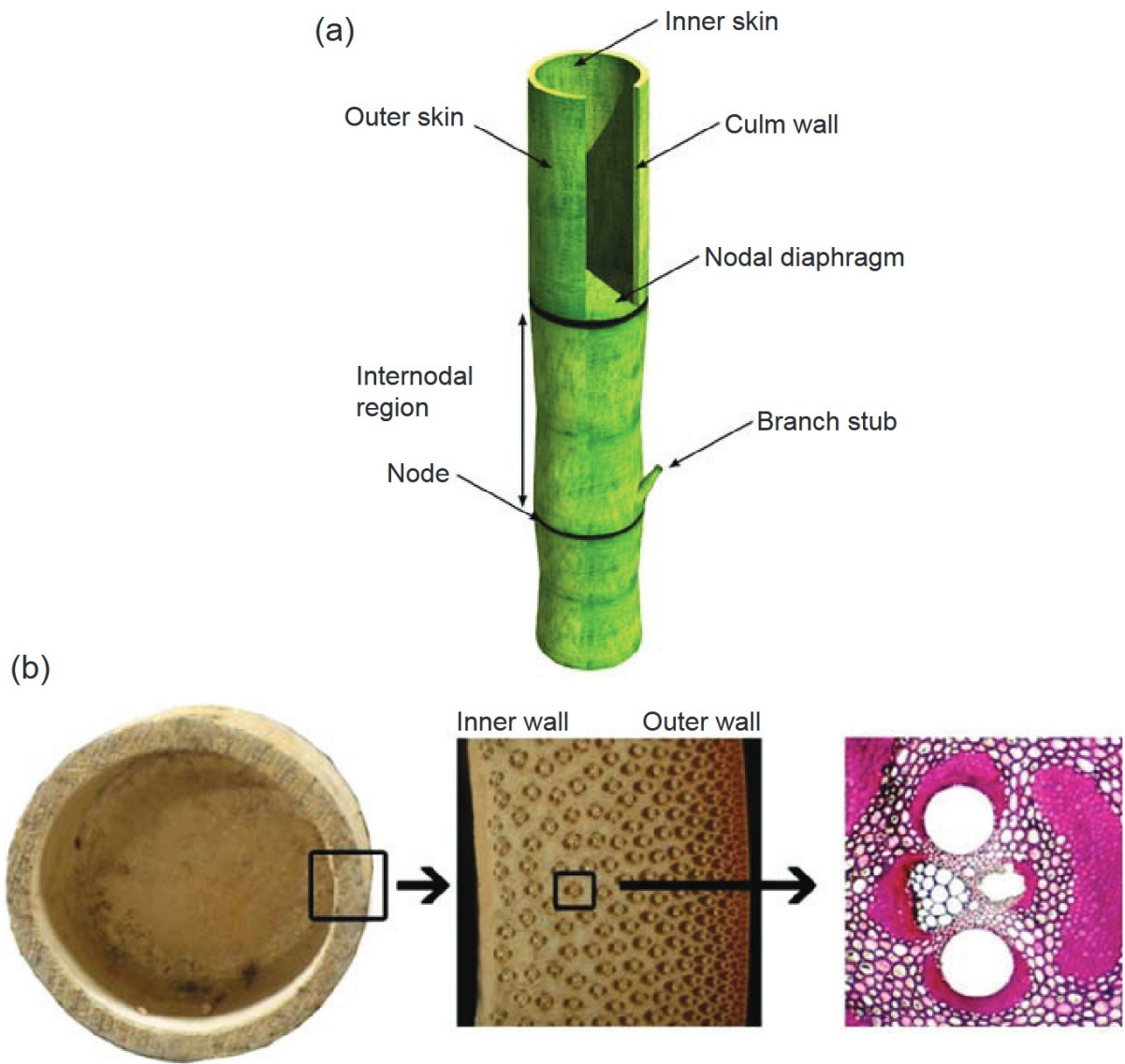


*Figure 2.1. Anatomy of a bamboo culm: (a) schematic view of a culm segment, © Sebastian Kaminski, David Trujillo and Andrew Lawrence, (b) section of culm wall showing grading of vascular bundles (Gottron, Harries and Xu, 2014)*

naturally intelligent and self-optimising, designed to have uniform strength at all positions of its culm (Nogata and Takahashi, 1995; Amada *et al.*, 1997; Dixon and Gibson, 2014).

### **2.1.2 Vascular bundles**

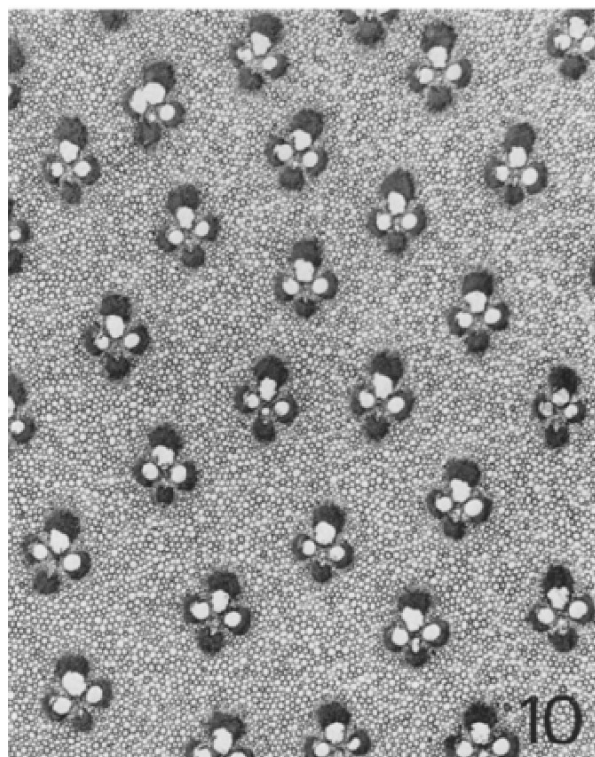
The vascular bundle is considered the most varied structural component of a bamboo culm (Liese, 1998). Differences in the shape, size, and grouping of these bundles have important diagnostic and taxonomic value, forming the basis for anatomical classification systems (Liese, 1998). The Liese and Grosser (1971) typology identifies various bundle types, including I, II, III and IV shown in Figure 2.2. These vascular bundles are embedded in the ground parenchyma tissue.

Nodes are transverse walls that interrupt the strictly axial arrangement of vascular bundles (Arce, 1993; Liese and Tang, 2015). Within the nodes, the bundles bend towards the lacuna (the hollow part of the culm), forming irregular patterns in their distribution and orientation. Anatomical studies have shown that the nodes negatively contribute to the axial and bending stiffness of the culm and limit its parallel tension capacity (Arce, 1993). The ground tissue of the diaphragm within the nodes consists of short parenchyma cells interspersed with sclerified cells, and tyloses are often present (Liese and Tang, 2015).

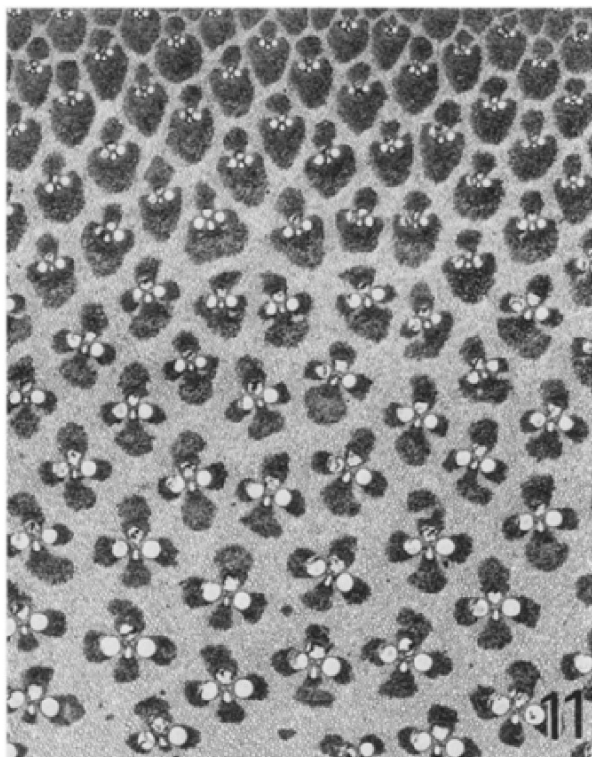
### **2.1.3 Fibres and Parenchyma**

Bamboo fibres are characterised by their slender form, being long and tapered at both ends, and sometimes forked (Liese, 1998; Ximena Londoño *et al.*, 2002). Their length is important, influencing both the culm's strength and its pulping properties. Average fibre lengths are approximately 1.9 mm, with a reported range from 1.04 mm to 2.64 mm, varying by species (Liese, 1998). The fine structure of bamboo fibres consists of numerous layers (lamellae) that make up the cell wall, with up to 18 layers reported (Liese, 1998).

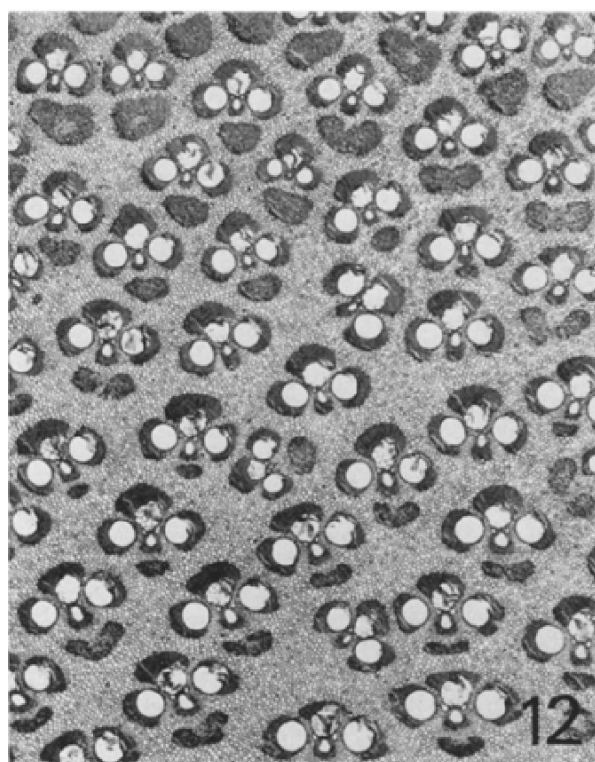
The parenchyma tissue matrix, which embeds the fibres, lignifies (hardens) as the culm matures (Liese and Köhl, 2015). Lignification is the formation of a polymer within the cell wall that provides strength to the culm, and its content is presumed to increase with culm development (Liese and Köhl, 2015). While the morphologic characteristics of parenchyma are observed to vary through the culm wall, their



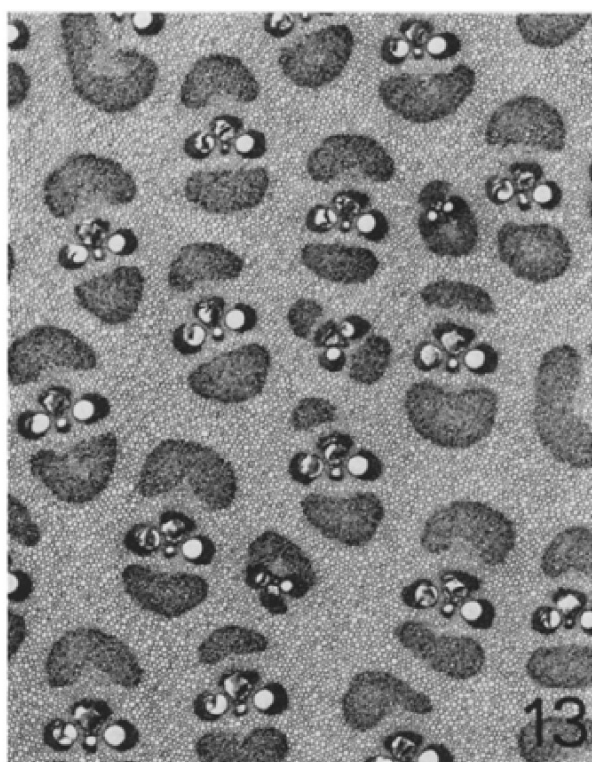
10



11



12



13

Figure 2.2. Vascular bundle types. (10) Type I - e.g. *Phyllostachys edulis*. (11) Type II - e.g. *Cephalostachyum pergamile*. (12) Type III - e.g. *Oxytenanthera albociliata*. (13) Type IV – e.g. *Bambusa polymorpha*. (Grosser and Liese, 1971)

precise impact on mechanical behaviour requires further research (Akinbade *et al.*, 2019).

## **2.2. Mechanical Properties of Bamboo Culms**

Bamboo is a highly orthotropic material, meaning its mechanical properties vary considerably depending on the direction of loading relative to the culm's axis (Akinbade *et al.*, 2019). The mechanical properties of bamboo are intrinsically linked to its density, fibre content, fibre diameter, and cell wall thickness. A strong correlation between bamboo's strength and its density has been widely observed, similar to timber (Trujillo and López, 2016). A summary of average bamboo mechanical property values have been summarised in Table 2.1.

### **2.2.1 Compressive Properties**

The compressive strength of bamboo is also a vital mechanical property. For *Phyllostachys edulis* (Moso) bamboo, axial compressive strength values typically range from 45 to 65 MPa (Dixon *et al.*, 2015). Specific species reported include *Guadua angustifolia* Kunth with an average compressive strength of 45–65 N/mm<sup>2</sup> (Correal D and Arbeláez C, 2010). *Bambusa Pervariabilis* (Kao Jue) shows a range of 44–99 N/mm<sup>2</sup>, and *Phyllostachys Pubescens* (Mao Jue) ranges from 48–114 N/mm<sup>2</sup>.

Compressive strength is highly sensitive to MC changes, generally increasing as MC falls below the FSP (Jiang *et al.*, 2012; Wang *et al.*, 2022). When subjected to compressive loads, the mechanical properties are dictated by the density variation (Krause *et al.*, 2016). Longitudinal splitting is a dominant failure mode for bamboo in structural applications, often exacerbated by connection details (Mitch, Harries and Sharma, 2010; Akinbade *et al.*, 2019). Bamboo culms can also fail by buckling under critical loads. Studies on longitudinal variation in compressive properties show mixed results: some species like Mao Jue exhibit an increase in compressive strength and stiffness from bottom to top, while others, such as Kao Jue, show constant values (Chung and Yu, 2002).

### **2.2.2 Shear properties**

Longitudinal shear strength is another mechanical property studied. It has been shown to be sensitive to moisture content changes, similar to compressive strength. Shear governs many bamboo connection details (bolts, dowels, pins) and transfer of torsional or transverse loads in full-culm members. Among standard strength tests, shear parallel to grain consistently shows the highest coefficient of variation (COV), so design codes adopt conservative characteristic values (Vivas *et al.*, 2019). For shear testing following ISO 22157:2019, single-plane shear along fibres dominates. Two-plane diagonal failures occur when wall thickness is high; three-plane failures are rare. Initiation generally near a parenchyma-rich zone; fibre bundles bridge the crack, giving some post-peak resistance.

### **2.2.3 Influence of moisture content (MC)**

MC is arguably the most considerable factor governing the mechanical properties of bamboo (Chung and Yu, 2002). Bamboo is a hygroscopic material, meaning it readily absorbs and releases moisture from its environment. The mechanical properties of bamboo are a function of MC below the fibre saturation point (FSP), which is typically between 20% and 30% depending on the species (Jiang *et al.*, 2012; Wang *et al.*, 2022). Above the FSP, additional moisture generally has no further influence on mechanical properties (Sánchez Cruz and Morales, 2019). Studies indicate that an increase in MC generally reduces the mechanical strength of the material. The reduction in maximum stress values is particularly considerable for MC values between 12% and the FSP, and this is accompanied by dimensional changes that can impair mechanical performance. The primary dimensional changes due to MC variations occur in the transverse direction, while the longitudinal direction remains almost constant. It is important for structural design to account for MC, with recommendations to adjust indicating properties to a standardised 12% MC (Bahtiar, Trujillo and Nugroho, 2020).

#### **2.2.4 Factors influencing mechanical properties**

Beyond the fundamental properties, several factors contribute to the variability and characteristics of bamboo's mechanical behaviour. The mechanical properties of bamboo are notably influenced by its age (Liese and Weiner, 1996). Culms typically reach their full height in the first year but come to maturity, where they are suitable for harvest, at 3 to 6 years old (Dixon *et al.*, 2015). During maturation, the parenchyma tissue lignifies, contributing to increased density and improved mechanical properties (Liese and Köhl, 2015; Akinbade *et al.*, 2019). Investigations on *Phyllostachys viridiglaucescens* culms up to 12 years old have shown definite anatomical changes during maturation and in later years, specifically cell wall thickening of the fibres (Liese and Weiner, 1996).

Mechanical properties vary along the culm's length. Fibre concentration is higher towards the top and the outer layer of the cross-section. The wall thickness also decreases from the base to the top (Chung and Yu, 2002).

The distribution of fibres is not uniform across the culm wall thickness, with a higher concentration towards the outer layers (up to 60% at the exterior face compared to 10–15% at the interior) (Akinbade *et al.*, 2019). This radial variation in fibre content and density impacts mechanical properties, and these variations are often more pronounced than longitudinal variations. The presence of nodes can act as limiting factors for the parallel tension capacity of bamboo culms, as they tend to weaken the material in tensile tests (Arce, 1993).

The mechanical properties of bamboo can vary considerably between different species (Chung and Yu, 2002). This highlights the importance of selecting the appropriate bamboo species for specific applications, as different species exhibit distinct mechanical characteristics.

### **2.3. Short and long tubes**

When a tube specimen is loaded while its ends are clamped, gripped or otherwise restrained inside a test rig, the stress and strain distribution close to those boundaries is no longer the same as in the free body of the sample. This disturbance, commonly

called the end effect, causes the material within roughly one diameter of each end to experience radial restraint and friction that stiffen it and alter its failure mode. In tube tests this can: (1) inflate the measured modulus and compressive/tensile strength by (Mujdeci, Bompa and Elghazouli, 2021; Bompa *et al.*, no date) and (2) suppress or shift the location of shear planes, giving “barrel-shaped” deformation.

The magnitude of the end effect grows as the length-to-diameter ratio ( $L/D$ ) decreases, as surface roughness and normal pressure at the platens increase, and when testing stiff or brittle materials that localise strain quickly. ISO 22157:2019 tests use stub bamboo specimens ( $L/D \approx 1$ ). End effects in these short tubes inflate measured compressive strength, therefore designs based on them are unconservative (Mujdeci, Bompa and Elghazouli, 2021; Bompa *et al.*, no date). Real, longer culms fail earlier by local buckling, shifting failure from strength-controlled to stability-controlled (Nie *et al.*, 2021). This is especially important given bamboo’s anisotropy and large internodal lengths. Length also skews splitting tests: short pieces crack and fail fast, giving overly low splitting strengths (Bompa *et al.*, no date). Hence, short specimens do not represent the behaviour of full-length bamboo members.

#### **2.4. Rule of mixtures**

The Rule of Mixtures (RoM) is an approach to predicting the mechanical properties of composite materials. For bamboo, this theory is applied by treating the material as composite material consisting of high-strength cellulosic fibres embedded within a softer parenchyma matrix. The longitudinal elastic modulus is calculated assuming parallel loading of the constituents (Akinbade *et al.*, 2019):

$$E_L = E_f V_f + E_m (1 - V_f)$$

where  $E_L$  is the composite longitudinal modulus,  $E_f$  is the fibre modulus,  $E_m$  is the matrix modulus, and  $V_f$  is the fibre volume fraction.

The rule of mixtures has demonstrated success in predicting bamboo’s longitudinal mechanical properties. Janssen’s seminal work established typical values of  $E_f = 35$  GPa and  $E_m = 1.8$  GPa for bamboo fibres and parenchyma matrix, respectively

(Janssen, 1981). Subsequent studies have consistently confirmed these values through experimental validation (Akinbade and Harries, 2021).

The success of RoM in the longitudinal direction is attributed to bamboo's highly anisotropic nature, with  $E_f/E_m$  ratios typically exceeding 20. Under these conditions, the longitudinal behaviour becomes entirely dominated by fibre properties, allowing the approximation  $E_L \approx V_f E_f$ . Dixon et al. (2015) demonstrated this relationship across three bamboo species (Moso, Guadua, and Tre Gai), showing linear relationships between modulus of elasticity and density that are consistent with rule of mixtures predictions.

An important parameter in applying RoM to bamboo is the accurate determination of fibre volume fraction ( $V_f$ ). Bamboo exhibits a functionally graded structure with  $V_f$  varying from approximately 0.10–0.15 near the interior surface to 0.60 at the exterior surface of the culm wall (Akinbade and Harries, 2021). The gross section fibre volume fraction typically ranges around 0.30 (Akinbade and Harries, 2021).

However, challenges exist in accurately measuring  $V_f$ . Dixon and Gibson (2014) highlighted the importance of distinguishing between load-bearing fibres and vessels (voids) within vascular bundles, noting that incorrect inclusion of vessels leads to overestimated fibre volume ratios. The variation in  $V_f$  through the culm wall has been modelled using various functions (linear, quadratic, exponential, or power functions) and is species-dependent.

*Table 2.1. Average bamboo mechanical property values. (Vivas et al., 2019)*

Mechanical Property	Symbol	Average Value (N)	Mid 50% Values
Shear Strength Parallel to Grain	$F_v$	9 MPa (18)	6.8–11.7 MPa
Compressive Strength	$F_c$	52 MPa (59)	40.7–61.9 MPa
Modulus of Rupture, Bending Strength (MOR)	$F_\beta$	120 MPa (52)	79.6–149 MPa
Tensile Strength	$F_t$	159 MPa (21)	89.5–206 MPa
Compressive Modulus of Elasticity (MOE)	$E_c$	16 GPa (19)	9–20.7 GPa
Bending Modulus of Elasticity (MOE)	$E_\beta$	17 GPa (34)	14.3–20 GPa

Tensile Modulus of Elasticity (MOE)	$E_t$	14 GPa (10)	9.5–18 GPa
Combined Modulus of Elasticity (MOE)	$E$	16 GPa (63)	11.8–19.7 GPa
Notes: N is the number of studies from which the data were collected. Mid 50% values is the range of values for the middle 50% of values.			

## 2.5. Bamboo species

### 2.5.1 *G. angustifolia*

*G. angustifolia* (often referred to simply as Guadua) is a significant tropical bamboo species, primarily endemic to South and Central America, with widespread use as a construction material, particularly in Colombia, Ecuador, and Venezuela (Aicher and Simon, 2022). It is considered one of the three largest and most economically important bamboo species globally due to its size, high performance, and impact on local economies (Ximena Londoño *et al.*, 2002; Osorio *et al.*, 2011).

*G. angustifolia* is widely used in construction due to its high strength-to-weight ratio, durability, ease of use, abundance, and low cost. Notable projects include the Colombian ZERI Pavilion at the Hannover Expo in 2000 and the DIHAD Pavilion (Aicher and Simon, 2022). Its structural integrity was notably tested during the 1999 earthquake in Colombia (6.2 Richter scale), leading to its standardization in the seismic-resistant Colombian code (NSR, 2010).

The *G. angustifolia* culm (stem) reaches its full height, diameter, and wall thickness within the first four to six months of life, followed by tissue consolidation through secondary thickening until maturity (Ximena Londoño *et al.*, 2002; Archila-Santos, Ansell and Walker, 2012). It is one of the world's fastest-growing plants, with growth rates up to 90 cm per day (Archila-Santos, Ansell and Walker, 2012; Aicher and Simon, 2022). *G. angustifolia* can grow by about 10 cm per day within the first six months and reaches a height of 20 to 30 m. It matures between three and five years of age, with some studies suggesting optimal maturity for mechanical properties is reached between three and four years (Correal D and Arbeláez C, 2010). It is commonly found at altitudes between 500 and 1500 m, with temperatures between 18°C and 24°C, and relative humidity of 80% to 90%, thriving in regions with 1200

mm to 2500 mm of precipitation per year (Ximena Londoño *et al.*, 2002; Archila-Santos, Ansell and Walker, 2012).

Typical *G. angustifolia* culm dimensions range from 76 mm to 143 mm in outer diameter and 9 mm to 19 mm in wall thickness (Aicher and Simon, 2022). The culm diameter and wall thickness generally decrease from the base to the apex, while internode length increases (Gnanaharan, Janssen and Arce, 1995; Ximena Londoño *et al.*, 2002; Harries *et al.*, 2017; Aicher and Simon, 2022; Rivera-Segura *et al.*, 2024). The ratio of culm wall thickness can be used to categorize bamboo as 'thick-' or 'thin-walled'. For *G. angustifolia*, a D/δ ratio (diameter to wall thickness) averaging approximately 10 classifies it as a thin-walled species (Harries *et al.*, 2017).

Research on *G. angustifolia* from Colombia suggests a characteristic 5%-quantile compressive strength ( $f_{c,0,k}$ ) of 40 N/mm<sup>2</sup> and a mean modulus of elasticity ( $E_{c,0,\text{mean}}$ ) of 18500 N/mm<sup>2</sup> (Aicher and Simon, 2022). Other studies report mean compressive strengths ranging from 35.0 to 50.6 N/mm<sup>2</sup> depending on the presence of nodes and culm section. The mean compressive strength for all the DIHAD project specimens was  $54.0 \pm 8.7$  N/mm<sup>2</sup>. The top portion of the culm often exhibits the maximum strength and modulus of elasticity compared to other portions, largely due to its higher density (Correal D and Arbeláez C, 2010).

The presence of nodes can influence mechanical properties; for instance, compressive strength was found to be maximally 10% higher for specimens without a node compared to those with a node at mid-length (Aicher and Simon, 2022). However, this effect is highly dependent on culm diameter, wall thickness, and wall area, becoming negligible for large values (external diameter  $\geq 130$  mm, thickness  $\geq 15$  mm, Area  $\gtrsim 5000$  mm<sup>2</sup>). The varying findings on node effects in literature suggest it might be species-dependent (Vivas *et al.*, 2019; Aicher and Simon, 2022).

In the literature, the shear strength of *G. angustifolia* has been extensively studied using the standardized bow-tie shear test described in ISO 22157:2019. A large-scale experimental campaign carried out across three Colombian regions (Quindío, Cundinamarca, and Valle del Cauca) reported green-condition shear strengths of 5.66 MPa, 5.52 MPa, and 6.44 MPa, respectively, with an overall mean of

approximately 5.87 MPa based on 246 samples (Correal & López, 2008). Complementary studies on dry-condition culms have shown slightly higher bow-tie shear strength values, typically ranging between 7.10 and 7.47 MPa (Lozano, Luna and Takeuchi, 2010). These results highlight the sensitivity of *G. angustifolia* to moisture content and confirm that, while its shear resistance is relatively modest compared to its axial tension and compression capacities, it remains an important parameter in structural applications and design codes where shear governs connection behaviour.

The mechanical characterization of *G. angustifolia* has also included the determination of its elastic modulus. Correal and López (2008) reported values obtained from bending tests across the three Colombian regions, with mean elastic moduli of 17,338 MPa in Quindío, 18,664 MPa in Cundinamarca, and 19,774 MPa in Valle del Cauca, yielding an overall average of approximately 18,792 MPa based on a dataset of more than 400 specimens. These findings are consistent with other studies on dry culms, which reported moduli in the range of 17,000–20,000 MPa, reinforcing the high stiffness of *G. angustifolia* relative to other bamboo species (Lozano, Luna and Takeuchi, 2010).

### 2.5.2 *D. asper*

*D. asper*, commonly known as Giant bamboo or Bamboo Betung, is a large bamboo species with great commercial importance, particularly in Southeast Asia (A.N. Rao, V. Ramanatha Rao, and J.T. Williams, 1998). It is widely cultivated for various applications, including construction, food, and composite materials (Hartono *et al.*, 2022).

*D. asper* culms typically reach heights of 20–30 meters, with lower nodes featuring a circle of rootlets. The internodes are 20–45 cm long, and their diameter ranges from 8–20 cm, with relatively thick walls (11–20 mm), which tend to be thinner towards the top of the plant (A.N. Rao, V. Ramanatha Rao, and J.T. Williams, 1998). Leaf dimensions are approximately 30x2.5 cm. The species' total internode count averages around 60 per culm. Studies have shown that internode length for *D. asper* generally increases from the lower to middle sections of the culm (e.g., from

internode 5 to 16), with slight variations thereafter (A.N. Rao, V. Ramanatha Rao, and J.T. Williams, 1998). Conversely, internode diameter and culm wall thickness tend to decrease with increasing culm height. The flowers are sterile, and fruits are typically collected from hybrids.

*D. asper* compressive strength lies around showed compressive strength values of 40.2 to 48.0 N/mm<sup>2</sup> parallel to the grain along the culm height. The highest average compressive strength found by Adam and Jusoh (2019) was 65 MPa and the lowest was 42 MPa. The highest compressive strength (48.0 N/mm<sup>2</sup>)for *D. asper* was observed in the top portion quarter of the culm, which is linked to its higher density compared to other bamboo species.

Bautista's (2021) shear tests on 30 specimens of *D. asper* following ISO 22157:2019 on returned an average shear strength of 10.3 MPa and a 5%-characteristic value of 7.0 MPa, placing *D. asper* in the same capacity bracket as other structural bamboos such as *Gigantochloa apus* and *Bambusa vulgaris* but below *B. blumeana* ( $\approx$ 11 MPa). Shear strength is substantially lower than the species' compressive capacity (40–65 MPa) because shear is governed by the thin parenchymatous matrix rather than the dense fibre bundles. Along the culm the mean value climbs gently from  $\approx$ 9 MPa at the base to  $\approx$ 11 MPa at mid-height before tapering again in the top quarter; however, the statistical analysis showed no significant difference between internode and node specimens, confirming that nodes do not penalise shear resistance. Comparative testing of seven Philippine bamboos under identical conditions ranked *D. asper* third for shear, behind *B. blumeana* and *G. apus* but ahead of *B. philippinensis* and *B. vulgaris*, indicating that its fibre-rich wall gives moderate transverse strength without the variability seen in thinner-walled species.

## 2.6. Standards and codes

Although it has been pointed numerously in literature (Harries et al., 2022) that bamboo standards are the catalyst to the use of bamboo, Janssen (2000) explained that developing building standards for bamboo is not an easy task, contrary to conventional construction materials. Janssen (2000) noted that bamboo is a local-first materials, and that means standards should (1) align with local traditions (2) balance

the interests of both the economically privileged and underprivileged to improve housing for lower-income groups and acknowledge their financial constraints and (3) reflect community priorities, utilize local materials and traditional housing resources while avoiding unnecessary bureaucracy. However, bamboo construction has been able to take place in developing countries due to the ability to bypass approvals which would have been an issue in developing countries (*NEBgS Lecture Series #3 with Jörg Stamm \_ Bamboo in the Future of Design: Long, light and strong*, 2024). Without bamboo building standards, the current bamboo construction practice involves modelling of a physical prototype of a structure, loading the model using actual dead loads to determine deformations (seen in Figure 1.6) and feeding back data into an analysis model. This design process is laborious and consumes time, money and labour therefore discouraging to clients.

The journey towards international bamboo standards began over two decades ago, with initial efforts culminating in the 2004 publication of ISO 22157-1:2004 for test methods and ISO 22156:2004 for structural design. These were based on traditional knowledge and early seminal work by researchers like Janssen (2000) and Arce-Villalobos (1993). However, they were considered "fundamentally inadequate for performing holistic design for most potential end-users" and provided little specific guidance beyond indicating an intent for design by calculation or experiment (Harries, Sharma and Richard, 2012).

Progress was made over the following 15 years, leading to updated ISO standards. ISO 22157:2019 describes methods for determining moisture content, density, mass per unit length, and six key mechanical properties: compressive strength and stiffness parallel to fibres; tension strength and stiffness parallel to fibres; bending strength and stiffness parallel to fibres; shear strength parallel to fibres; tension strength perpendicular to fibres; and bending strength and stiffness perpendicular to fibres (ISO, 2019). It evolved from the 2004 version by adding methods for perpendicular tension and bending, and revising the tension test method.

ISO 19624:2018 provides a framework for grading bamboo culms based on defined selection criteria, differentiating between non-destructive "indicating properties" and destructively measured "grade-determining properties" (ISO, 2018).

ISO 22156:2021 revises the 2004 edition, enabling allowable capacity design alongside allowable stress design approaches. However, the standard's scope is limited to one- and two-storey residential, small commercial or institutional, and light industrial buildings not exceeding 7m in height, where the primary load-bearing structure is full-culm bamboo (ISO, 2021). The standard specifies a practical minimum diameter of 50 mm for structural load-bearing elements and recommends a diameter-to-wall thickness ratio ( $D/\delta$ ) less than 12 to prevent local buckling. ISO 22156:2021 also introduces modification factors for in-service equilibrium moisture content, load duration, and service temperature (ISO, 2021). For safety, the component factor of safety is 2 for longitudinal actions (compression, tension, bending) and 4 for brittle splitting behaviour.

Beyond these international efforts, several countries where local bamboo is endemic have developed their own national building codes and standards (see Table 2.2 and Table 2.3) focusing on whole culm bamboo:

*Table 2.2. Codes for bamboo structural design (Amede et al., 2021)*

Country	Year of publication	Code name
Colombia	2010	Reglamento Colombiano de Construcción Sismoresistente—chapter G.12 Estructuras de Guadua (Guadua Structures)
China	2011	JGJ 254: Technical code for the safety of bamboo scaffold in construction
Ecuador	2011	Norma Ecuatoriana de la Construcción—chapter 17 Utilización de la <i>Guadua Angustifolia</i> Kunth en la Construcción (Use of <i>Guadua angustifolia</i> Kunth in construction)
India	2005	National Building Code of India—developed a Code of Practice for Bamboo Design-Section 3—Timber and Bamboo: 3B
	1979	9096: Code of practice for preservation of bamboo for structural purposes
Peru	2012	Reglamento Nacional de Edificaciones, Section 3. Code E100—Diseño y Construcción con Bamboo (ICG)

*Table 2.3. Standards for bamboo structural design (Amede et al., 2021)*

<b>Country</b>	<b>Year of publication</b>	<b>Code name</b>
International	2004	ISO 22156 Bamboo—Structural Design
	2004	ISO 22157-1 Bamboo—Determination of Physical and Mechanical Properties—Part 1: Requirements ISO
	2004	ISO 22157-2: Bamboo—Determination of Physical and Mechanical Properties—Part 2: Laboratory Manual
	2018	ISO 19624 Bamboo structures—Grading of Bamboo Culms—Basic Principles and Procedures
China	2014	JG/T 428: Composite ply bamboo form with steel frame
	2014	GB/T 30762: Quality grading standards of main bamboo shoot
	2007	JG/T 199: A testing method for physical and mechanical properties of bamboo used in building
	2000	GB/T 2690—Bamboo timber
	1995	GB/T 15780: Testing methods for physical and mechanical properties of bamboo
India	2012	IS 6874: Method of tests for bamboos
	2010	IS 6874: Method of tests for round bamboos
	2008	IS 6874: Method of tests for round bamboos
	1994	13958: Specification for bamboo mat board for general purposes
	1976	8242: Method of test for split bamboo
	1973	IS:6874: Method of test for round bamboo
	2007	NTC 5525: Me' todos de Ensayo para Determinar las Propiedades Físicas y Mecánicas de la Guadua angustifolia Kunth (methods and tests to determine the physical and mechanical properties of <i>Guadua angustifolia</i> Kunth)
	2006	NTC 5407: Uniones de Estructuras con Guadua angustifolia Kunth (structural unions with <i>Guadua angustifolia</i> Kunth)
Ecuador	1976	INEN 42: Bamboo Caña Guadua (bamboo cane Guadua)
USA	2013	ASTM D5456: Standard specification for evaluation of structural composite lumber products

Despite these advances, the call for further standardisation and codification continues. Several key challenges and areas for future development have been identified by Harries (2024):

1. While ISO standards provide a foundation, they are considered insufficient for widespread use and need to be updated and expanded to reflect ongoing research and new structural bamboo products. A shortcoming in existing literature is the inconsistent use of test methods, leading to widely varying results. For example, tension test results can vary by more than a factor of two depending on specimen orientation and grip conditions. The presence of a node also affects tension results by a factor of about two, and tension strength should always be reported using specimens containing a node in the gauge length for structural design relevance.
2. Important needs include improved performance of standard shear and flexural tests. The third-point bending test in ISO 22157:2019 is performed on full culms, but the behaviour is often governed by longitudinal shear rather than pure flexure, and the test itself is cumbersome. Alternative small rectangular bending samples and torsion-based shear tests are being explored.
3. Current standards, including ISO 22157:2019, do not adequately address the change of material and mechanical properties over time due to bamboo's viscoelastic nature or environmental degradation. Existing ISO 22156:2021 provisions for viscoelastic behaviour and environmental exposure are conservative due to a lack of long-term data. There is a need to formalise tests and sampling protocols to establish time-dependent changes in mechanical parameters. Bamboo is known to be less resistant to decay vectors (insect, fungal, hygrothermal) than wood, and much of the available durability data is anecdotal.
4. The impact of preservation treatments on mechanical properties is another poorly studied area. While treatment is universally understood as necessary for load-bearing applications with a longer life, there's a need to quantify the

efficacy of different treatment methods, especially emerging ecologically friendly ones.

5. ISO 19624:2018 provides a framework for grading but does not identify specific indicating properties (IP) and grade-determining properties (GDP) or their inference relationships. Due to significant inter- and intraspecies variation, generalising IP selection and IP-to-GDP inference is challenging. Machine learning and material informatics approaches are proposed to accelerate this development.
6. There is a need for tools and data to allow bamboo to be treated as any other material in the realm of digital design, promoting innovation in engineered bamboo.

A promising pathway for future standardisation is to create standards and codes analogous to timber-based standards (Gat  o *et al.*, 2014). Recent research is shifting towards using timber standards for testing and characterising engineered bamboo products that no longer resemble whole culm bamboo. This approach provides a comparison to other timber products and could broaden market potential for structural and engineered bamboo (Gat  o *et al.*, 2014). For example, ASTM D143, a standard test method for small clear specimens of timber, has been used for laminated bamboo (ASTM, 2023).

## **2.7. Summary**

Bamboo functions as an intelligent functionally graded material with hollow, segmented culms characterized by nodes separating internodal regions. The culm wall comprises approximately 52% parenchyma cells, 40% fibres, and 8% conducting elements, with fibre density increasing dramatically from inner walls (10-15% fibre volume) to outer walls (up to 60%). This natural optimization results in relatively uniform engineering properties along the culm height, with bamboo being naturally intelligent and self-optimizing.

Mechanical properties demonstrate bamboo's highly orthotropic nature, with compressive strengths typically ranging 45-65 MPa for various species. Moisture

content emerges as the most critical factor governing mechanical properties, with the fibre saturation point occurring between 20-30% depending on species. Above this point, additional moisture generally has minimal influence on properties, while increases in moisture content between 12% and the fibre saturation point cause particularly notable strength reductions.

Current testing methodologies present some limitations, particularly the ISO 22157:2019 specification using short specimens with length-to-diameter ratios of approximately 1.0. These create end effects that inflate measured compressive strength, leading to unconservative strength predictions for actual structural members. Real structural elements fail earlier by local buckling, shifting failure from strength-controlled to stability-controlled modes.

Species-specific analysis reveals *G. angustifolia* achieving characteristic compressive strengths of 40 N/mm<sup>2</sup> with shear strengths of 5.5-6.4 MPa, while *D. asper* demonstrates superior performance with compressive strengths of 40.2-48.0 MPa and shear strengths averaging 10.3 MPa. The development of bamboo standards remains challenging, with the first international standard appearing in 2004, yet comprehensive structural design standards still lacking, necessitating empirical approaches to bamboo structure design.

### **3. Methodology**

#### **3.1. Material procurement**

Four full-length bamboo culms, each 5.85 m in length, were obtained from UK Bamboo Supplier Limited (see Figure 3.2a). The bamboo culms comprised two *G. angustifolia* poles and two *D. asper* poles. The two bamboo species are one of the 20 taxa of bamboo accorded high priority for international action (A.N. Rao, V. Ramanatha Rao, and J.T. Williams, 1998). The culms were sourced from the Department of Suchitepeques plantation in Guatemala (UK Bamboo Suppliers Limited, 2025). The age of the culms was between 3–5 years. For the treatment method of the culms, the culms were washed, perforated, cured and then treated by immersion for 5 days in a 5% solution of pentaborate salts i.e. borax and boric acid. External diameters ranged from 80–100 mm for *G. angustifolia* and 130–150 mm for *D. Asper*. On arrival, the culms were stored for 30 days in the structural laboratory at  $23\pm2^\circ\text{C}$  and  $65\pm2\%$  relative humidity to achieve hygroscopic equilibrium with the testing environment.

#### **3.2. Specimen preparation**

A final total of 108 specimens (roughly 50% with nodes and 50% without nodes) were generated from the four full-length culms. 65 samples belonged to *G. angustifolia* species and 38 samples to *D. Asper*. Each culm was first divided into three equal segments representing the basal (bottom), middle, and apical (top) portions (see Figure 3.2b). This segmentation was done to allow each segment to have an assumed external diameter which would then dictate the specimen lengths that would achieve the appropriate aspect ratios (aspect ratios of 1.0 and 2.0). This was done as for both species, the diameter variation across the full-length pole was large.

The segmentation resulted in twelve primary segments, which provided material for testing under different moisture conditions and loading configurations. Each segment was subsequently cut into test specimens with dimensions conforming to aspect ratio requirements as detailed in Table 3.1. The *D. asper* poles had numerous long splits, resulting in fewer usable specimens compared to *G. angustifolia*.

A labelling system was implemented for each specimen using the format DT-2-001, where: D = species designation (D for *D. Asper*, G for *G. angustifolia*), T = culm segment (T = top, M = middle, B = bottom), 2 = pole number (1-2 for each species), 001 = sequential specimen number within the segment. This approach enabled traceability in regard to the type of species and location along the full length culm. The specimens were then assigned sample groups (see Table 3.1) with the format DLOC, where D = species designation (D for *D. Asper*, G for *G. angustifolia*), L = specimen length (L = long i.e. 2.0 aspect ratio, S = short i.e. 1.0 aspect ratio), O = conditioning (O = oven-dry, A = ambient-dry, W = wet), C = test type (C = compression parallel to grain, S = shear parallel to grain). The sample groups were used for analysis in Section 4.

*G. angustifolia* specimens were cut using a band saw machine, which produced acceptable cuts but resulted in burning at the cut surfaces. Sanding was done to some specimens after cutting to remove the burned zone and expose the underlying microstructure clearly for subsequent image analysis described in Section 3.4. This surface preparation was done to prevent the burnt zones inflating the fibre and matrix volume values in the image analysis process described in Section 4.1.

*D. asper* specimens, due to their larger diameter and greater stiffness, required workshop-based cutting using industrial equipment. The cutting process for *D. Asper* produced clean surfaces without thermal damage, eliminating the need for surface preparation thereafter. However, cutting of *D. asper* resulted in fewer useable specimens due to larger diameter which meant longer specimens as compared to *G. angustifolia*. Also, the inherent brittleness of *D. asper* led to longitudinal splitting during cutting and therefore some samples were lost.

The specimen end faces were machined to achieve parallel surfaces perpendicular to the longitudinal axis, with a maximum deviation tolerance of 1% from perfect alignment. This preparation is essential for ensuring uniform stress distribution during mechanical testing and preventing premature failure due to geometric irregularities.

Mass measurements were carried out using a calibrated electronic balance with a precision of 0.1 g. Recordings were taken at multiple stages: initial (as-received), pre-

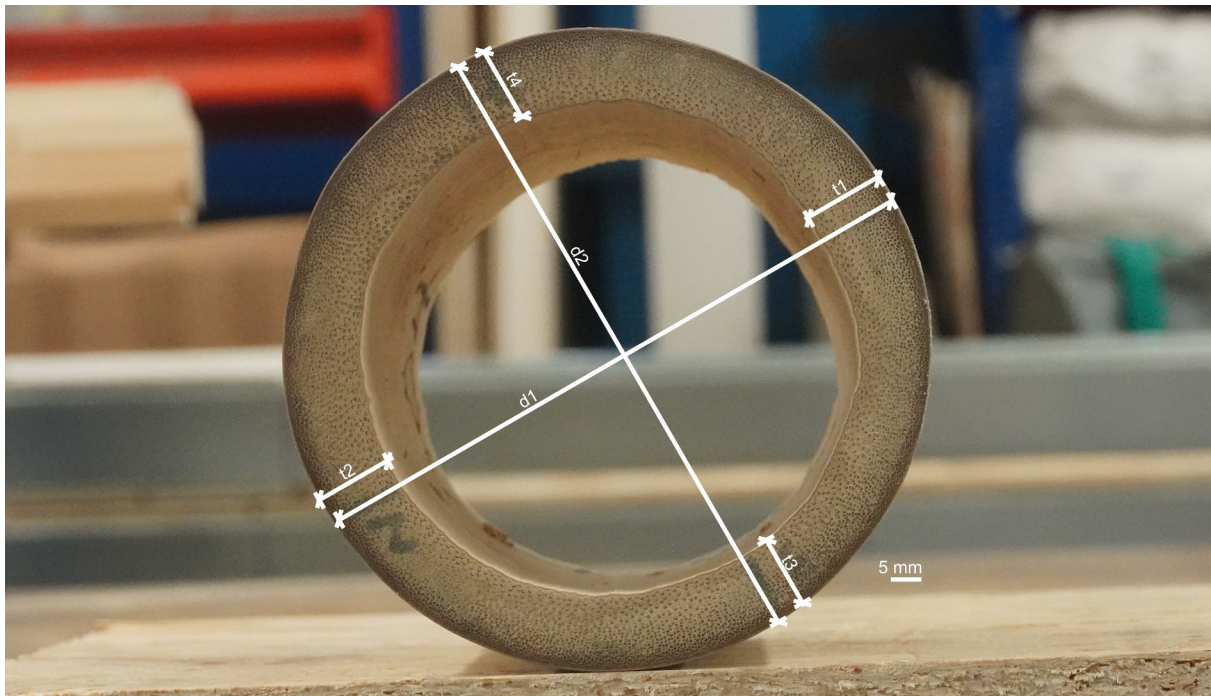


*Figure 3.1. Typical section of bamboo culm. To account for the oval shape of the culms, how diameters and thickness measurements were carried out were adjusted. For the outside diameter was equal to the average value of the measurements along the major axis and minor axis of the oval culm. In similar fashion the thickness was taken as the average value of the four measurements, two along each axis. These four thickness measurements also represented the shear planes in the bowtie test.*

conditioning, post-conditioning/pre-testing, and post-oven drying. This approach enabled calculation of moisture content variations throughout the testing programme.

All dimensional measurements (Error: Reference source not found) were conducted in accordance to ISO 22157:2019 (ISO, 2019) using digital callipers with 0.01 mm precision for small measurements and a ruler with a precision of 0.5 mm. Bamboo's inherent irregularity in geometry was addressed through averaging of the below dimensions (see Figure 3.1):

1. External diameter  $D$ : Two measurements per end face along major and minor axes ( $90^\circ$  intervals), with final diameter calculated as the arithmetic mean of four measurements per specimen.

2. Wall thickness  $\delta$ : Eight measurements per specimen (four per end face) along the major and minor axes, with mean thickness used for stress calculations.
3. Length  $L$ : Measured using digital calliper ( $\pm 0.5$  mm precision) and a steel ruler ( $\pm 0.5$  mm precision) at four locations corresponding to the diameter measurement points, with specimen length calculated as the mean of the four measurements.

*Table 3.1. Sample details*

<b>Sample group</b>	<b>Count</b>	<b>D</b>	<b><math>\delta</math> (mm)</b>	<b>L (mm)</b>	<b><math>L/D (-)</math></b>	<b><math>D/\delta (-)</math></b>
DLAC	1	132.1(0.0)	9.5(0.0)	260.5(0.0)	2	13.9
DLOC	2	136.7(1.3)	11.9(2.2)	274.8(20.4)	2	11.7
DLWC	1	138.5(0.0)	10.5(0.0)	290.0(0.0)	2.1	13.2
DSAC	6	135.0(2.7)	10.9(1.5)	137.0(6.7)	1	12.5
DSOC	4	137.5(3.7)	10.9(1.3)	139.1(7.9)	1	12.8
DSWC	5	135.5(3.9)	10.5(0.8)	135.0(6.1)	1	12.9
DLAS	3	137.7(3.1)	11.4(1.6)	140.9(5.7)	2.1	12.2
DLOS	2	138.3(4.1)	12.6(4.0)	280.7(14.8)	2	11.6
DLWS	3	137.1(2.8)	12.2(2.2)	283.8(11.9)	2.1	11.4
DSAS	3	139.0(2.9)	11.9(2.5)	284.0(11.1)	1	12
DSOS	4	137.6(4.3)	11.7(2.8)	137.7(6.4)	1	12.2
DSWS	3	136.6(2.8)	11.3(1.8)	138.2(7.8)	1	12.3
GLAC	5	99.7(9.1)	9.0(1.6)	186.8(32.3)	1.9	11.3
GLOC	1	98.6(0.0)	9.0(0.0)	189.9(0.0)	1.9	11
GLWC	5	104.8(7.4)	11.1(3.1)	207.5(17.4)	2	9.9
GSAC	10	102.5(6.9)	10.0(2.5)	109.4(31.6)	1.1	10.6
GSOC	8	99.2(8.0)	9.2(1.5)	98.0(4.8)	1	11
GSWC	7	103.1(8.6)	10.4(1.7)	99.9(5.3)	1	10.1
GLAS	2	108.6(2.4)	9.7(0.8)	207.4(16.8)	1.9	11.2
GLOS	1	105.7(0.0)	11.3(0.0)	201.4(0.0)	1.9	9.3
GLWS	2	102.3(4.3)	9.5(2.0)	199.1(2.0)	1.9	11

GSAS	6	106.6(7.4)	10.9(2.3)	101.6(4.9)	1	10.1
GSOS	9	103.0(6.4)	10.0(2.2)	100.4(6.8)	1	10.6
GSWS	9	105.3(4.7)	11.0(2.5)	101.8(6.0)	1	9.9

Notes: The values in brackets represent the standard deviation of the value attached to it.  $D$  is the average diameter of the specimen,  $\delta$  is the average thickness of the specimen and  $L$  is the average length of the specimen.

### 3.2.1 DIC

Two opposite faces, each roughly a quarter of the external wall, of every specimen were coated with two light passes of matte white acrylic spray paint (see Figure 3.3a). The paint layer provided a uniform, non-reflective background while adding  $<10\ \mu\text{m}$  thickness, which is negligible relative to the section dimensions.

A commercial rubber stamp with a nominal dot diameter of 1.27 mm was inked on a flat pad charged with black ink. The stamp was laid flat face up. Each specimen was then rolled once across the mat in a single, steady motion, transferring the pattern without smearing (see Figure 3.3b). Sparse regions within the DIC pattern were filled using an ultra-fine black permanent marker of matching diameter. The chosen dot size yielded 6–8 pixels per dot for the cameras positioned at the planned 90 mm field-of-view, satisfying the  $\geq 5$  pixel criterion for reliable correlation (Jones *et al.*, 2018). Preliminary images were captured and the dot sizes were measured in ImageJ (Ferreira and Rasband, 2012).

During the tests, twin Sony EV 710 cameras (25.2 megapixels,  $6000\times4000$  pixel resolution) were positioned to capture images of opposite specimen surfaces at 10-second intervals throughout each test described in section 3.3.1 and 3.3.2. Camera aperture was set to f/16 with manual focus adjustment for optimal pattern resolution. Supplementary LED lighting provided consistent illumination throughout the test duration. The images from the tests were analysed for strain distributions using DICe and Paraview (Engine (DICe), 2025; Paraview, 2025).



**Figure 3.2. Specimen preparation.** (a) Full-length culms. (b) Segmenting of full-length culms into thirds. (c) Marking of cutting points along the length of thirds. (d) cutting of specimens using band-saw. (e) Labelling of specimens. (f) Sanding of specimens. (g) Cut specimens. (h) Weighing of specimens. (i) Measuring of specimen dimensions. (j) Oven-drying of specimens. (k) Soaked specimens

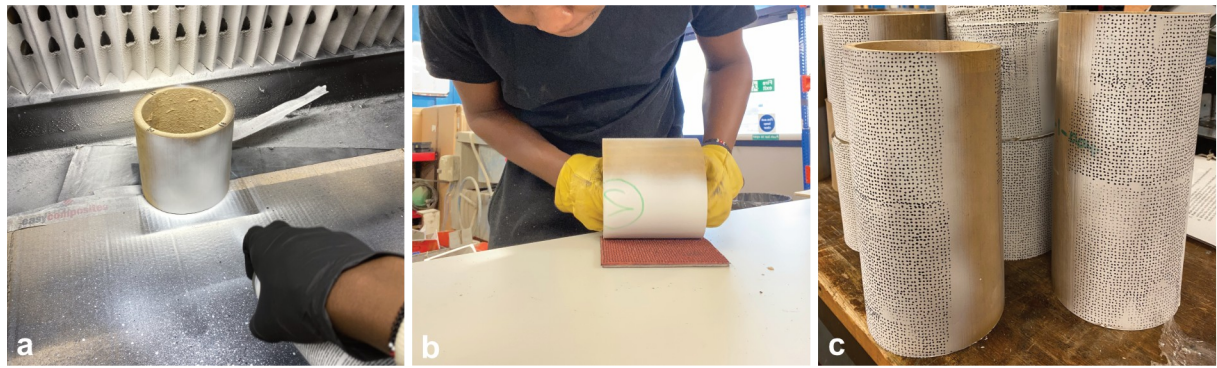


*Figure 3.3. DIC preparation for specimens. (a) Spray painting of specimens. (b) Application of speckle pattern. (c) Bamboo specimens with speckle pattern.*

### 3.2.2 Conditioning

Specimens were divided into three conditioning groups:

1. Ambient conditioning: Specimens maintained at laboratory conditions ( $25\pm2^{\circ}\text{C}$ ,  $60\pm2\%$  RH) until equilibrium moisture content was achieved. During this conditioning, no specimens were lost.
2. Oven-dry conditioning: Specimens were dried for 24 hours at  $103 \pm 2^{\circ}\text{C}$  immediately prior to testing. During this conditioning, samples across both species were lost due to splitting in the oven and after removal from the oven. Splitting was prevalent among long tubes and tubes with internodes as seen in Figure 3.2j.
3. Wet conditioning: Specimens were immersed in tap water for 24 hours to achieve fibre saturation point, the length of period was determined from previous studies which show that the fibre saturation point (>30% moisture content) of bamboo specimens was achieved in less than 24 hours (Xu *et al.*, 2014). During this conditioning, samples were lost only in the *D. asper* species. This was an early indicator of the brittleness of *D. asper* species discussed in Section 4.3. Majority of the samples lost were long tubes, with almost equal splitting in tubes with nodes and without nodes as seen in Figure 3.2k. For both *G. angustifolia* and *D. asper*, the tap water turned brown.

### **3.3. Experimental setup**

All mechanical tests were conducted using an Instron 8805 universal testing machine equipped with a 1 MN load cell using a displacement-control rate of 1 mm/min. This loading rate was selected based on preliminary testing to ensure test completion within the recommended time-frame of  $300 \pm 200$  seconds, as specified in ISO 22157:2019 (ISO, 2019). Two primary test configurations were implemented: compression parallel to fibre and shear parallel to fibre with a general setup shown in Figure 3.4.

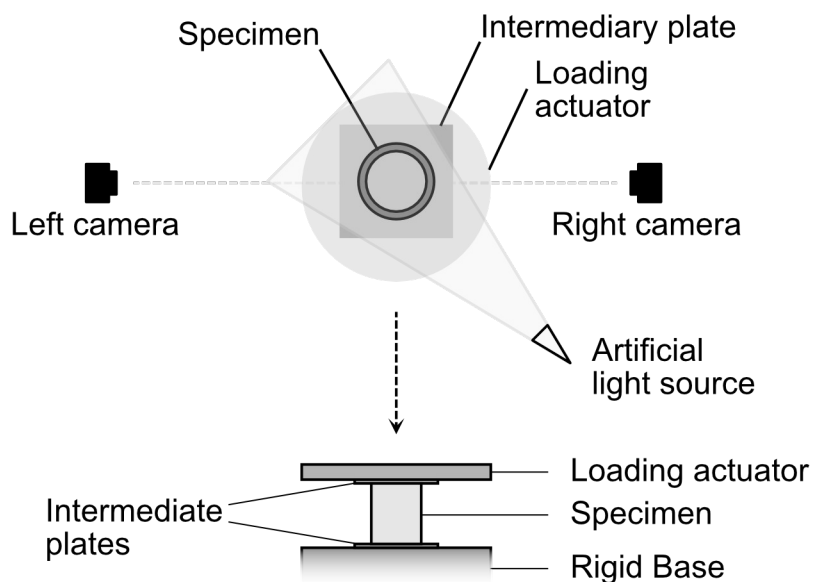


*Figure 3.4. Typical experimental setup*

#### **3.3.1 Compression testing**

For compression testing, specimens were loaded in compression parallel to the fibre direction (Figure 3.5). The bottom grip of the testing machine was fitted with a rigid steel base. An intermediary steel plate was placed on top of the bases. At the top grip, a hinge was incorporated to allow smooth load transfer and to prevent the influence of any minor inclinations on the upper surface of the samples. For compression tests, each specimen was topped with a steel plate. This arrangement ensured an even distribution of stress across the cross-section and reduced friction, which could otherwise create radial restraint at the specimen ends.

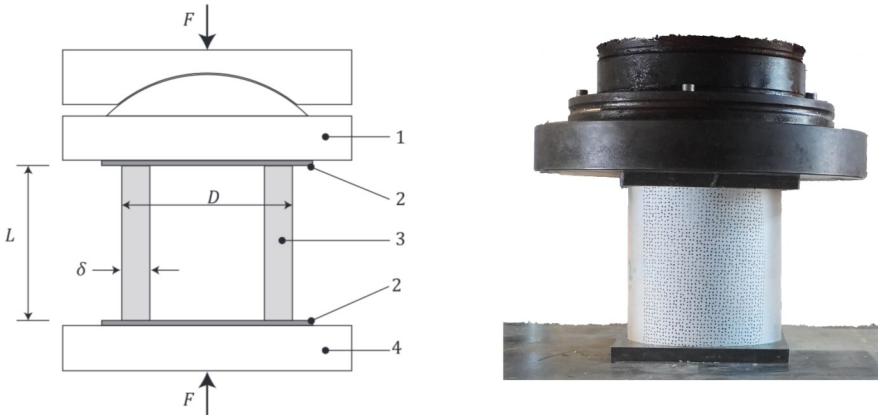


*Figure 3.5. Compression test setup. ISO setup diagram on the left and actual test setup on the right. D is outer diameter,  $\delta$  is wall thickness, F is load, L is length of specimen, 1 is upper loading platen with spherical bearing, 2 is intermediate layer, 3 is bamboo specimen, 4 intermediate layer and 5 is lower loading platen (ISO, 2019).*

Specimens were centred and a seating load not exceeding 1% of the anticipated failure load was applied to establish full contact. Thereafter, displacement-controlled loading proceeded at 1.0 mm/min. The test was halted at a post-peak load of  $0.8F_{\max}$ . Following failure, the specimen was oven-dried at  $103 \pm 2^\circ\text{C}$  for 7 days for subsequent moisture-content determination.

The compression strength parallel to the fibres,  $f_{c,0}$ , was calculated by dividing the maximum load ( $F_{\max}$ ) by the measured cross-sectional area of the bamboo culm:

$$A = \pi/4(D^2 - (D - 2\delta)^2)$$

where  $D$  represents the average external diameter of the specimen and  $\delta$  represents the average thickness of the specimen.  $E_{c,0}$  was evaluated as the secant slope between 20% and 60% of  $F_{\max}$ :

$$E_{(c,0)} = (F_{60} - F_{20}) / A(\varepsilon_{60} - \varepsilon_{20})$$

with  $F_{20}$  and  $F_{60}$  denoting the loads, and  $\varepsilon_{20}$  and  $\varepsilon_{60}$  the corresponding average axial strains, at the specified load levels. All load-displacement data from machine was exported and analysed using python libraries; the code is presented in and the results are presented in Section 3.

### 3.3.2 Shear testing

Shear tests were performed on an Instron 8805 1000 kN universal testing machine equipped with a compression load cell calibrated to  $\pm 1\%$  accuracy. The upper platen incorporated a spherical bearing to guarantee concentric loading, eliminating artefacts caused by slight end-plane irregularities and permitting self-alignment under load.

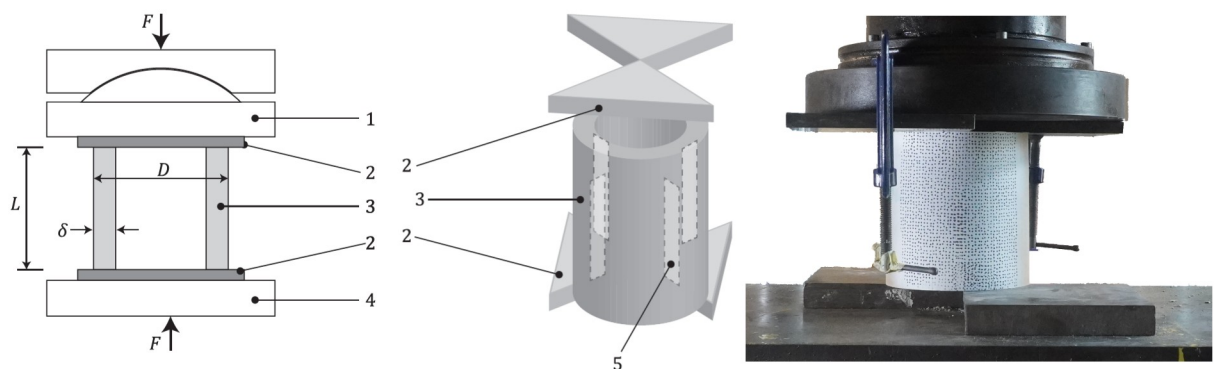


*Figure 3.6. Shear setup. ISO recommended setup on the left and actual experiment setup on the far right.  $\delta$  is wall thickness,  $D$  is outer diameter,  $F$  is load,  $L$  is length of specimen, 1 is upper loading platen with spherical bearing, 2 is shear plate, 3 is bamboo specimen, 4 is lower loading platen, 5 is shear area, normally calculated from  $\delta \times L$*

A pair of rigid square steel plates were positioned diagonally using a Leica Lino L6R as shown in Figure 3.7 to create a “bow-tie” shape. Precise alignment between the upper and lower bow-tie plates was critical for producing pure shear in the bamboo wall. Two steel plates were clamped to the top machine platen and two steel plates were placed on the rigid base. The lower plates bore the specimen over two opposing quadrants, while the upper plate applied load to the remaining quadrants. This configuration generated four discrete shear planes within the culm wall, reproducing the arrangement prescribed in ISO 22157:2019 (ISO, 2019). The centres of both plates were rigidly aligned with the machine axis to prevent lateral slip during testing.

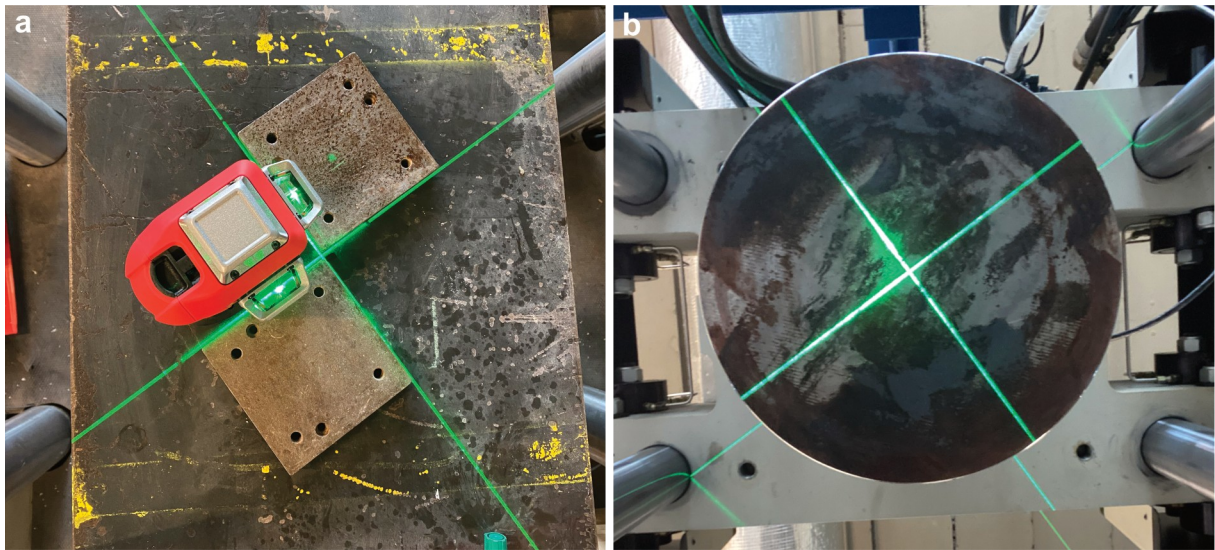


*Figure 3.7. Alignment of shear plates. (a) Alignment of bottom plates. (b) Locating of centre of machine platen.*

Specimens were then placed on the bowtie shape formed. Visual alignment ensured parallel orientation between specimen ends and loading platens before test initiation. A preload of 1-2 kN was applied to seat the specimen and lay parallel the load cell on the surface of the specimen.

The peak load  $F_{ult}$  and the number of failed shear planes were logged. After the test was completed the specimen was then oven-dried at  $103\pm2^\circ\text{C}$  for 7 days for subsequent moisture-content determination.

Nominal shear strength  $f_v$  was calculated as

$$f_v = F_{ult} / \sum(d * L)$$

where  $F_{ult}$  was the recorded maximum load and  $\sum(\delta \times L)$  was the combined area of the four shear planes. Because fracture rarely propagated through all planes simultaneously, the value represented a conservative lower-bound estimate of the true parallel-to-grain shear capacity.

### 3.4. Section analysis

6 digital images each of *G. angustifolia* and *D. asper* bamboo cross-sections, (3 for each culm to represent the top, middle and bottom section) were captured using a

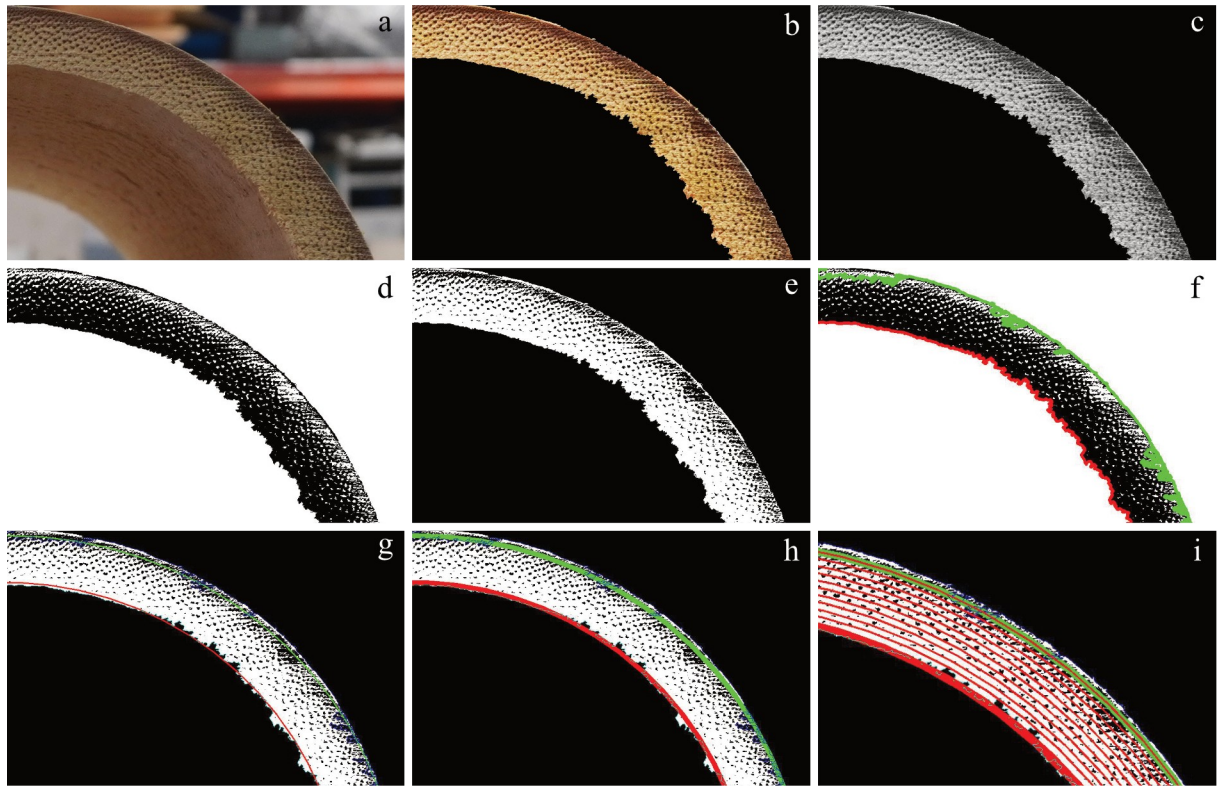


*Figure 3.8. Section analysis process. (a) Original image. (b) Isolated and enhanced image. (c) Equalised image. (d) Inverted binary image. (e) Noise-reduced image. (f) Detected external and internal contour. (g) Fitted ellipses used for calculating cross-section properties. (h) Fitted ellipses. (i) Tangential segments.*

mirrorless camera equipped with a APS-C-format 24.2 megapixel Exmor CMOS sensor. The dimensions of the images were 6000×4000 pixels with a resolution of 350 dpi. The images were first enhanced in Affinity Photo to (1) isolate the cross section through masking (2) improve brightness and contrast and (3) ensure consistent quality across all specimens. This pre-processing stage made it easier to distinguish between different parts of the bamboo microstructure during analysis.

A contour analysis tool by Hutchinson and Koepferl (2024), modified by Bompa (2024), was utilised to conduct the processing stage. The python code is presented in Appendix. The first step of the processing stage was to improve the visibility of fibres against the background matrix, by applying histogram equalisation. This technique redistributes the brightness values across the entire range, making it easier to distinguish between different structural components. This step is particularly

important for bamboo analysis since fibres and matrix materials can have similar brightness levels under normal imaging conditions.

The processed images were converted to binary (black and white) format using Otsu's automatic thresholding method. This technique automatically found the best threshold value to separate the solid bamboo material from empty spaces and cavities. The result was clear black and white images that showed the bamboo structure against the background.

To remove noise and small imperfections that could interfere with analysis, morphological closing was performed using a small elliptical filter ( $1 \times 1$  pixels). This process fills in small gaps within fibre regions and removes tiny spurious features while preserving the overall shape and size of genuine structural elements. This cleaning step ensures more accurate measurements by eliminating artifacts from the specimen preparation or imaging process.

The cleaned images were processed to identify the outer and inner boundaries of the bamboo cross-section using contour detection algorithms. The system automatically found the largest contours representing the external wall and internal cavity boundaries. These boundaries were then fitted with ellipses to measure the geometric properties of the bamboo tube. The ellipse fitting process provided key measurements including: (1) major and minor diameters of both outer and inner boundaries (2) centre positions and shape characteristics and, (3) orientation angles of the fitted ellipses.

To study how material properties vary across the wall thickness, the bamboo wall was divided into ten equal sections from inside to outside. This division was created by drawing concentric elliptical boundaries between the inner and outer walls, with each section representing an equal portion of the wall thickness.

Within each wall section, the relative amounts of fibre and matrix material were measured by counting pixels. The analysis calculated the ratio of white pixels (representing fibres) to total pixels in each section to determine the local fibre content. The matrix content was calculated as the remaining portion within each section.

All the data from the section analysis were automatically exported to spreadsheet format for further statistical analysis and comparison with mechanical test results. The resulting datasets provide detailed information about fibre distribution patterns that can be correlated with mechanical properties and used to understand how bamboo structure varies under different moisture conditions.

### **3.5. Limitations and rationale**

1. To prevent splitting of specimens, a lower temperature and longer duration moisture conditioning protocol should have been employed to achieve gradual moisture content changes. However, *D. asper* demonstrated inherent sensitivity to moisture content variations, which would likely result in splitting regardless of conditioning methodology. This sensitivity aligns with research indicating that bamboo species exhibit significant variability in their response to moisture changes, with certain species being particularly susceptible to dimensional instability during moisture transitions.
2. The reduced specimen count resulting from losses during preparation adversely affected the statistical power of the dataset. This limitation is commonly encountered in bamboo research due to the material's natural variability and processing challenges. The impact on data reliability necessitates careful consideration when drawing conclusions from limited sample sizes.
3. The 1 mm/min loading rate may have been suboptimal for DIC strain measurement accuracy. Although a reduced rate of 0.5 mm/min was attempted, this resulted in excessively long test durations and unwieldy data volumes, creating practical limitations for experimental efficiency.
4. The large diameter and splitting tendency of *D. asper* resulted in reduced specimen yields compared to other bamboo species, compromising sample size adequacy. Additional full-length culms should have been procured for *D. asper* specimens; however, financial constraints prevented this optimisation.

This limitation reflects common challenges in bamboo research where material procurement and processing costs can impact experimental design.

5. An aspect ratio of 2.0 was selected to ensure specimens contained no more than two nodes, facilitating complete water ingress during soaking treatments.
6. The irregular internal surface geometry and pronounced oval nature of bamboo culms created significant difficulties during cross-sectional analysis and contouring procedures. These geometric irregularities particularly affected measurements of the innermost and outermost segments, compromising the accuracy of wall thickness and area calculations. The clarity of the cross-section of *G. angustifolia* specimens was inferior to that of *D. asper*, suggesting that microscopic analysis methods would be more appropriate for detailed morphological characterisation.

## 4. Results

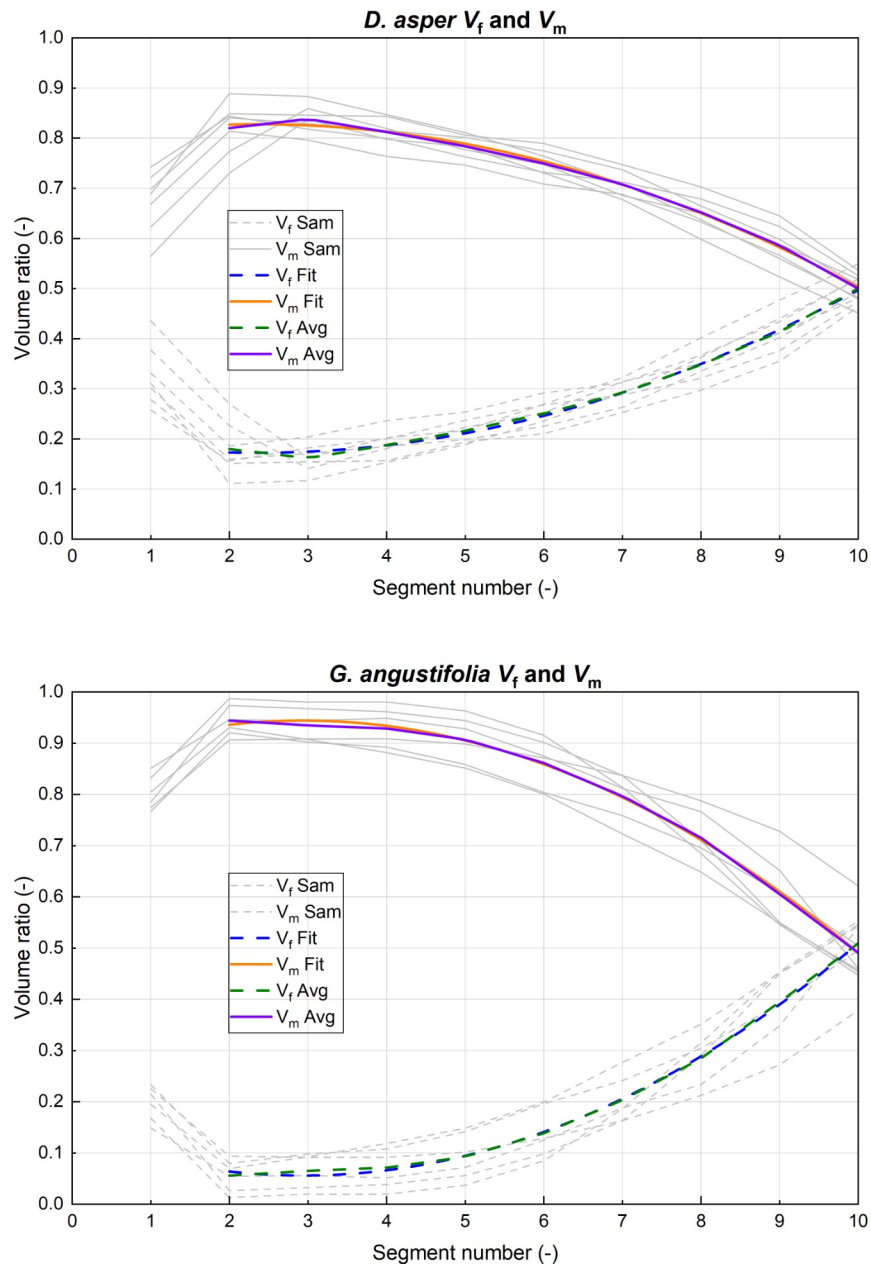
### 4.1. Sectional analysis

Figure 4.1 demonstrates a summary of the fibre volumes and matrix volumes. Due to the rough nature of the inner walls of both species, the fibre volume fractions and matrix volume fractions were inflated due to false counting of pixels. Excluding the first segment, the concentric-segment analysis revealed a clear, graded architecture in both *D. asper* and *G. angustifolia*, but with quantitative differences between the two species.

For *D. asper*, the fibre volume fraction ( $V_f$ ) increased from the inner cavity, peaked at approximately 0.51 in the last segment, where it converged with the matrix fraction at about 0.55. The complementary matrix volume fraction ( $V_m$ ) exhibited the inverse trend, peaking at 0.83 in the third segment and decreased up to 0.51 in the tenth segment. Mid-wall bands (third to sixth) showed low scatter, with coefficients of variation below 5 %, which indicated a highly uniform fibre-rich belt that dominated the mechanical response of the culm. Exponential fits explain more than 90 % of the variance in both  $V_f$  and  $V_m$ , confirming that a simple decay model adequately captures the through-thickness gradation in this species. A simple quadratic relationship,

$$V_f = 0.00556^2 - 0.021619x + 0.20314$$

where  $x$  is the concentric segment number (1 = inner wall, 10 = epidermis), reproduced the averaged experimental profile with an  $R^2 = 0.922$ .



*Figure 4.1. Results of segmentation for both *D. asper* and *G. angustifolia*. The first segment was ignored when fitting the curves.*

In *G. angustifolia* the overall shape of the profiles was similar, but the entire curve was shifted downward by roughly 10%. Peak  $V_f$  reached 0.52, again in the third band, and fell to about 0.48 at the epidermis. The corresponding  $V_m$  peaked at just over 0.50. Scatter was larger (up to 12 % in the outer bands) owing to the smaller

diameter, stronger curvature and lower image contrast of this species. Even so, the same exponential model still accounted for nearly 90 % of the observed variance, indicating that identical mathematical form can be used for both species despite their optical differences. For *G. angustifolia*, the polynomial fit for  $V_f$  was,

$$V_f = 0.00909^2 - 0.5341x + 0.86556$$

where  $x$  is the concentric segment number (1 = inner wall, 10 = epidermis), reproduced the averaged experimental profile with an  $R^2 = 0.916$ .

#### **4.2. Physical properties**

The resultant moisture content for the specimens of both species after conditioning was: <2% for oven-dry, 9-11% for ambient-dry and 30-40% for wet. *D. asper* specimens exhibited larger dimensions compared to *G. asper*. The mean external diameter averaged  $134.2 \pm 9.6$  mm for *D. asper*, exceeding the  $103.3 \pm 3.2$  mm recorded for *G. angustifolia*. Similarly, wall thickness measurements showed *D. asper* specimens averaging  $11.2 \pm 0.9$  mm compared to  $10.1 \pm 0.9$  mm for *G. angustifolia*. Height measurements reflected the intended aspect ratio targets, with *D. asper* specimens averaging  $200.2 \pm 76.9$  mm and *G. angustifolia* specimens  $154.8 \pm 50.9$  mm.

The slenderness ratios ( $D/\delta$ ) were relatively consistent between species, with *D. asper* showing values between 11.4 and 12.3, while *G. angustifolia* exhibited ratios from 9.3 to 11.2. This indicates that despite the size differences, both species maintained proportionally similar wall thickness relationships.

The average external diameter of *D. asper* specimens ranged from 136.6 to 139.0 mm, while *G. angustifolia* specimens were notably smaller with diameters ranging from 102.3 to 108.6 mm. Wall thickness measurements showed *D. asper* specimens averaging 11.3 to 12.6 mm compared to *G. angustifolia* specimens with 9.5 to 11.3 mm thickness.

#### **4.3. Mechanical properties**

The compression and shear test results are summarised in Table 4.1 and Table 4.2 below.

*Table 4.1: Compression test results*

Sample Group	D (mm)	$\delta$ (mm)	L (mm)	$D/\delta$ (-)	E (MPa)	$f_c$ (N/mm <sup>2</sup> )	$P_{max,c}$ (kN)
DLAC	132.1(0.0)	9.5(0.0)	260.5(0.0)	13.9	6479.5(0.0)	77.0(14.5)	282.1(0.0)
DLOC	136.7(1.3)	11.9(2.2)	274.8(20.4)	11.7	7082.0(1638.3)	108.2(12.7)	496.9(20.0)
DLWC	138.5(0.0)	10.5(0.0)	290.0(0.0)	13.2	5320.0(0.0)	45.9(16.2)	193.7(0.0)
DSAC	135.0(2.7)	10.9(1.5)	137.0(6.7)	12.5	3584.8(587.7)	76.3(6.8)	323.9(52.6)
DSOC	137.5(3.7)	10.9(1.3)	139.1(7.9)	12.8	4394.5(400.6)	105.8(12.1)	454.9(56.0)
DSWC	135.5(3.9)	10.5(0.8)	135.0(6.1)	12.9	3156.7(370.7)	52.2(10.1)	215.4(40.3)
GLAC	99.7(9.1)	9.0(1.6)	186.8(32.3)	11.3	4502.8(1129.7)	68.3(10.1)	171.8(26.5)
GLOC	98.6(0.0)	9.0(0.0)	189.9(0.0)	11	5431.6(0.0)	86.0(0.0)	217.2(0.0)
GLWC	104.8(7.4)	11.1(3.1)	207.5(17.4)	9.9	2700.6(706.8)	34.4(5.8)	109.6(23.9)
GSAC	102.5(6.9)	10.0(2.5)	109.4(31.6)	10.6	2454.5(1002.2)	65.0(10.3)	183.9(31.4)
GSOC	99.2(8.0)	9.2(1.5)	98.0(4.8)	11	2932.0(495.4)	88.2(14.6)	232.7(70.6)
GSWC	103.1(8.6)	10.4(1.7)	99.9(5.3)	10.1	1401.7(377.5)	33.1(5.8)	99.0(15.5)

Notes: The values in brackets represent the standard deviation of the value attached to it. D is the average diameter of the specimen,  $\delta$  is the average thickness of the specimen,  $D/\delta$  is the wall slenderness, E is the elastic modulus,  $f_c$  is the compressive strength,  $P_{max,c}$  is the maximum compression load and L is the average length of the specimen.

*Table 4.2: Shear test results*

<b>Sample Group</b>	<b>D (mm)</b>	<b><math>\delta</math> (mm)</b>	<b>L (mm)</b>	<b><math>D/\delta</math> (-)</b>	<b>E (MPa)</b>	<b><math>f_v</math> (N/mm<sup>2</sup>)</b>	<b><math>P_{max,v}</math> (kN)</b>
DLAS	137.7(3.1)	11.4(1.6)	140.9(5.7)	12.2	1077.8(65.0)	9.0(1.6)	115.9(18.3)
DLOS	138.3(4.1)	12.6(4.0)	280.7(14.8)	11.6	1002.8(23.9)	7.3(0.1)	103.9(40.0)
DLWS	137.1(2.8)	12.2(2.2)	283.8(11.9)	11.4	767.7(163.3)	5.5(0.7)	76.9(22.6)
DSAS	139.0(2.9)	11.9(2.5)	284.0(11.1)	12	822.1(31.3)	11.9(2.2)	81.4(31.4)
DSOS	137.6(4.3)	11.7(2.8)	137.7(6.4)	12.2	895.7(142.9)	9.9(2.2)	62.2(12.3)
DSWS	136.6(2.8)	11.3(1.8)	138.2(7.8)	12.3	730.6(275.4)	8.7(1.1)	55.0(16.8)
GLAS	108.6(2.4)	9.7(0.8)	207.4(16.8)	11.2	564.1(64.8)	7.4(1.3)	58.5(0.8)
GLOS	105.7(0.0)	11.3(0.0)	201.4(0.0)	9.3	581.1(0.0)	3.6(0.0)	33.1(0.0)
GLWS	102.3(4.3)	9.5(2.0)	199.1(2.0)	11	421.1(0.0)	4.8(0.4)	35.9(5.0)
GSAS	106.6(7.4)	10.9(2.3)	101.6(4.9)	10.1	365.1(112.8)	6.1(1.7)	26.0(5.7)
GSOS	103.0(6.4)	10.0(2.2)	100.4(6.8)	10.6	356.5(122.1)	4.0(0.9)	15.9(3.3)
GSWS	105.3(4.7)	11.0(2.5)	101.8(6.0)	9.9	249.8(44.6)	4.7(0.5)	21.2(5.8)

Notes: The values in brackets represent the standard deviation of the value attached to it.  $D$  is the average diameter of the specimen,  $\delta$  is the average thickness of the specimen,  $D/\delta$  is the wall slenderness,  $E$  is the elastic modulus,  $f_v$  is the shear strength,  $P_{max,v}$  is the maximum shear load and  $L$  is the average length of the specimen.

#### **4.4. Compression**

The compression test results reveal considerable variations in mechanical properties between the two bamboo species and across different moisture conditioning states. Table 4.1 presents the comprehensive test results for both *D. asper* and *G. angustifolia* specimens under ambient-dry, oven-dry, and wet conditions. During the test *G. angustifolia* gave a warning sign just before reaching failure mode by cracking. *D. asper* stayed silent until after failure load.

##### *4.4.1 Effect of moisture conditioning*

The moisture conditioning had a pronounced effect on compression strength for both species. For *D. asper*, oven-dry conditioning consistently produced the highest compression strengths, with long specimens (DLOC) achieving  $108.2 \pm 12.7$  MPa and short specimens (DSOC) reaching  $105.8 \pm 12.1$  MPa. This represents increases of 40.5% and 38.6% respectively compared to their ambient-dry counterparts.

Conversely, wet conditioning resulted in substantial strength reductions. *D. asper* long specimens (DLWC) exhibited a compression strength of  $45.9 \pm 16.2$  MPa, representing a 40.4% decrease from ambient-dry conditions (DLAC:  $77.0 \pm 14.5$  MPa). Similarly, short specimens showed a 31.6% reduction from ambient-dry (DSAC:  $76.3 \pm 6.8$  MPa) to wet conditions (DSWC:  $52.2 \pm 10.1$  MPa).

*G. angustifolia* demonstrated similar moisture sensitivity patterns. Oven-dry long specimens (GLOC) achieved 86.0 MPa, while wet specimens (GLWC) dropped to  $34.4 \pm 5.8$  MPa, representing a 49.6% reduction from ambient-dry conditions (GLAC:  $68.3 \pm 10.1$  MPa). Short specimens showed even more dramatic variations, with oven-dry specimens (GSOC) reaching  $88.2 \pm 14.6$  MPa compared to wet specimens (GSWC) at  $33.1 \pm 5.8$  MPa.

##### *4.4.2 Species comparison*

*D. asper* generally exhibited superior compression performance compared to *G. angustifolia*. Under ambient-dry conditions, *D. asper* long specimens demonstrated 12.7% higher strength than *G. angustifolia* (77.0 vs 68.3 MPa). However, this

advantage was more pronounced under oven-dry conditions, where *D. asper* showed 25.8% higher strength (108.2 vs 86.0 MPa) for long specimens. The species difference was still consistent for short specimens, with *G. angustifolia* showing lower ambient-dry strength ( $65.0 \pm 10.3$  MPa) compared to *D. asper* ( $76.3 \pm 6.8$  MPa). For short oven-dry specimens, *D. asper* achieved 19.9% higher compressive strength than *G. angustifolia* (105.8 vs 88.2 MPa).

#### 4.4.3 Aspect ratio

The aspect ratio effect varied between species and conditioning states. For *D. asper*, long specimens consistently showed minimal difference in strength as compared to short specimens across all conditions. Long ambient-dry specimens achieved  $77.0 \pm 14.5$  MPa compared to  $76.3 \pm 6.8$  MPa for short specimens.

*G. angustifolia* also showed a similar pattern with minimal difference in strength between short and long specimens across all conditioning states. Short oven-dry specimens ( $88.2 \pm 14.6$  MPa) outperformed long specimens (86.0 MPa) by 2.6%, while under ambient-dry conditions, the difference was still minimal (65.0 vs 68.3 MPa).

#### 4.4.4 Elastic modulus

The elastic modulus followed similar trends to compression strength regarding moisture sensitivity. *D. asper* long specimens showed the highest modulus under oven-dry conditions ( $7082.0 \pm 1638.3$  MPa), decreasing to 6479.5 MPa under ambient-dry and 5320.0 MPa under wet conditions.

*G. angustifolia* demonstrated lower overall stiffness values, with oven-dry long specimens achieving 5431.6 MPa compared to  $4502.8 \pm 1129.7$  MPa under ambient-dry conditions. Wet specimens showed the most significant reduction, dropping to  $2700.6 \pm 706.8$  MPa for long specimens and  $1401.7 \pm 377.5$  MPa for short specimens.

#### 4.4.5 Variance

The coefficient of variation in compression strength was generally higher for wet specimens compared to oven-dry specimens. *D. asper* wet specimens showed standard deviations ranging from 10.1 to 16.2 MPa, while oven-dry specimens exhibited more consistent performance with standard deviations of 12.1 to 12.7 MPa.

*G. angustifolia* displayed higher overall variability, particularly evident in the elastic modulus measurements where standard deviations reached up to 1129.7 MPa for ambient-dry long specimens. This suggests greater natural variation in *G. angustifolia* material properties compared to *D. asper*.

### 4.5. Shear

The shear test results revealed considerable differences in mechanical properties between the two bamboo species and across different moisture conditioning states. *D. asper* consistently demonstrated superior shear performance compared to *G. angustifolia* across all testing conditions. Moisture content notably influenced the shear behaviour of both bamboo species. For *D. asper* specimens, ambient-dry conditions produced the highest shear strengths, with short specimens (DSAS) achieving  $11.9 \pm 2.2$  MPa and long specimens (DLAS) reaching  $9.0 \pm 1.6$  MPa. Oven-drying reduced these values to  $9.9 \pm 2.2$  MPa and  $7.3 \pm 0.1$  MPa for short and long specimens respectively. Wet conditioning resulted in the lowest shear strengths at  $8.7 \pm 1.1$  MPa for short specimens and  $5.5 \pm 0.7$  MPa for long specimens.

*G. angustifolia* displayed a similar trend but with generally lower absolute values. Short ambient-dry specimens (GSAS) achieved  $6.1 \pm 1.7$  MPa, while long ambient-dry specimens (GLAS) reached  $7.4 \pm 1.3$  MPa. Interestingly, the long specimens of *G. angustifolia* showed less pronounced differences between conditioning states compared to *D. asper*, with oven-dry specimens achieving 3.6 MPa and wet specimens  $4.8 \pm 0.4$  MPa.

#### 4.5.1 Elastic modulus

The elastic modulus measurements revealed substantial differences between species and moisture conditions. *D. asper* specimens exhibited notably higher

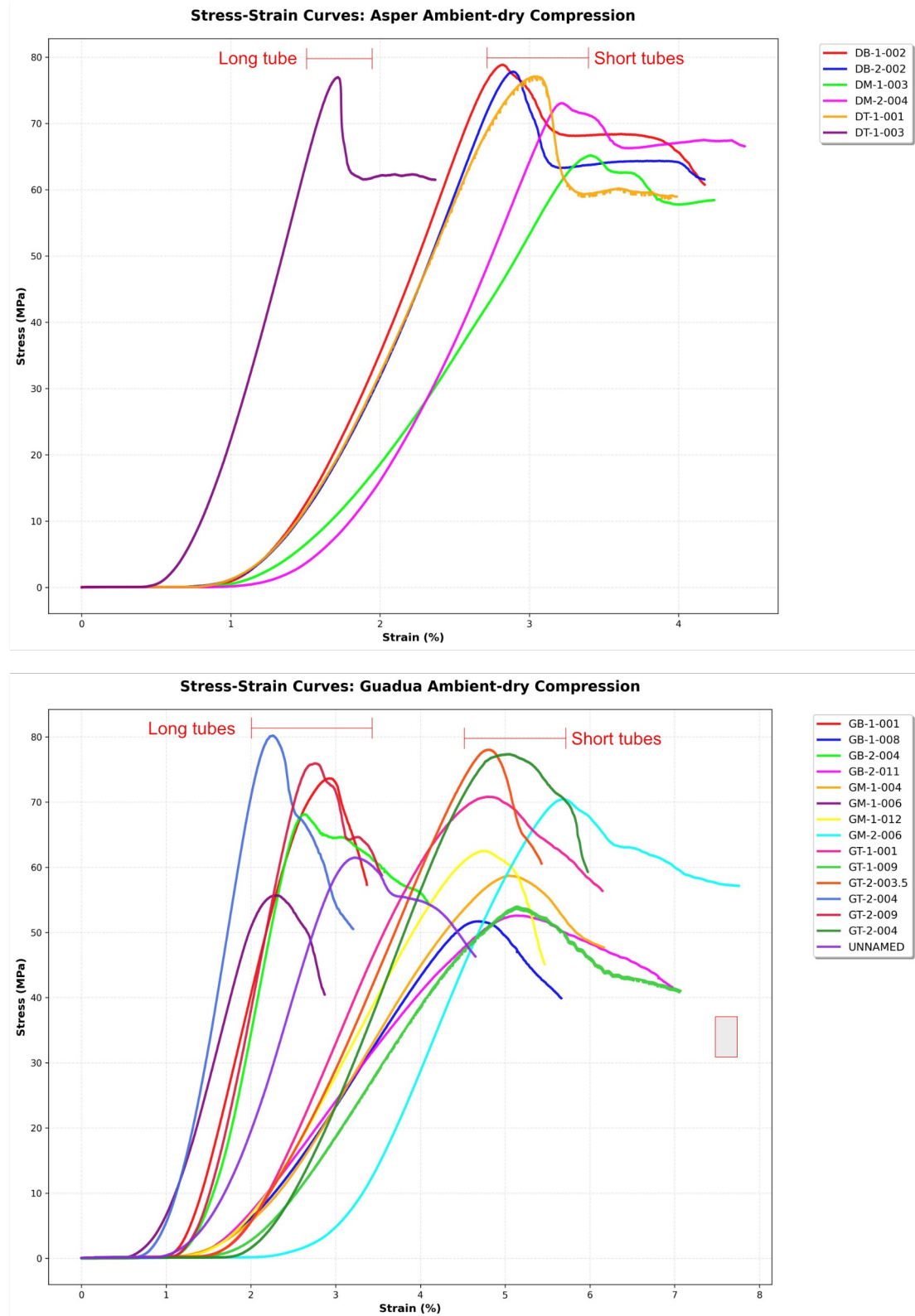


*Figure 4.2. Ambient-dry compression stress-strain curves*

stiffness values, with ambient-dry long specimens (DLAS) achieving  $3087.6 \pm 217.7$  MPa, followed by oven-dry long specimens (DLOS) at  $2849.2 \pm 80.2$  MPa. Wet conditioning reduced the elastic modulus to  $2218.7 \pm 468.2$  MPa, representing approximately a 28% reduction from the ambient-dry condition.

Short *D. asper* specimens showed lower elastic modulus values overall, with ambient-dry conditions yielding  $1161.5 \pm 71.9$  MPa, oven-dry conditions  $1243.9 \pm 168.4$  MPa, and wet conditions  $1015.9 \pm 357.5$  MPa. *G. angustifolia* specimens consistently demonstrated lower elastic modulus values across all conditions, with the highest value of 1579.0 MPa observed in oven-dry long specimens and the lowest value of  $343.5 \pm 61.3$  MPa in wet short specimens.

#### 4.5.2 Load capacity

Maximum shear load capacity followed patterns consistent with strength measurements. *D. asper* specimens demonstrated superior load-bearing capacity, with ambient-dry long specimens (DLAS) sustaining  $115.9 \pm 18.3$  kN, while wet long specimens (DLWS) carried  $76.9 \pm 22.6$  kN. Short specimens showed more modest load capacities, ranging from  $81.4 \pm 31.4$  kN in ambient-dry conditions to  $55.0 \pm 16.8$  kN in wet conditions.

*G. angustifolia* specimens exhibited considerably lower load capacities across all conditions. Long specimens achieved maximum loads of  $58.5 \pm 0.8$  kN in ambient-dry conditions, while short specimens reached peak loads of only  $26.0 \pm 5.7$  kN under the same conditions. Wet and oven-dry conditions further reduced these capacities, with some specimens carrying as little as  $15.9 \pm 3.3$  kN.

#### 4.5.3 Aspect ratio

The aspect ratio influence on shear behaviour varied between species. For *D. asper*, short specimens generally exhibited higher shear strengths than their long counterparts under ambient-dry conditions, suggesting that the reduced length-to-diameter ratio enhanced the shear resistance. However, this trend was less consistent across other moisture conditions.

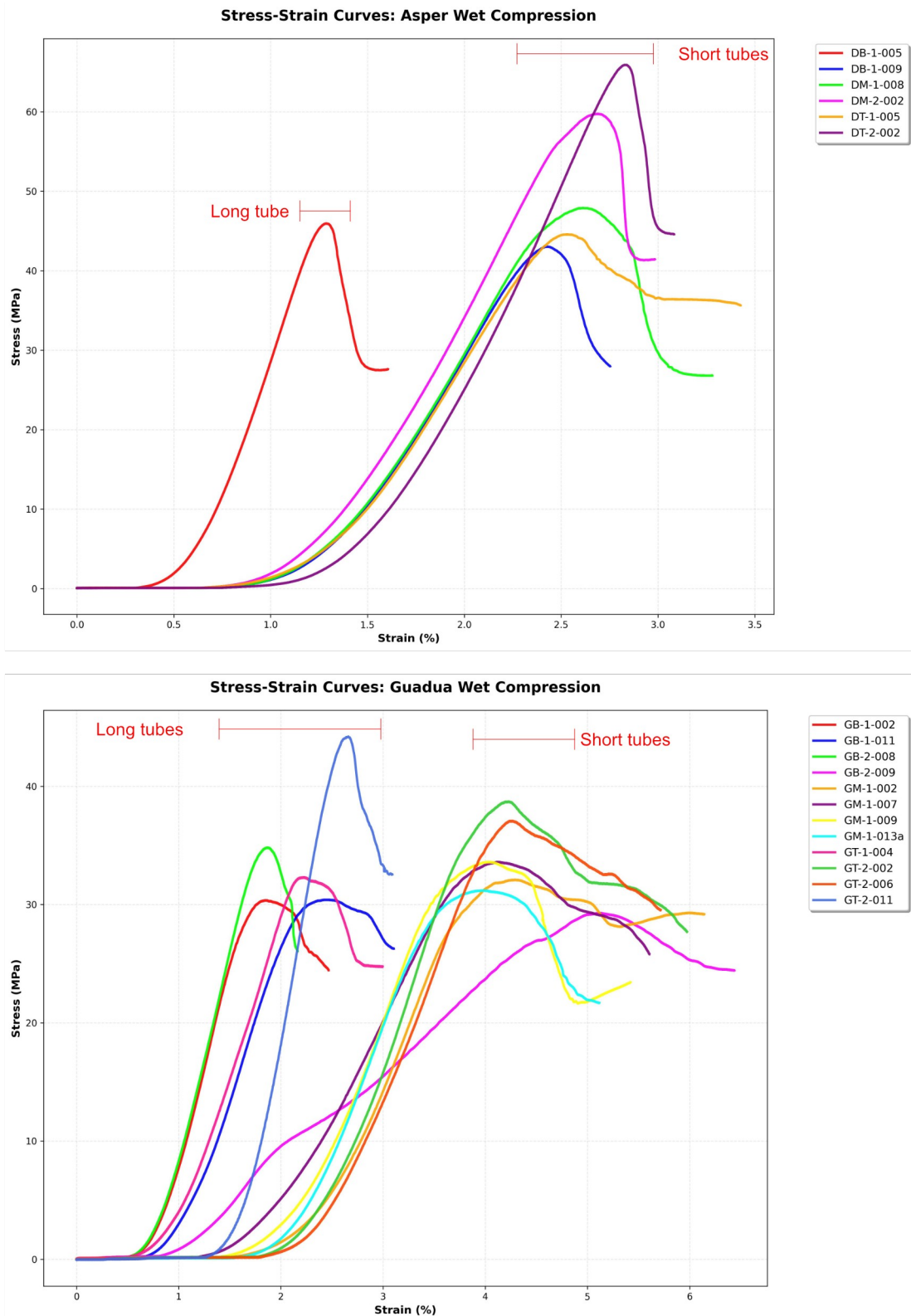


*Figure 4.3. Wet compression stress-strain curves*

*G. angustifolia* showed a different pattern, with long specimens sometimes outperforming short specimens in terms of shear strength, particularly under ambient-dry conditions. This species-specific geometric sensitivity indicates different failure mechanisms may be governing the shear behaviour of the two bamboo types.

#### 4.5.4 Variability

The variability in measurements, as indicated by standard deviations, was generally higher for *G. angustifolia* specimens, suggesting greater material inconsistency or higher sensitivity to testing conditions. *D. asper* specimens showed more consistent behaviour, particularly under controlled oven-dry conditions, indicating better material uniformity and potentially more predictable engineering properties.

### 4.6. Stress stain curves

#### 4.6.1 Ambient-dry compression (Figure 4.2)

Both *D. asper* and *G. angustifolia* follow the same three-step pattern when they are compressed along the fibre direction. First, there is a gentle rise while tiny gaps inside the wall close. Next comes a fairly straight, elastic rise up to the peak stress. After that peak, the load drops because cracks and fibre buckling start to spread.

For *D. Asper*, the six curves sat close together. They reached their highest stresses between 74 MPa and 80 MPa at strains of about 2.6% to 2.9%. The single long tube peaked earliest, then suddenly dropped by roughly 20 MPa. For the short tubes, their peak came a little later and the post-peak drop was smoother. Their residual strength settled near 55 MPa, roughly one-quarter below the peak.

*G. angustifolia* showed more scatter because twelve samples were tested. Peak stresses ranged from 59 MPa to 81 MPa. The highest values belonged to the long tubes, which load more evenly along their length and delay local crushing. Once they peaked, however, they lost 35%–40% of their capacity within a small extra strain. The short tubes peaked at slightly larger strains, around 3.5% to 4%, and then dropped in a series of steps rather than one big collapse. Post-test inspection shows many ring-like arrest lines that slow the cracks and create the “saw-tooth” curves.

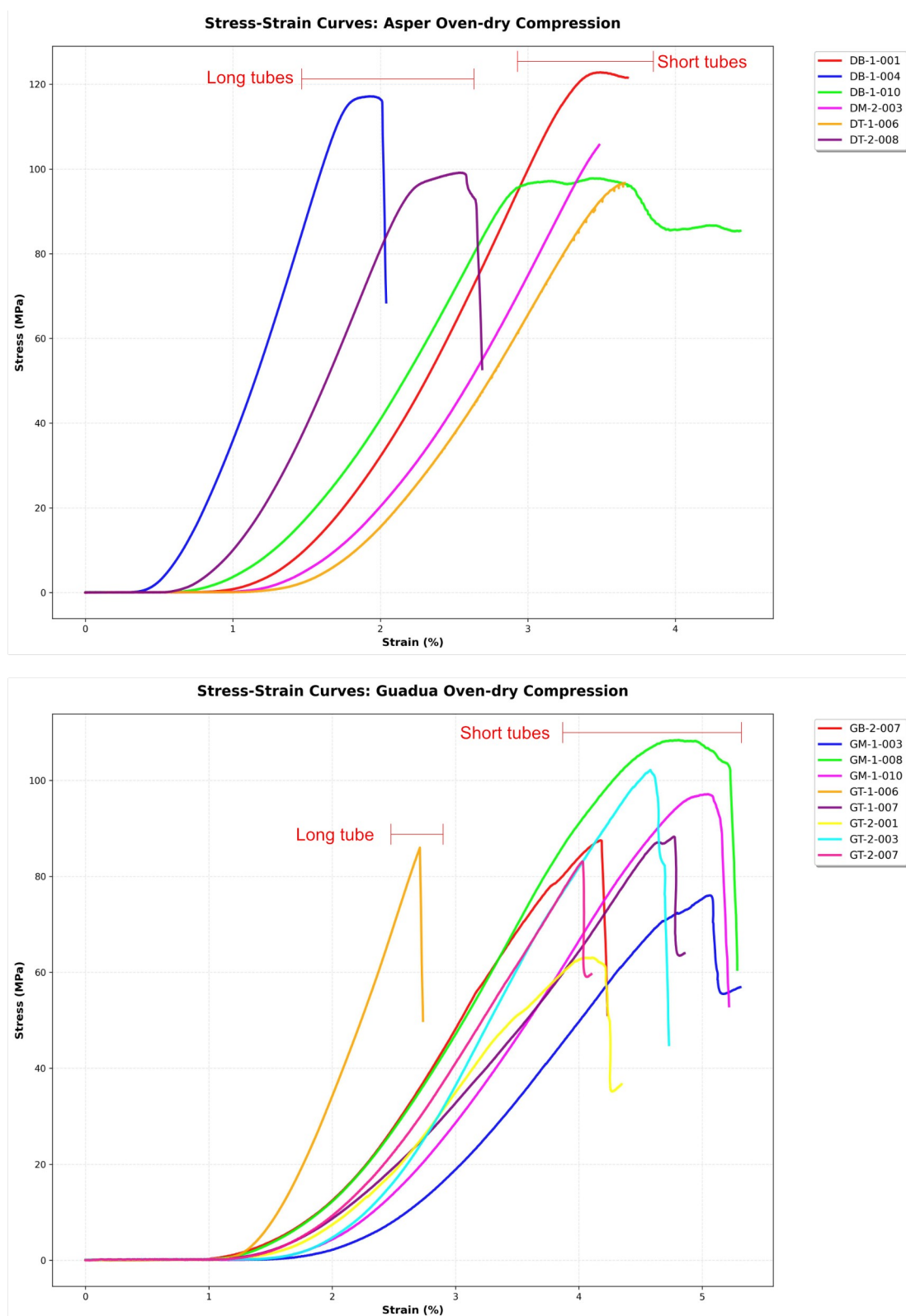


Figure 4.4. Oven-dry compression stress-strain curves

When we compare the two species, *D. Asper* was about 10 MPa stronger at its peak thanks to a higher fibre content and thicker walls. Yet *G. angustifolia* was more ductile; it kept stresses above 50 MPa up to 4.5% strain, while *D. Asper* fell below that level by 3.2% strain. Tube length affected both bamboos in the same way:  $L/D \approx 2.0$  long tubes peak earlier and failed faster because they can buckle, whereas  $L/D \approx 1.0$  short tubes were held in place by the steel platens and crush progressively, giving a longer, flatter post-peak tail.

Post peak failure shows that *D. Asper* underwent a strength drop followed by a yield plateau. For *G. angustifolia*, the strength dropped gradually indicating ductile behaviour.

#### 4.6.2 Wet compression (Figure 4.3)

For *D. asper* the short tubes ( $L/D \approx 1.0$ ) failed at markedly higher stresses than the single long tube ( $L/D \approx 2.0$ ) that was available for wet testing. Peak values ranged from 43 MPa to 66 MPa in the short specimens, whereas the long specimen reached only 46 MPa. Strain at maximum stress lay between 2.1% and 2.8% for the short tubes, but almost doubled to 4.5% in the long one. After the peak, all curves showed an immediate stress drop of 15%–35%, followed by a sharp strength drop. The curve then followed into a yield plateau.

The *G. angustifolia* set exhibited greater scatter but the same size effect. Short tubes reached between 32 MPa and 39 MPa, while long tubes peaked at 30 MPa to 44 MPa. The corresponding ultimate strains were 4%–5% for short specimens and 6%–6.5% for long ones. Unlike *D. asper*, many *G. angustifolia* curves displayed a soft strength drop for the short tubes. The long *G. angustifolia* tube curves displayed a sharper drop as compared to their shorter counterparts.

#### 4.6.3 Oven-dry compression (Figure 4.4)

The oven-dry compression tests revealed distinct behavioural patterns for both *D. asper* and *G. angustifolia* bamboo species across different specimen geometries. Figure 1 presents the complete stress-strain relationships obtained from the compression testing program.

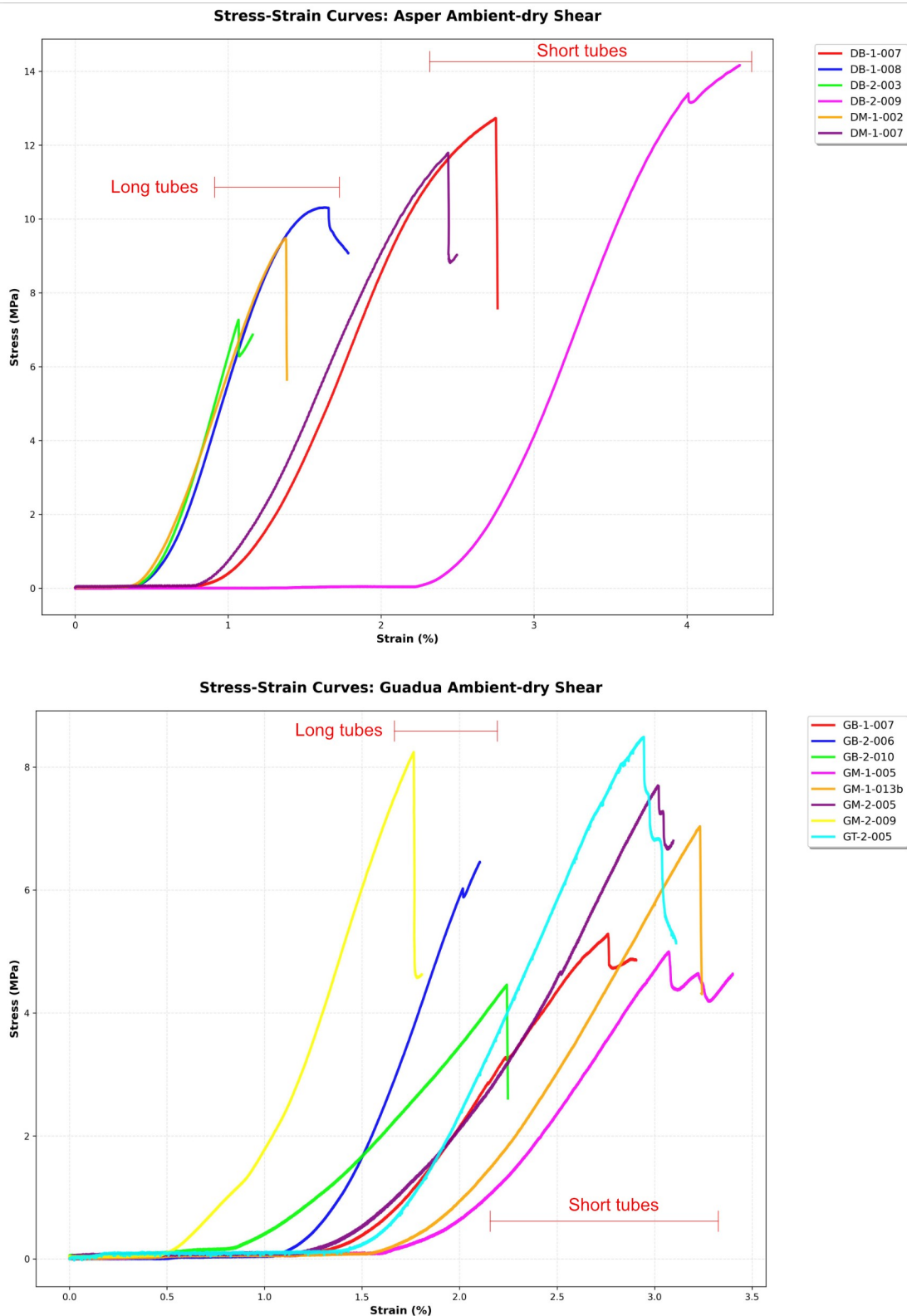


*Figure 4.5: Ambient-dry shear stress-strain curves*

For *D. asper* specimens, the oven-dry compression strength showed no significant variation between specimen geometries. Short tubes ( $L/D = 1.0$ ) demonstrated superior performance with peak compressive stresses reaching approximately 115-120 MPa, while long tubes ( $L/D=2.0$ ) achieved lower peak stresses in the range of 85-100 MPa. All of the oven-dry *D. asper* specimens failed in an explosive manner. Therefore some of the tests were halted before failure as the bursting of the tubes which was considered unsafe.

The stress-strain curves for *D. asper* exhibited characteristic brittle behaviour with relatively linear elastic regions extending to approximately 1.5-2.0% strain before reaching peak stress. Post-peak behaviour showed rapid strength degradation with minimal ductility, particularly evident in the long tube specimens where stress dropped sharply after peak load was achieved.

*G. angustifolia* specimens demonstrated different behavioural characteristics under oven-dry compression conditions. Peak compressive strengths were generally lower than *D. asper*, with short tubes achieving maximum stresses of approximately 70-110 MPa and long tubes reaching 70-85 MPa. The strength reduction between short and long specimens was more pronounced, showing approximately 20-30% decrease in capacity.

Notably, *G. angustifolia* specimens exhibited more variable stress-strain behaviour with some specimens showing multi-peak characteristics and more gradual post-peak strength degradation. The elastic modulus appeared lower compared to *D. asper*, with the linear portion extending to similar strain levels but with reduced slope.

The aspect ratio significantly influenced the compression performance of both species. Short tubes ( $L/D=1.0$ ) outperformed long tubes ( $L/D = 2.0$ ) in terms of peak strength, likely due to reduced susceptibility to global buckling instabilities. The strength reduction factor ranged from 0.75-0.85 for long tubes compared to short tubes across both species.

Strain capacity at peak load remained relatively consistent between geometries, typically occurring between 1.5-2.5% compressive strain. However, long tubes showed more variable behaviour with some specimens exhibiting premature failure at

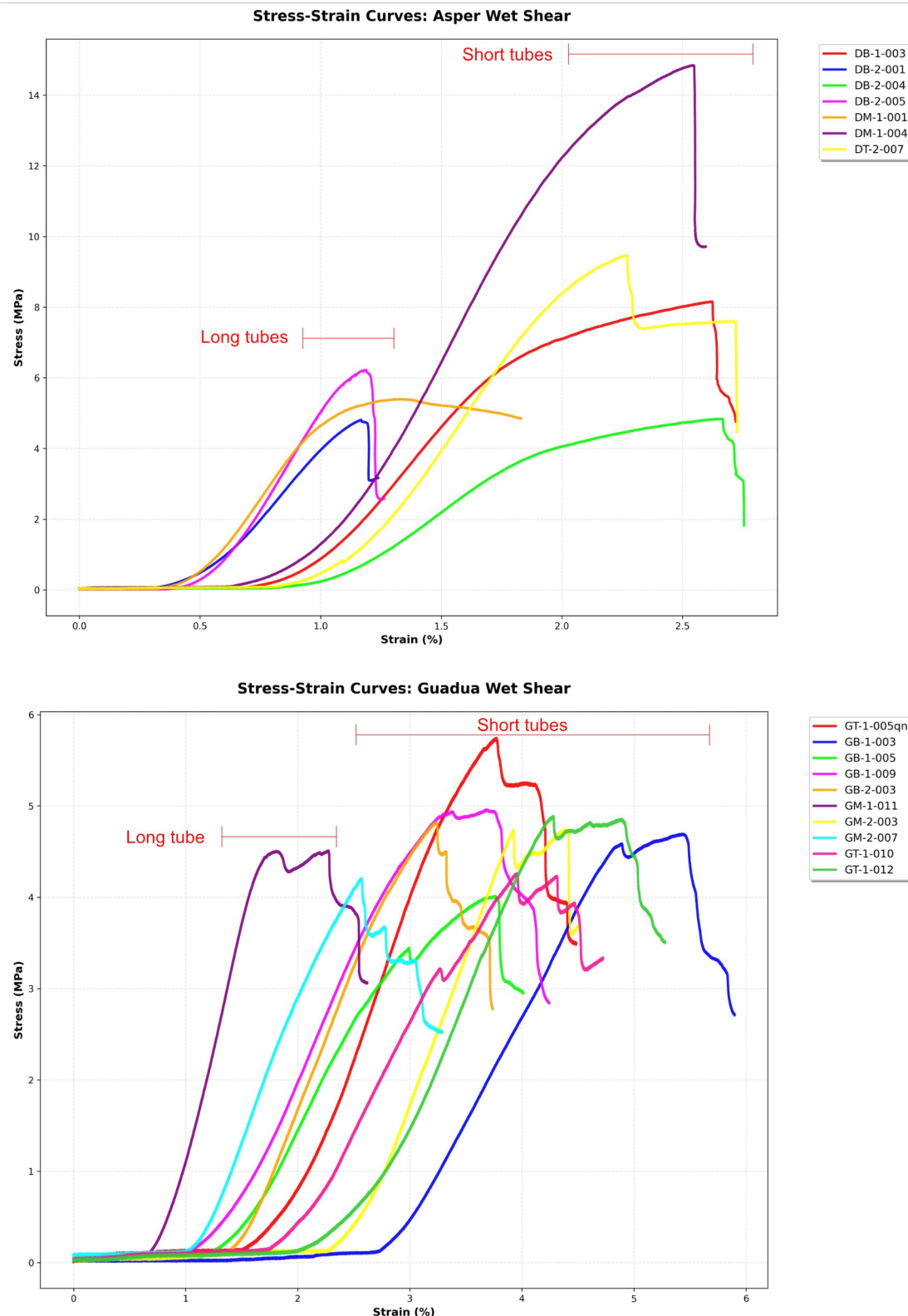


*Figure 4.6. Wet shear stress-strain curves*

lower strain levels, suggesting potential influence of material defects or geometric imperfections.

The oven-dry conditioning resulted in brittle failure characteristics for both species. The reduced moisture content appeared to increase the brittleness of both species, with post-peak behaviour showing minimal energy absorption capacity compared to ambient-dry and wet conditions.

#### 4.6.4 Ambient shear (Figure 4.5)

In both bamboo species, the curves shared the same overall shape: an initially linear rise, and a brief non-linear zigzag range as the specimen continues to fail along other shear planes. The highest resistances were measured in *D. asper*. The three long *D. asper* tubes reached ultimate shear stresses of 7.2-10.2 MPa, with failure occurring at roughly 1.2% shear strain. The response up to that point was essentially elastic and the ensuing collapse was sudden: a single shear split through the wall thickness and the load dropped. The three short *D. asper* tubes displayed a similar behaviour with their peak stresses between 11.8 and 13.9 MPa.

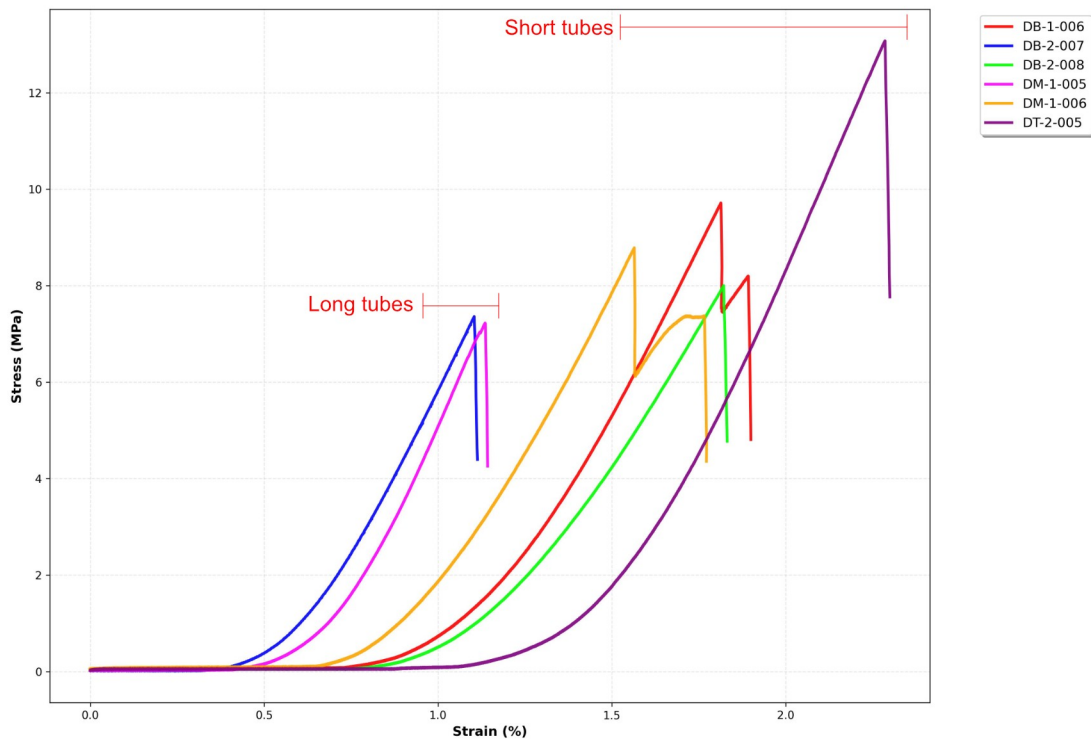
*G. angustifolia* reproduced the same aspect ratio effect, albeit at lower absolute levels. The two long *G. angustifolia* specimens achieved 8.6 and 6.0 MPa at about 1.7% strain; the five short ones peaked between 4.2 and 8.3 MPa. The long specimens had a steeper stress-strain curve as compared to the shorter specimens.

A direct comparison therefore establishes a clear performance hierarchy. At identical moisture content *D. asper* is roughly 30% stronger and 40% stiffer than *G. angustifolia* irrespective of aspect ratio, a result that correlates with the higher fibre volume fraction determined for *D. asper* in the sectional analysis. Geometry, on the other hand, dictates the manner of failure: the long tubes of both species behave in a more brittle fashion, forming lesser shear planes than the short tubes.

#### 4.6.5 Wet shear (Figure 4.6)

The shear tests carried out on wet tubes revealed markedly different responses for *D. asper* and *G. angustifolia* and highlighted the strong influence of specimen slenderness on both strength and deformability. In the *D. asper* series the long

**Stress-Strain Curves: Asper Oven-dry Shear**



**Stress-Strain Curves: Guadua Oven-dry Shear**

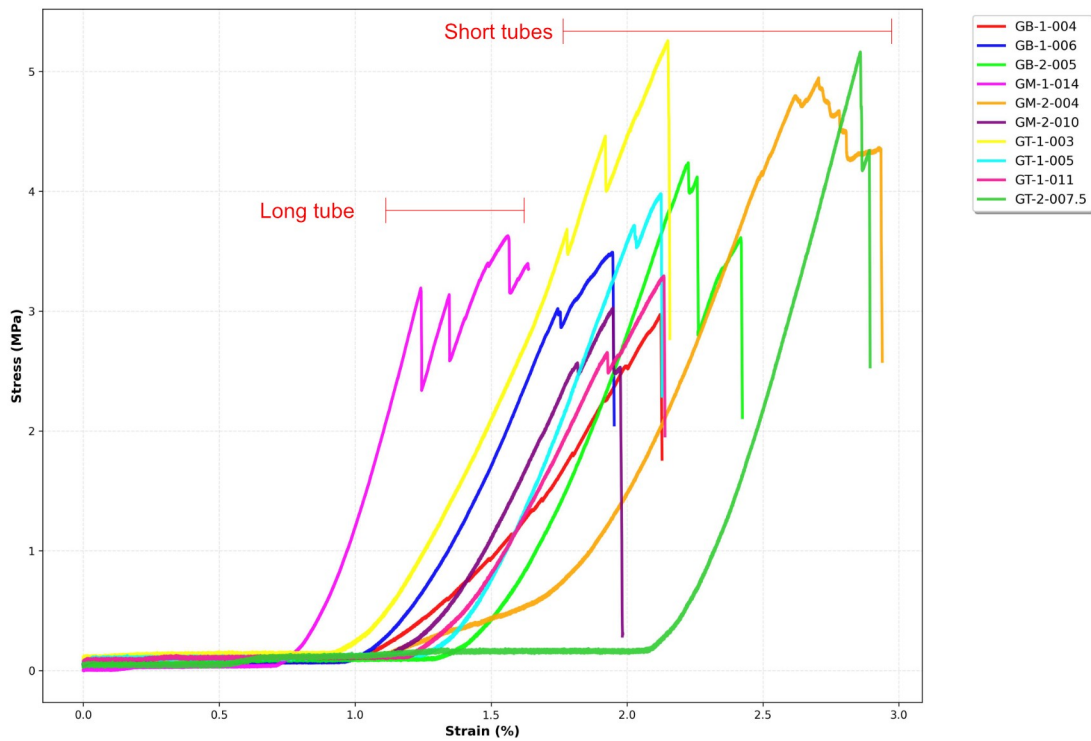


*Figure 4.7. Oven-dry shear stress-strain curves*

specimens attained relatively low stresses. All three long tubes behaved almost identically up to about 1.2% strain, where the stress peaked between 4.4 and 6.2 MPa. A sudden stress drop followed. The short *D. Asper* tubes ( $H/D \approx 1$ ) started from similar elastic moduli but reached their maximum stress later and at higher levels forming a “humped” trajectory. Peak stresses clustered around 4.3–14.6 MPa and occurred at strains close to 2.3%.

The *G. angustifolia* set reproduced the same qualitative trends but at a lower stress scale. The single long specimen achieved 4.5 MPa at about 1.7% strain. All eight short *G. angustifolia* tubes followed a characteristic “humped” trajectory: stresses rose slowly, reached between 4.1 and 5.7 MPa at 2.4–5.0% strain and then oscillated along a broad plateau while successive splits propagated through the wall. Failure was therefore governed less by a singular event than by a sequence of local fractures that redistributed the load among the four nominal shear planes created by the bow-tie fixture.

Direct comparison of the two species under identical wet conditioning shows that *D. asper* retains a considerably higher shear capacity than *G. angustifolia*, irrespective of aspect ratio. Both species, however, experienced a slight strength increase when the tube was shortened. In *D. Asper* the average peak stress increases by about one fifth but the ultimate strain doubles; in *G. angustifolia* the increase in strength is negligible while the ultimate strain is multiplied by almost three.

*G. angustifolia* achieve failure strain later at around 3% as compared to *D. asper* which achieved failure strain at 1.2% for long tubes and 2.4% for short tubes.

#### 4.6.6 Oven-dry shear (Figure 4.7)

Figure 4 condenses the stress–strain response of all oven-dry specimens loaded in bow-tie shear. For *D. asper* the curves shared a common shape. After about 0.6% strain the response is essentially linear. Long tubes attained their peak stress much earlier than the short ones, between 1.1 and 1.2% strain, and they did so at lower stress levels. The best performing long specimen, DB-2-007, reached 7.2 MPa, while its companion recorded 7.5 MPa. Short tubes peaked between 1.5 and 2.4% strain and topped out at 7.0–12.8 MPa. Once the peak has been passed, the stress drops

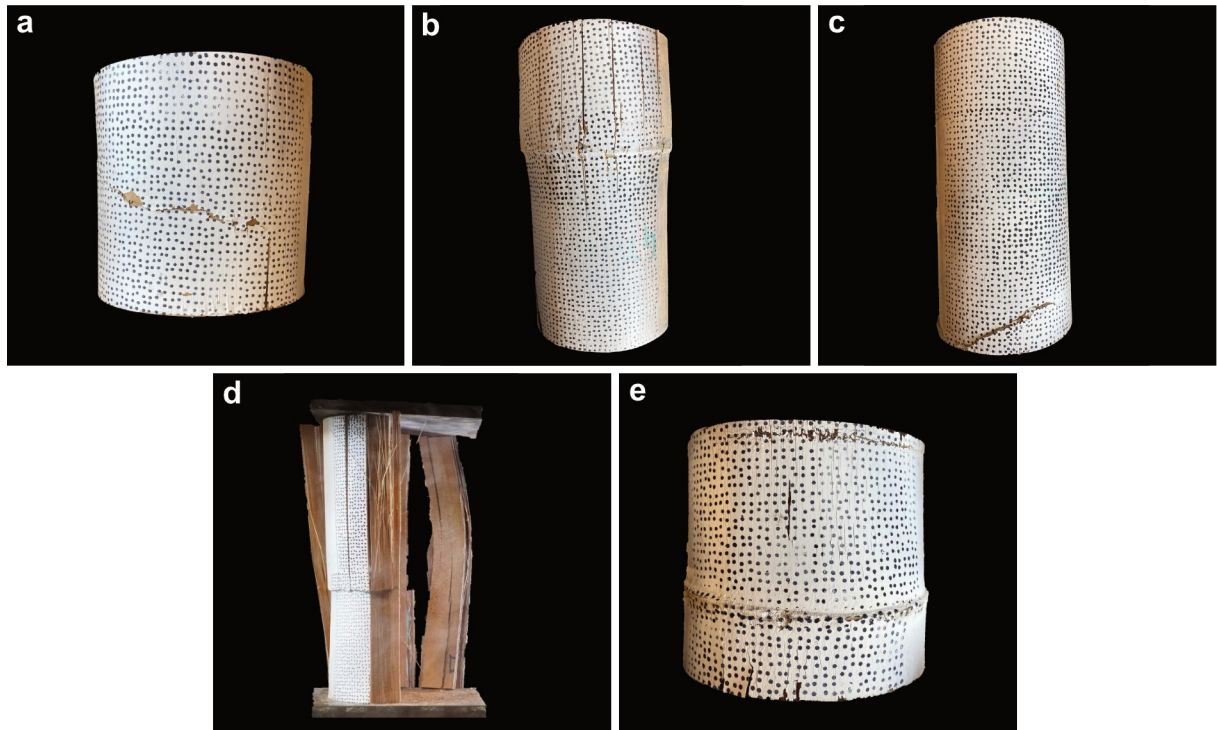


*Figure 4.8. Compression test failure modes. (a) Combined failure mode for an ambient-dry specimen (b) Splitting failure mode for an oven-dry specimen. The specimen was held together by the node. (c) Crushing failure mode (d) Splitting failure mode for an oven-dry specimen without node (e) Crushing failure mode for a wet specimen. Crushing occurred at the top and bottom.*

almost instantaneously and sharply in all the tubes, leaving practically no post-peak load-bearing reserve. In the short series, the same two planes appeared as opposed to one plane in long tubes.

*G. angustifolia* responded in a distinctly different manner. The initial linear segment extends over 0.4% strain, followed by formation of more than two shear planes. The sole long-tube specimen achieved a maximum stress of 3.2 MPa at 1.3% strain. Short tubes bunched between 1.6 and 2.9% strain and registered peak stresses in the 2.4–5.2 MPa range, yielding a higher stress compared to the sole long tube.

A direct cross-species comparison highlights two important points. First, even after oven-dry conditioning *D. asper* is two to three times stronger in shear than *G. angustifolia*. This difference originate in the contrasting microstructures: the denser,

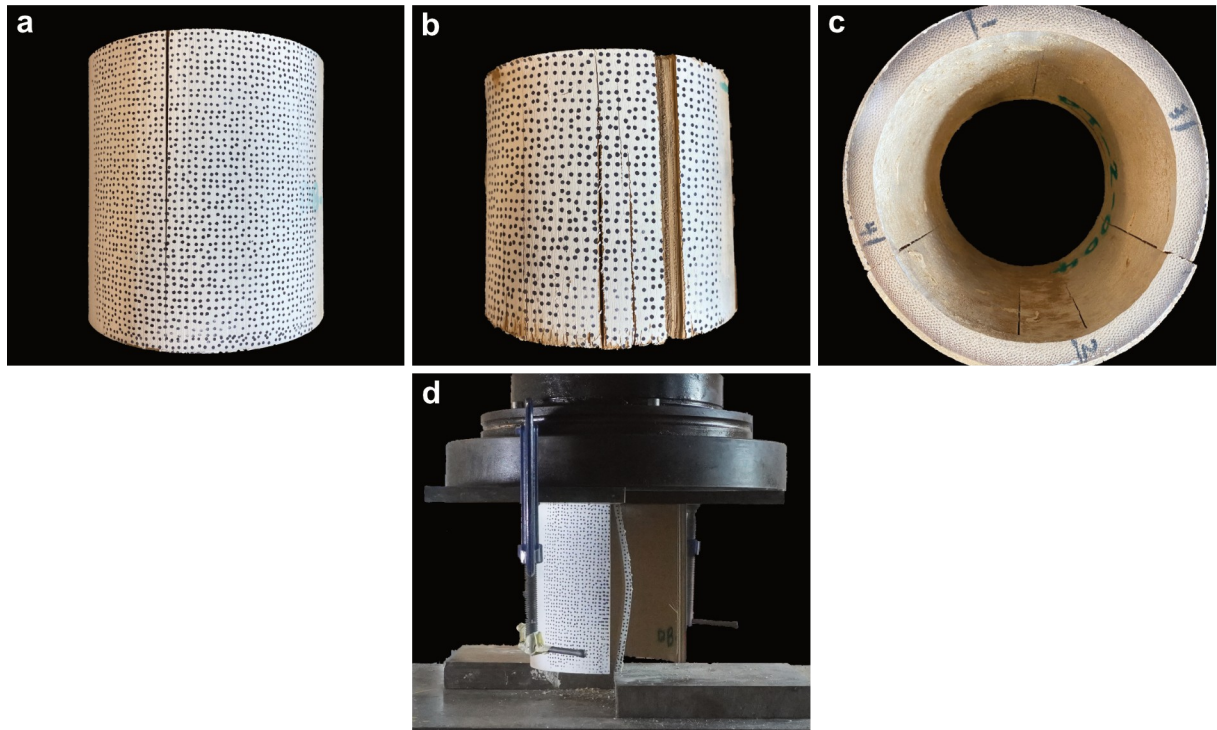


*Figure 4.9. Shear test failure modes. (a-b) Splitting failure mode for an ambient-dry specimen. (b) Splitting failure mode for an oven-dry specimen. (c) Internal splitting. (d) Splitting failure mode where a quarter of the specimen was sheared off.*

thin-walled vascular bundles of *D. asper* confer high stiffness and strength but fail abruptly once the matrix has been sheared, whereas *G. angustifolia* distributes the shear more evenly and postpone localisation at the cost of lower peak stress.

Oven-drying amplifies the intrinsic contrast between the two species. *D. asper* behaves as a stiff, high-strength but brittle material whose strength is sensitive to end restraint; *G. angustifolia* shows a far more compliant response with extending the yielding over other shear planes, though at the expense of a much lower ultimate resistance.

#### 4.7. Failure modes

Splitting failure was characterised by longitudinal cracks parallel to the fibres (Figure 4.8b), a common behaviour due to bamboo's unidirectional grain structure, particularly between nodes. Crushing failure involved a perpendicular or diagonal

deformation of the culm wall (Figure 4.8e), which can appear on the outer or inner surface and may penetrate the entire thickness. As noted by Li et al. (2015), crushing was typical in short-column specimens. Combined failure involved the simultaneous occurrence of both splitting and crushing within a single specimen (Figure 5c).

#### 4.7.1 Compression

The prevalence of these failure modes during compression tests was influenced by species, moisture content, and nodal presence. Under ambient-dry conditions, *D. asper* failed primarily by splitting, while *G. angustifolia* failed by crushing. Combined failure was exclusive to *G. angustifolia*. In oven-dry conditions, both species exhibited splitting. Splits typically occurred on the inner wall and rarely penetrated the full culm thickness, especially at nodes in ambient-dry samples. In contrast, wet samples did not split but failed via non-visible crushing at the specimen ends.

A clear correlation emerged between failure mode, sample dimensions, and compressive strength. The longer *D. asper* samples, which possess a higher average compressive strength ( $f_{c,0}$ ), failed predominantly by splitting which is a mode analogous to buckling in longer culms. Conversely, the shorter *G. angustifolia* samples, with a lower  $f_{c,0}$ , were most prone to crushing. This aligns with the findings of Li et al. (2015) and suggests that splitting is associated with high-strength bamboos, while crushing is more common in those with lower compressive strength.

#### 4.7.2 Shear

Figure 4.9 illustrates the shear test failure modes. Figure 4.9a illustrates splitting failure that occurred commonly in *D. Asper* for ambient-dry condition. Figure 4.9b illustrates failure for *G. angustifolia* for the oven dry condition, whereby specimens formed many splits. Figure 4.9c and Figure 4.9d illustrates failure across two nearby planes which sheared off a quarter of the specimen. For the shear tests the number of shear planes formed were mostly 1 to 2 planes in the ambient condition. 3 and 4 shear planes were common in the oven-dry conditions. In two tests, shear planes occurred in between the intended planes of failure. This was attributed to either pre-existing defects or the intermediary plates sliding during the test.

#### 4.7.3 DIC

DIC revealed the full-field strain patterns for some specimens shown in Appendix B, highlighting how damage evolves under different loading scenarios. In the plots, red denotes tensile strains, while blue indicates compressive strains.

- Appendix B Figure 2 captures a mixed-mode response in which longitudinal splitting coincides with localized crushing.
- Appendix B Figure 3 shows the same mixed-mode behaviour, but also makes the characteristic “elephant-foot” flare at the loaded end unmistakable—a consequence of end-bearing effects.
- Appendix B Figure 4 depicts the bow-tie test, where the specimen ultimately fails in shear.

#### 4.8. Summary

- Image-based segmentation confirmed a functionally graded wall in both species, with fibre fraction rising toward the epidermis and well fit by simple exponential/polynomial models ( $R^2 \approx 0.90\text{--}0.92$ ) across ten concentric bands. *D. asper* exhibited a uniform, fibre-rich mid-wall belt with low scatter and a peak  $V_f \approx 0.51$  near the outer wall, while *G. angustifolia* showed similar profiles but slightly lower and more scattered outer-band values.
- *D. asper* specimens were larger ( $D \approx 134$  mm,  $\delta \approx 11.2$  mm) than *G. angustifolia* ( $D \approx 103$  mm,  $\delta \approx 10.1$  mm), yet both maintained comparable  $D/\delta \approx 10\text{--}13$  across groups, supporting fair geometric comparability between species.
- Oven-dry conditioning maximized strength and stiffness and wet minimized both. For *D. asper*, long-tube  $f_c$  rose from  $45.9 \pm 16.2$  MPa (wet) to  $108.2 \pm 12.7$  MPa (oven-dry), while *G. angustifolia* long tube  $f_c$  shifted from  $34.4 \pm 5.8$  MPa (wet) to 86.0 MPa (oven-dry). Species-wise, *D. asper* was stronger in all states (e.g., ambient long  $f_c \approx 77.0 \pm 14.5$  MPa vs  $68.3 \pm 10.1$  MPa for *G. angustifolia*), with modulus trends aligned (e.g., *D. asper* long  $E \approx 5320$  MPa wet to 7082 MPa oven-dry; *G. angustifolia* long  $E \approx 2701$  MPa wet to 5432 MPa oven-dry).

Changing aspect ratio from  $\approx 1.0$  to  $\approx 2.0$  produced minimal strength differences in compression at these lengths, indicating end-effects still dominate over stability effects at  $L/D \leq 2$  for the tested geometries.

- Shear was more geometry-sensitive: short tubes were generally stronger and less brittle than long tubes, with *D. asper* ambient-dry  $f_v$  rising from  $9.0 \pm 1.6$  MPa (long) to  $11.9 \pm 2.2$  MPa (short) and *G. angustifolia* ambient-dry  $f_v \approx 7.4 \pm 1.3$  MPa (long) vs  $6.1 \pm 1.7$  MPa (short). Moisture depressed shear across both species; for *D. asper* long tubes,  $f_v$  fell from  $9.0 \pm 1.6$  MPa (ambient) to  $5.5 \pm 0.7$  MPa (wet), and for *G. angustifolia* long tubes from  $7.4 \pm 1.3$  MPa (ambient-dry) to  $4.8 \pm 0.4$  MPa (wet), with corresponding elastic modulus reductions and lower peak loads. Overall, *D. asper* displayed  $\approx 30\text{--}60\%$  higher shear capacity and stiffness than *G. angustifolia* across states, consistent with its fibre-rich microstructure observed in section analysis.
- Ambient-dry compression curves showed an initial seating phase, a near-linear hardening to peak, and then species-distinct softening: *D. asper* peaked higher but dropped sharply, while *G. angustifolia* showed more gradual, ductile post-peak with audible cracking, maintaining load to larger strains. Wet compression increased strains at peak and softened post-peak further, whereas oven-dry conditions amplified brittleness (especially in *D. asper*), which sometimes failed explosively, prompting premature test stops for safety. In shear, tubes of both species exhibited early, sharp peaks with abrupt drops (multi-plane failures).
- Compression failures transitioned with moisture: oven-dry favoured longitudinal splitting, ambient-dry favoured combined failure mode, and wet favoured end-crushing without visible full-thickness splits, with longer *D. asper* tubes more prone to splitting. Shear failures concentrated along 1–2 planes in ambient-dry, expanding to 3–4 planes under oven-dry.

## 5. Discussion

### 5.1. MC sensitivity

The pronounced moisture sensitivity observed in both species aligns with already established bamboo research principles. The compression strength reductions of 31.6% for *G. angustifolia* when transitioning from ambient-dry to wet conditions corroborate findings by Sánchez Cruz and Morales (2019), who reported strength reductions of 28.0% in *G. angustifolia* for moisture content increases between 12% and the fibre saturation point. The current results extend this understanding by demonstrating that strength degradation beyond the traditionally cited fibre saturation point, is not significant. The specimens had already exceeded the fibre saturation point (>30%) after being immersed in water for 24 hours.

The observed moisture effects align with the hygroscopic nature of bamboo documented by Bahtiar et al. (2020), who noted that bamboo exhibits improved mechanical properties in dry conditions. The differential response between species reflects their distinct microstructural characteristics, with *D. asper* showing more pronounced brittleness in wet conditions compared to *G. angustifolia*'s more gradual strength degradation. This species-specific behaviour supports Harries et al. (2017) observations that bamboo properties vary considerably between genera and species.

The elastic modulus reductions followed similar patterns to strength degradation, with wet conditions producing decreases of 18% and 40% for *D. asper* and *G. angustifolia* respectively. These findings parallel research by Jiang et al. (2012) on Moso bamboo, which demonstrated moisture sensitivity in mechanical properties below the fibre saturation point. The greater sensitivity of *G. angustifolia* to moisture variations may relate to its distinct anatomical structure and parenchyma distribution compared to *D. asper*.

### 5.2. Species mechanical performance

The superior performance of *D. asper* in both compression and shear testing confirmed its classification among the stronger bamboo species (A.N. Rao, V.

Ramanatha Rao, and J.T. Williams, 1998). With ambient-dry compression strengths of  $77.0 \pm 14.5$  MPa for long specimens and shear strengths reaching  $11.9 \pm 2.2$  MPa for short specimens, *D. asper* demonstrated mechanical properties consistent with high-performance bamboo species documented in literature (Hartono *et al.*, 2022). These values exceed those reported by Hartono *et al.* (2022) for the same species, suggesting potential regional variations that warrant further investigation.

*G. angustifolia*'s mechanical performance, while lower than *D. asper*, remained within expected ranges for this species. The compression strengths of  $68.3 \pm 10.1$  MPa (ambient-dry, long specimens) align closely with values reported by Aicher and Simon (2022) for Colombian *G. angustifolia*, who documented characteristic compression strengths of  $40$  N/mm $^2$  and mean values around  $54\text{--}86$  N/mm $^2$ . The shear strength results for *G. angustifolia* (6.1 MPa for GSAS) corroborate findings by Correal and López (2008), who reported shear strengths of  $5.52\text{--}6.44$  MPa for the same species across different Colombian regions.

The species comparison reveals differences in failure characteristics. *D. asper* exhibited more brittle failure modes with rapid post-peak load drops, while *G. angustifolia* demonstrated more ductile behaviour with gradual strength degradation. This distinction has important implications for structural applications, as the warning capacity of *G. angustifolia* (and audible cracking before failure) provides valuable safety advantages over *D. asper*'s sudden failure mode.

### **5.3. Geometric effects and sectional analysis**

The influence of specimen slenderness on mechanical performance highlighted important considerations for bamboo testing standards. The current ISO 22157:2019 specification of aspect ratio  $\approx 1.0$  was shown to produce different failure mechanisms compared to longer specimens (aspect ratio  $\approx 2.0$ ). Short specimens across short and long specimens demonstrated similar compressive strengths. However in shear, long specimens performed lesser than their shorter counterparts., supporting Harries *et al.* (2017) arguments for slenderness-based testing protocols rather than fixed aspect ratios.

The buckling failure mode in compression was not as pronounced with an aspect ratio of 2.0. However a larger aspect ratio such as 3.0 as seen in (Bompa *et al.*, no date), would have amplified the effect of the buckling failure mode in order to validate concerns raised by Aicher and Simon (2022) regarding current testing methodologies they recommend for slenderness ratios as opposed to a fixed length that is based on the external diameter.

In compression testing, the minimal strength differences observed between short ( $L/D = 1.0$ ) and long ( $L/D = 2.0$ ) specimens across both species initially appear to contradict theoretical expectations about end effects and local buckling. However, this observation can be explained by the competing influences of two distinct phenomena. Short specimens benefit from end restraint effects that suppress local instabilities and provide confining pressure, effectively increasing the measured strength above the true material capacity. Long specimens, while experiencing reduced end effects, remain below the critical slenderness ratio for global buckling instability in the tested geometries, allowing them to develop material-limited failure modes similar to their shorter counterparts.

The critical insight is that both geometries remain within the "end-effect dominated" regime rather than representing true material behaviour. The measured strengths therefore represent upper-bound estimates that may not be achievable in practical structural applications where members experience different boundary conditions and length scales. This finding supports the hypothesis that current standard test methods may provide unconservatively high design values, particularly for compression-dominated structural elements.

The investigation of aspect ratio effects revealed complex interactions between specimen geometry, failure mechanisms, and property measurement accuracy that challenge current standardized testing approaches. The results demonstrate that the ISO 22157:2019 specification of short specimens with  $L/D \approx 1.0$  may not provide representative data for structural design applications, confirming theoretical predictions about end effects while revealing species-specific geometric sensitivities.

The shear testing results revealed more pronounced geometric effects, with consistently lower strengths observed in longer specimens across both species and moisture conditions. For *D. asper*, the strength reduction from short to long specimens ranged from 17% (ambient) to 24% (oven-dry), while *G. angustifolia* showed more variable geometric sensitivity. This pattern can be attributed to the different mechanisms governing shear failure in short versus long specimens.

Short specimens develop multiple shear planes simultaneously, creating a distributed failure mechanism that utilizes the full wall thickness and provides some degree of redundancy. The bow-tie loading configuration creates four nominal shear planes, and the observed "zigzag" stress-strain curves indicate progressive activation of these planes as local stress concentrations develop. Long specimens, by contrast, tend to develop single dominant shear planes with limited redistribution capacity, resulting in more brittle failures with abrupt strength degradation.

The implications for testing standards are significant. The current ISO 22157:2019 approach of using stub specimens may systematically overestimate both compressive and shear strengths available in practice. For compression testing, the end restraint effects create artificial confinement that inflates measured capacity. For shear testing, the short specimen configuration promotes multi-plane failure mechanisms that may not be representative of actual structural connections where single-plane shear typically governs.

A revised testing approach should consider implementing multiple specimen geometries to characterize both material properties and geometric effects. For compression, longer specimens approaching  $L/D = 3-4$  might provide more representative material properties by minimizing end effects while remaining below global buckling thresholds. For shear, both short and long specimen configurations should be tested to bound the range of expected performance under different constraint conditions.

The DIC analysis provided valuable insights into the development of these geometric effects. The characteristic "elephant-foot" flaring observed at loaded ends in

compression specimens confirms the presence of radial restraint effects that alter local stress distributions.

The species-specific differences in geometric sensitivity also warrant consideration in testing standards. *D. asper*'s higher sensitivity to aspect ratio effects may require more conservative geometric factors in design, while *G. angustifolia*'s more consistent performance across geometries might permit less conservative approaches. This finding suggests that universal testing standards may be inadequate for the full range of bamboo species, necessitating species-specific modifications to existing protocols.

#### **5.4. Section analysis**

The sectional analysis revealed distinct fibre volume fraction distributions between species, with *D. asper* achieving maximum  $V_f \approx 0.51$  and *G. angustifolia* reaching  $V_f \approx 0.52$  in outer regions. These values align with literature ranges of 0.40-0.60 for outer culm regions reported by Dixon and Gibson (2014) and validate the rule of mixtures applications in bamboo mechanics. The successful curve fitting ( $R^2 > 0.90$ ) supports the use of simple mathematical models for describing bamboo's functionally graded structure.

The comprehensive sectional analysis successfully quantified the functionally graded nature of both bamboo species while providing validation for rule of mixtures predictions and revealing species-specific microstructural characteristics that explain observed mechanical property differences. The systematic variation in fibre volume fraction from inner wall (approximately 0.20 for both species) to outer wall (0.51 for *D. asper*, 0.48 for *G. angustifolia*) confirms the intelligent design of bamboo's natural optimization strategy.

The mathematical modelling of fibre distribution through polynomial relationships ( $R^2 = 0.916-0.922$ ) provides a robust framework for predicting mechanical properties based on sectional analysis. For *D. asper*, the relationship  $V_f = 0.00556x^2 - 0.021619x + 0.20314$  accurately captures the experimental distribution and enables prediction of local mechanical properties through rule of mixtures calculations. The

high correlation coefficients indicate that simple mathematical functions can reliably represent complex biological optimization patterns.

The species differences revealed through sectional analysis provide mechanistic explanations for observed performance variations. *D. asper*'s higher and more uniform fibre volume fraction in the critical outer wall regions directly translates to superior mechanical properties through increased load-carrying capacity of the high-stiffness fibres. The lower coefficient of variation in *D. asper* (less than 5% in mid-wall regions) compared to *G. angustifolia* (up to 12%) suggests better manufacturing quality control in nature, potentially reflecting more stable growing conditions or genetic optimization.

The implications for non-destructive evaluation and quality grading are significant. The strong correlation between sectional properties and mechanical performance suggests that image-based analysis could provide a practical method for bamboo culm grading without destructive testing. The established mathematical relationships enable prediction of mechanical properties from cross-sectional images, potentially supporting automated grading systems for commercial bamboo production.

However, several limitations in the sectional analysis approach require acknowledgment. The image-based segmentation method may not distinguish between load-bearing fibres and non-structural vessels within vascular bundles, potentially overestimating effective fibre volume fractions (Akinbade and Harries, 2021). The analysis also assumes uniform properties along the culm length, which may not account for variations in fibre maturity, lignification, or local defects that influence mechanical performance.

The irregular internal geometry of bamboo culms created measurement challenges, particularly for specimens with pronounced oval cross-sections or internal surface irregularities. These geometric variations may have influenced the accuracy of wall thickness measurements and concentric segment analysis, introducing uncertainty in the calculated fibre volume fractions. Future work should consider three-dimensional analysis techniques or microscopic validation of image-based measurements.

Despite these limitations, the sectional analysis results provide valuable insights into bamboo's natural optimization strategies and offer a foundation for developing predictive models linking microstructure to mechanical performance. The identification of critical outer wall regions with maximum fibre concentrations suggests that structural applications should focus on protecting these areas from damage or degradation to maintain optimal performance.

### **5.5. Failure mechanisms**

The documentation of failure modes across moisture conditions reveals a transition in failure mechanisms that reflects changes in the relative properties of bamboo's constituent materials. This evolution from splitting-dominated failures in dry conditions to crushing-dominated failures in wet conditions provides important insights into the underlying mechanical processes and has implications for structural design and safety assessment.

Under oven-dry conditions, both species exhibited predominantly splitting failures characterized by longitudinal cracks parallel to the fibre direction. These failures initiated at or near the inner wall surface and propagated outward, often arresting at vascular bundle interfaces or node locations. The splitting pattern reflects the highly anisotropic nature of dried bamboo, where the stiff, brittle fibres maintain strong longitudinal integrity while the desiccated matrix provides minimal transverse restraint. In this state, failure occurs when radial stresses generated by Poisson contraction under axial loading exceed the limited tensile capacity of the brittle matrix.

The transition to wet conditions altered this failure pattern, with crushing becoming the dominant mode. Under wet conditions, the plasticized matrix can no longer provide effective lateral support to individual fibres, allowing local buckling and progressive deformation to occur. The increased moisture content transforms the failure mechanism from a sudden, brittle fracture to a gradual, ductile process involving progressive fibre buckling and matrix deformation. This transition explains the observed increases in strain capacity and the more gradual post-peak behaviour under wet conditions.

The intermediate ambient-dry condition produced mixed failure modes that varied between species, reflecting their different microstructural characteristics and moisture sensitivity. *D. asper* specimens showed primarily splitting behaviour similar to oven-dry conditions, while *G. angustifolia* exhibited more combined failures involving both splitting and crushing. This species difference may reflect variations in the critical moisture content at which the failure mode transition occurs, potentially related to differences in cell wall porosity, lignin content, or fibre-matrix bonding characteristics.

The presence of nodes influenced failure patterns, particularly under ambient and wet conditions. Nodes provided crack arrest mechanisms that prevented full-thickness splitting and forced failure redistribution to adjacent internodal regions. In several specimens, longitudinal splits initiated in internodal regions but terminated at nodal boundaries, creating a segmented failure pattern that maintained overall structural integrity. This behaviour highlights the important role of nodes as natural reinforcement elements that improve bamboo's damage tolerance.

The implications of these failure mode transitions for structural applications are important. The shift from predictable, brittle failures in dry conditions to more ductile but potentially less predictable failures in wet conditions affects both design approaches and safety assessment procedures. Structures designed based on dry-condition properties may experience unexpected failure modes under service moisture conditions, potentially affecting their overall reliability and safety margins.

The observed failure patterns also influence connection design considerations. The predominance of splitting failures suggests that connection details should be designed to accommodate and arrest longitudinal crack propagation. Traditional bamboo construction techniques often incorporate wrapping or binding elements that provide circumferential restraint, effectively preventing or controlling splitting failures.

### **5.6. *Implications for structural applications***

The mechanical characterisation of bamboo conducted provides valuable data for structural bamboo applications. The moisture-dependent strength variations emphasise the importance of environmental control in bamboo structures. The

strength reduction factors observed (40-50% from oven-dry to wet conditions) emphasize the need for careful consideration of moisture in structural applications.

The species-specific performance characteristics suggest different optimal applications for each bamboo type. *D. asper*'s higher strength but brittle failure characteristics make it suitable for compression-dominated applications where sudden failure can be accommodated through appropriate design measures. Conversely, *G. angustifolia*'s more ductile behaviour and warning capacity before failure make it preferable for applications where structural robustness and damage tolerance are paramount.

The geometric effects documented support the development of more sophisticated testing protocols that better represent actual structural behaviour. The transition from stub column to slender column behaviour observed in longer specimens provides crucial data for developing buckling design equations for bamboo structural members.

### **5.7. Limitations**

The research limitations included the restricted sample sizes due to specimen loss during conditioning, particularly for *D. asper*. The inherent brittleness of *D. asper* resulted in fewer usable specimens, which may have affected the statistical reliability of some conclusions. Additionally, the study focused on two specific species from particular geographical origins (Guatemala), limiting the ability to generalise the findings to other bamboo species or growth conditions.

The geometric limitations of the tested aspect ratios ( $L/D \leq 2.0$ ) in compression prevented full characterization of the transition from material-dominated to stability-dominated failure modes. While the current results provide insights into end effects and short-column behaviour, longer specimens approaching  $L/D > 2$  would be necessary to identify true material properties free from constraint effects.

The image-based sectional analysis, while providing valuable microstructural insights, may not capture the full complexity of bamboo's hierarchical structure. The resolution limitations of optical imaging prevent detailed analysis of cell wall structure,

lignification patterns, and fibre-matrix interfaces that influence mechanical behavior. Integration of microscopic techniques, potentially including scanning electron microscopy or micro-computed tomography, would provide higher-resolution validation of image-based measurements.

The sectional analysis, though successful in quantifying fibre distribution patterns, encountered challenges with the rough interior surfaces of bamboo culms, particularly for *G. angustifolia* specimens. More sophisticated imaging techniques, such as microscopy, could provide enhanced accuracy in microstructural characterisation.

The rule of mixtures applications for predicting bamboo mechanical properties received support through the successful correlation between fibre volume fractions and mechanical performance. The functionally graded nature of bamboo culms, with exponential increases in fibre density toward outer regions, was confirmed through quantitative sectional analysis.

### **5.8. Future research**

Future research priorities should focus on several key areas. Long-term durability studies are critically needed to understand how mechanical properties change over time under realistic service conditions. The current investigation considered only short-term moisture effects, but bamboo structures experience cyclical wetting and drying that may produce cumulative damage through mechanisms not captured in single-cycle tests.

The development of accelerated testing methods for durability assessment represents another critical need. While natural weathering studies provide the most realistic data, the time scales involved make such studies impractical for design code development. Accelerated testing protocols that can reliably predict long-term performance within practical timeframes would support more confident structural applications.

Connection behaviour under varying moisture conditions requires dedicated investigation. This research focused on material properties of isolated specimens, but

structural performance depends critically on connection details that may be even more sensitive to moisture variations. The interaction between bamboo culms and steel, concrete, or composite connection elements under moisture cycling represents a significant knowledge gap.

Scale effects in bamboo structures remain poorly understood. The transition from laboratory specimen behaviour to full-scale structural performance involves complex interactions between material properties, geometric effects, and construction tolerances. Full-scale testing programs, while expensive, are necessary to validate laboratory-based design approaches and identify scale-dependent phenomena.

The development of standardized quality control procedures for structural bamboo represents both a research need and a practical requirement for industry adoption. The sectional analysis techniques demonstrated in this research provide a foundation for non-destructive evaluation methods, but validation across broader species ranges and correlation with long-term performance data are necessary for practical implementation.

Integration of advanced modelling techniques, including finite element analysis with moisture-dependent material properties and multi-scale modelling approaches that capture bamboo's hierarchical structure, would support more sophisticated design methods. Such models could enable optimization of bamboo structures for specific applications while accounting for the complex interactions between geometry, material properties, and environmental conditions identified in this research.

The economic and environmental lifecycle assessment of bamboo structural applications represents another important research direction. While bamboo's rapid growth and carbon sequestration potential are well-established, comprehensive analyses comparing bamboo structures to conventional alternatives across their full lifecycle, including maintenance, durability, and end-of-life considerations, are needed to support policy and investment decisions.

Finally, the development of engineered bamboo products that address the limitations of natural culms while preserving their environmental benefits represents a promising research frontier. Techniques such as densification, lamination, or composite

reinforcement could potentially overcome issues related to moisture sensitivity, geometric variability, and connection limitations while maintaining bamboo's fundamental advantages as a sustainable structural material.

## **6. Conclusions**

This dissertation has provided an experimental investigation into the mechanical behaviour of *G. angustifolia* and *D. asper* bamboo culms under varying moisture conditions and geometric configurations. Through testing of 108 specimens across compression and shear loading conditions, combined with detailed sectional analysis and digital image correlation techniques, this study has progressed understanding of bamboo's fundamental structural behaviour whilst addressing gaps in current testing methodologies and design standards.

The primary research objective to characterise the mechanical behaviour of *G. angustifolia* and *D. asper* bamboo culms under compression and shear loading parallel to grain across different moisture contents and slenderness ratios has been successfully accomplished. The experimental programme yielded datasets encompassing three moisture conditioning states (oven-dry <2%, ambient equilibrium 9-11%, and saturated >30%) and two aspect ratios (1.0 and 2.0).

The evaluation of existing testing methods through variable aspect ratios has revealed fundamental limitations in current protocols and established the critical importance of geometric effects on apparent material properties. The investigation of moisture content influence has quantified the dramatic property variations across hygroscopic ranges, with strength reductions of 40-50% observed between oven-dry and wet conditions. These findings provide essential data for developing moisture-dependent design procedures that accurately reflect bamboo's environmental sensitivity.

The comparative analysis between *G. angustifolia* and *D. asper* has documented species-specific mechanical properties and behaviour patterns, establishing *D. asper*'s superior performance characteristics whilst identifying *G. angustifolia*'s enhanced ductility under certain conditions. The digital image correlation analysis has captured failure progression mechanisms, revealing complex crack propagation patterns.

The investigation of correlations between fibre packing density, sectional properties, and mechanical performance has validated the rule of mixtures approach for bamboo property prediction whilst establishing polynomial relationships that describe fibre distribution patterns with high statistical confidence ( $R^2 > 0.92$ ). This achievement represents a step toward developing non-destructive bamboo grading systems essential for industrial adoption.

### **6.1. Key findings**

1. This research demonstrated that moisture content represents the most influential factor governing bamboo mechanical properties, extending beyond simple strength scaling to encompass fundamental changes in failure mechanisms. The transition from brittle failure modes in dry conditions to quasi-ductile responses under saturation represents a shift in understanding bamboo structural behaviour.
2. The investigation of aspect ratio effects has exposed limitations in current testing standards. The consistent superior performance of short specimens ( $L/D \approx 1.0$ ) compared to long specimens ( $L/D \approx 2.0$ ) in shear demonstrates that standard test configurations may overestimate the strength of actual structural members. In compression tests the strengths for both long and short specimens were statistically insignificant, however a larger aspect ratio ( $>2.0$ ) would have amplified the difference in compression strength.
3. *D. asper* demonstrated superior overall mechanical performance across most testing conditions, achieving approximately 25% higher compression strengths and 60% higher shear strengths compared to *G. angustifolia* under equivalent conditions. This performance advantage correlates directly with *D. asper*'s higher fibre volume fraction and more uniform microstructural organisation. However, *G. angustifolia* exhibited enhanced ductility characteristics, maintaining substantial post-peak load capacity that may prove advantageous in seismic applications.

4. The sectional analysis has validated bamboo's functionally graded architecture through quantitative measurement of radial fibre distribution patterns. The successful fitting of polynomial functions to experimental data demonstrates the mathematical predictability of bamboo's internal organisation, providing the foundation for structure-property relationships essential for engineering applications. The strong correlation between fibre volume fraction and mechanical properties confirms the applicability of composite material theories to bamboo structural behaviour.
5. The detailed characterisation of failure modes has revealed progressive damage mechanisms that vary with moisture content, specimen geometry, and species characteristics. The observed transformation from splitting-dominated failures in dry conditions to crushing-dominated failures under saturation indicates moisture-induced changes in crack propagation characteristics and stress distribution patterns. These findings suggest that simple strength-based design approaches may be inadequate for capturing bamboo's actual structural behaviour.

## **6.2. *Implications***

The research findings expose fundamental inadequacies in current bamboo testing standards and highlight urgent needs for methodological refinements. The ISO 22157:2019 standard's recommendation for  $L/D = 1.0$  specimens in compression testing overestimates material strength for typical structural applications where internodal lengths produce significantly higher aspect ratios. The observed 15-25% strength reduction between short and long specimens indicates that current protocols may underestimate required safety factors by substantial margins.

The bow-tie shear test demonstrates even greater limitations, with factor-of-two differences in apparent shear strength between geometric configurations making direct application of results to structural design highly questionable. The research findings necessitate immediate revision of testing protocols to incorporate multiple aspect ratios representative of actual structural conditions, coupled with development of alternative testing approaches that provide structurally relevant property data.

More fundamentally, the findings question whether material-based testing protocols can adequately capture bamboo's performance as a structural material. The observed dominance of geometric effects and complex interactions between moisture content, specimen size, and failure mechanisms suggest that bamboo characterisation may require hybrid approaches combining material property determination with member-level structural testing.

For structural design practice, the research has immediate implications requiring explicit consideration of hygroscopic effects in design procedures. The moisture sensitivity observed across both species necessitates moving beyond simple safety factor adjustments to incorporate moisture-dependent failure mode transitions.

The species-specific behaviour patterns support arguments for species-dependent design approaches rather than universal bamboo properties. The superior performance and consistency of *D. asper* compared to *G. angustifolia* suggests that material selection should be a primary design consideration, with different species requiring distinct design parameters and safety factors.

### **6.3. Contributions**

This research contributes to the broader objectives of sustainable construction by advancing the scientific foundation required for bamboo's acceptance as a mainstream structural material. The quantitative characterisation of moisture effects and geometric dependencies provides essential data for developing reliable design procedures, addressing key barriers to bamboo adoption identified by construction industry stakeholders.

The validation of structure-property relationships through sectional analysis supports development of performance-based bamboo grading systems essential for quality assurance in structural applications. The ability to predict mechanical properties from fibre distribution measurements represents an advance toward standardised bamboo material assessment, potentially enabling quality-based pricing and specification systems similar to those established for timber products.

However, the research also highlights the complexity of bamboo as an engineering material and the substantial research effort still required before bamboo can achieve parity with conventional structural materials in terms of design confidence and predictability. The observed moisture sensitivities, geometric dependencies, and failure mode complexities indicate that bamboo structural design will require sophisticated approaches fundamentally different from current timber or steel design procedures.

#### **6.4. Limitations**

Several limitations in the current research require acknowledgement whilst highlighting priorities for future investigation. The limited specimen numbers, particularly for *D. asper* due to material brittleness during preparation, constrain statistical confidence in some findings. The loss of a high number of specimens during conditioning processes indicates inherent challenges in bamboo testing that require methodological solutions through modified conditioning protocols or alternative specimen preparation techniques.

The research scope requires extension to additional bamboo species and environmental conditions to establish broader applicability of the findings. Future research priorities should include development of standardised testing protocols incorporating the geometric effects and moisture dependencies identified in this study.

Investigation of dynamic and fatigue properties under varying moisture conditions would address important gaps in current understanding of bamboo's long-term structural performance. The promising findings regarding sectional analysis-based property prediction require validation through expanded testing programmes and development of practical implementation procedures.

#### **6.5. Recommendations**

Based on the research findings, several recommendations emerge for advancing bamboo structural applications. Testing protocols should be revised to incorporate multiple aspect/slenderness ratios representative of actual structural conditions,

abandoning the current emphasis on  $L/D=1.0$  specimens that provide unconservative strength estimates in shear tests.

Species-specific design approaches should be adopted, recognising the substantial performance differences between bamboo types and avoiding generic property assumptions. Quality control systems should incorporate sectional analysis techniques for performance-based material grading, enabling reliable property prediction and quality assurance.

For the adoption of bamboo in the construction industry, development of comprehensive training programmes is required addressing bamboo's unique characteristics and design requirements. Professional engineering organisations should establish bamboo-specific continuing education requirements, ensuring practitioners understand the material's complexities and appropriate design approaches.

Research institutions and funding agencies should prioritise bamboo research programmes addressing the identified knowledge gaps, particularly in areas of long-term performance, environmental durability, and standardised testing procedures. International collaboration should be enhanced to accelerate development of comprehensive bamboo design standards and facilitate knowledge transfer between regions with established bamboo construction traditions and those seeking to adopt sustainable building practices.

## **6.6. Remarks**

This research has advanced understanding of bamboo structural behaviour through experimental investigation and systematic analysis of moisture, geometric, and species effects. The findings provide crucial data for developing evidence-based design approaches whilst exposing fundamental limitations in current testing standards and design procedures.

The demonstrated complexity of bamboo mechanical behaviour underscores both the challenges and opportunities associated with this sustainable construction material. Whilst the observed moisture sensitivities and geometric dependencies present

immediate design challenges, the superior strength-to-weight ratios and environmental credentials of bamboo justify continued research investment and industry development efforts.

The path toward widespread bamboo adoption requires continued interdisciplinary collaboration combining materials science, structural engineering, and construction practice expertise. The research contributions presented in this dissertation provide a foundation for these future efforts whilst identifying priority areas for continued investigation.

As the construction industry faces increasing pressure to reduce environmental impact and embrace sustainable materials, bamboo represents a considerable opportunity for achieving these objectives. However, realising this potential requires sophisticated understanding of the material's behaviour and development of design approaches that acknowledge its unique characteristics rather than attempting to force conformity with conventional material paradigms.

The research presented here demonstrates that bamboo can achieve structural performance comparable to conventional materials when properly understood and appropriately applied. The challenge for the construction industry lies in developing the knowledge frameworks, design procedures, and quality assurance systems necessary to support bamboo's transition from vernacular building material to mainstream structural material.

Through continued research, standardisation efforts, and industry collaboration, bamboo has the potential to make substantial contributions to sustainable construction objectives whilst providing economic opportunities in regions where the material grows naturally. The findings presented in this research represent an important step toward achieving these goals, providing both immediate practical insights and a foundation for future developments in bamboo structural engineering.

## References

- Adam, N. and Jusoh, I. (2019) ‘Physical and Mechanical Properties of Dendrocalamus asper and Bambusa vulgaris’, *Advances in Science and Technology* [Preprint].
- Aicher, S. and Simon, K. (2022) ‘Compressive Strength and Modulus of Elasticity Parallel to Culm Axis of Guadua Bamboo (G. Angustifolia) – Effect of Specimen Aspect and Slenderness Ratios, Nodes, Density and Preservation Treatment’, *Otto Graf Journal*, 21.
- Akinbade, Y. et al. (2019) ‘Through-culm wall mechanical behaviour of bamboo’, *Construction and Building Materials*, 216, pp. 485–495. Available at: <https://doi.org/10.1016/j.conbuildmat.2019.04.214>.
- Akinbade, Y. and Harries, K.A. (2021) ‘Is the rule of mixture appropriate for assessing bamboo material properties?’, *Construction and Building Materials*, 267, p. 120955. Available at: <https://doi.org/10.1016/j.conbuildmat.2020.120955>.
- Alexander, C. (2002) *Notes on the synthesis of form*. 17. printing. Cambridge, Mass.: Harvard Univ. Press.
- Amada, S. et al. (1996) ‘The Mechanical Structures of Bamboos in Viewpoint of Functionally Gradient and Composite Materials’, *Journal of Composite Materials*, 30(7), pp. 800–819. Available at: <https://doi.org/10.1177/002199839603000703>.
- Amada, S. et al. (1997) ‘Fiber texture and mechanical graded structure of bamboo’, *Composites Part B: Engineering*, 28(1–2), pp. 13–20. Available at: [https://doi.org/10.1016/S1359-8368\(96\)00020-0](https://doi.org/10.1016/S1359-8368(96)00020-0).
- Amede, E.A. et al. (2021) ‘A Review of Codes and Standards for Bamboo Structural Design’, *Advances in Materials Science and Engineering*. Edited by A. Gloria, 2021(1), p. 4788381. Available at: <https://doi.org/10.1155/2021/4788381>.

A.N. Rao, V. Ramanatha Rao, and J.T. Williams (1998) *Priority species of bamboo and rattan*. Serdang, Malaysia: PGRI-APO.

Arce, O.O. (1993) 'Fundamentals of the design of bamboo structures'. Technische Universiteit Eindhoven. Available at: <https://doi.org/10.6100/IR402687>.

Arch2o (2021) 'Urban Park Micro Renovation | Atelier cnS + School of Architecture , South China University of Technology', 20 October. Available at: <https://www.arch2o.com/urban-park-micro-renovation-atelier-cns-school-of-architecture-south-china-university-of-technology/> (Accessed: 3 August 2025).

Archila-Santos, H.F., Ansell, M.P. and Walker, P. (2012) 'Low Carbon Construction Using Guadua Bamboo in Colombia', *Key Engineering Materials*, 517, pp. 127–134. Available at: <https://doi.org/10.4028/www.scientific.net/KEM.517.127>.

ASTM (2023) 'Test Methods for Small Clear Specimens of Timber'. ASTM International. Available at: <https://doi.org/10.1520/D0143-22>.

Bahtiar, E.T., Trujillo, D. and Nugroho, N. (2020) 'Compression resistance of short members as the basis for structural grading of Guadua angustifolia', *Construction and Building Materials*, 249, p. 118759. Available at: <https://doi.org/10.1016/j.conbuildmat.2020.118759>.

Bautista, B.E., Garciano, L.E.O. and Lopez, L.F. (2021) 'Comparative Analysis of Shear Strength Parallel to Fiber of Different Local Bamboo Species in the Philippines', *Sustainability*, 13(15), p. 8164. Available at: <https://doi.org/10.3390/su13158164>.

Bompa, D. (2025) 'Bamboo Section Image Analysis Script'.

Bompa, D.V. et al. (no date) 'Experimental and numerical assessment of bamboo culm tube properties under dry and wet conditions.'

Chung, K.F. and Yu, W.K. (2002) ‘Mechanical properties of structural bamboo for bamboo scaffoldings’, *Engineering Structures*, 24(4), pp. 429–442. Available at: [https://doi.org/10.1016/S0141-0296\(01\)00110-9](https://doi.org/10.1016/S0141-0296(01)00110-9).

Correal D, J.F. and Arbeláez C, J. (2010) ‘Influence of age and height position on colombian “Guadua Angustifolia” bamboo mechanical properties’, *Maderas. Ciencia y tecnología*, 12(2). Available at: <https://doi.org/10.4067/S0718-221X2010000200005>.

Correal, J.F. (2016) ‘Bamboo design and construction’, in *Nonconventional and Vernacular Construction Materials*. Elsevier, pp. 393–431. Available at: <https://doi.org/10.1016/B978-0-08-100038-0.00014-7>.

Dixon, P.G. *et al.* (2015) ‘Comparison of the structure and flexural properties of Moso, Guadua and Tre Gai bamboo’, *Construction and Building Materials*, 90, pp. 11–17. Available at: <https://doi.org/10.1016/j.conbuildmat.2015.04.042>.

Dixon, P.G. and Gibson, L.J. (2014) ‘The structure and mechanics of Moso bamboo material’, *Journal of The Royal Society Interface*, 11(99), p. 20140321. Available at: <https://doi.org/10.1098/rsif.2014.0321>.

Engine (DICe), D.I.C. (2025) ‘dicengine/dice’. Available at: <https://github.com/dicengine/dice> (Accessed: 23 August 2025).

Ferreira, T. and Rasband, W. (2012) ‘ImageJ’.

Gatóo, A. *et al.* (2014) ‘Sustainable structures: bamboo standards and building codes’, *Proceedings of the Institution of Civil Engineers - Engineering Sustainability*, 167(5), pp. 189–196. Available at: <https://doi.org/10.1680/ensu.14.00009>.

Gnanaharan, R., Janssen, J.A. and Arce, O.O. (1995) ‘Bending strength of Guadua bamboo: comparison of different testing procedures.’, *International Network for Bamboo and Rattan (INBAR)* [Preprint].

Göswein, V. *et al.* (2022) ‘Barriers and opportunities of fast-growing biobased material use in buildings’, *Buildings and Cities*, 3(1), pp. 745–755. Available at: <https://doi.org/10.5334/bc.254>.

Gottron, J., Harries, K.A. and Xu, Q. (2014) ‘Creep behaviour of bamboo’, *Construction and Building Materials*, 66, pp. 79–88. Available at: <https://doi.org/10.1016/j.conbuildmat.2014.05.024>.

Grosser, D. and Liese, W. (1971) ‘On the anatomy of Asian bamboos, with special reference to their vascular bundles’, *Wood Science and Technology*, 5(4), pp. 290–312. Available at: <https://doi.org/10.1007/BF00365061>.

Gutiérrez, J.A. (2000) *Structural adequacy of traditional bamboo housing in Latin America*. Beijing: INBAR (Technical report / International Network for Bamboo and Rattan, 19).

Gutiérrez, J.A. (2004) ‘Notes on the Seismic Adequacy of Vernacular Buildings’, in. *13th World Conference on Earthquake Engineering*, Vancouver, Canada.

Harries, K. and Molari, L. (2024) ‘Mechanical characterisation of bamboo for construction: the state-of-practice and future prospects’, *RILEM Technical Letters*, 8, pp. 150–157. Available at: <https://doi.org/10.21809/rilemtechlett.2023.188>.

Harries, K.A. *et al.* (2017) ‘Geometric and material effects on bamboo buckling behaviour’, *Proceedings of the Institution of Civil Engineers - Structures and Buildings*, 170(4), pp. 236–249. Available at: <https://doi.org/10.1680/jstbu.16.00018>.

Harries, K.A., Sharma, B. and Richard, M. (2012) ‘Structural Use of Full Culm Bamboo: The Path to Standardization’, *International Journal of Architecture, Engineering and Construction*, 1(2), pp. 66–75. Available at: <https://doi.org/10.7492/IJAEC.2012.008>.

Hartono, R. *et al.* (2022) ‘Physical, Chemical, and Mechanical Properties of Six Bamboo from Sumatera Island Indonesia and Its Potential Applications for Composite

Materials', *Polymers*, 14(22), p. 4868. Available at: <https://doi.org/10.3390/polym14224868>.

Hutchison, M.A. and Koepferl, C.M. (2024) 'Contour Analysis Tool: an interactive tool for background and morphology analysis', *The Astrophysical Journal*, 975(1), p. 27. Available at: <https://doi.org/10.3847/1538-4357/ad779f>.

IBUKU (no date) 'Our Work - Projects Portfolio', IBUKU. Available at: <https://ibuku.com/portfolio/> (Accessed: 3 August 2025).

ISO (2018) 'BS ISO 19624:2018: Bamboo structures. Grading of bamboo culms. Basic principles and procedures'.

ISO (2019) 'BS ISO 22157:2019: Bamboo structures. Determination of physical and mechanical properties of bamboo culms. Test methods'.

ISO (2021) 'BS ISO 22156:2021: Bamboo structures. Bamboo culms. Structural design'.

Janssen, J.J. (1981) 'Bamboo in building structures'. Technische Hogeschool Eindhoven. Available at: <https://doi.org/10.6100/IR11834>.

Janssen, J.J.A. (2000) *Designing and building with bamboo*. (INBAR technical report, 20).

Jiang, Z. et al. (2012) 'Sensitivity of Several Selected Mechanical Properties of Moso Bamboo to Moisture Content Change Under the Fibre Saturation Point', *BioResources*, 7(4), pp. 5048–5058. Available at: <https://doi.org/10.15376/biores.7.4.5048-5058>.

Jones, E. et al. (2018) *A Good Practices Guide for Digital Image Correlation*. 1st edn. International Digital Image Correlation Society. Available at: <https://doi.org/10.32720/idics/gpg.ed1/print.format>.

Kaminski, S. (2013) 'Engineered Bamboo Houses for Low-income Communities in Latin America', *The Structural Engineer*, 91(10), pp. 14–23. Available at: <https://doi.org/10.56330/LXJD4295>.

Kaminski, S., Lawrence, A. and Trujillo, D. (2016a) *Design Guide for Engineered Bahareque Housing*. 38. Beijing, China: International Network for Bamboo and Rattan (INBAR). Available at: <https://www.inbar.int/wp-content/uploads/2020/05/1491901273.pdf> (Accessed: 2 July 2025).

Kaminski, S., Lawrence, A. and Trujillo, D. (2016b) 'Structural use of bamboo. Part 1: Introduction to bamboo', *The Structural Engineer*, 94(8), pp. 40–43. Available at: <https://doi.org/10.56330/PNSC8891>.

King, C. et al. (2021) 'Integration of Bamboo Forestry into Carbon Markets'. International Bamboo and Rattan Organisation (INBAR). Available at: [https://www.inbar.int/wp-content/uploads/2021/03/Mar-2021\\_Integration-of-Bamboo-Forestry-into-Carbon-Markets-2.pdf](https://www.inbar.int/wp-content/uploads/2021/03/Mar-2021_Integration-of-Bamboo-Forestry-into-Carbon-Markets-2.pdf) (Accessed: 3 July 2025).

Krause, J.Q. et al. (2016) 'On the influence of *Dendrocalamus giganteus* bamboo microstructure on its mechanical behavior', *Construction and Building Materials*, 127, pp. 199–209. Available at: <https://doi.org/10.1016/j.conbuildmat.2016.09.104>.

Li, H. et al. (2015) 'Mechanical performance of laminated bamboo column under axial compression', *Composites Part B: Engineering*, 79, pp. 374–382. Available at: <https://doi.org/10.1016/j.compositesb.2015.04.027>.

Liese, W. (1998) *The Anatomy of Bamboo Culms*. BRILL. Available at: <https://doi.org/10.1163/9789004502468>.

Liese, W. and Köhl, M. (eds) (2015) *Bamboo: The Plant and its Uses*. Cham: Springer International Publishing (Tropical Forestry). Available at: <https://doi.org/10.1007/978-3-319-14133-6>.

Liese, W. and Tang, T.K.H. (2015) 'Properties of the Bamboo Culm', in W. Liese and M. Köhl (eds) *Bamboo*. Cham: Springer International Publishing (Tropical Forestry), pp. 227–256. Available at: [https://doi.org/10.1007/978-3-319-14133-6\\_8](https://doi.org/10.1007/978-3-319-14133-6_8).

Liese, W. and Weiner, G. (1996) 'Ageing of bamboo culms. A review', *Wood Science and Technology*, 30(2), pp. 77–89. Available at: <https://doi.org/10.1007/BF00224958>.

Lopez, M., Bommer, J. and Mendez, P. (2004) 'The Seismic Performance of Bahareque Dwellings in El Salvador', in. *13th World Conference on Earthquake Engineering*, Vancouver, Canada.

Lozano, J., Luna, P. and Takeuchi, C. (2010) 'Validación de la Guadua angustifolia como material estructural para diseño, por el método de esfuerzos admisibles.' Universidad Nacional de Colombia.

Maria S. Vorontsova *et al.* (2016) *INBAR Technical Report No. 37 - World Checklist of Bamboos and Rattans*. 37. INBAR International Network for Bamboo and Rattan. Available at: <https://www.inbar.int/wp-content/uploads/2020/05/1491869017.pdf> (Accessed: 4 July 2025).

Matos, L. (2022) 'Unique, Sustainable Architecture: Exploring Vernacular Bamboo Structures Around The World - Bamboo U', *Bamboo U*, 3 August. Available at: <https://bamboou.com/design-vernacular-bamboo-structures-around-the-world/> (Accessed: 3 July 2025).

Minke, G. *et al.* (2016) *Building with bamboo : design and technology of a sustainable architecture*. Second and revised edition. Basel, Switzerland: Birkhäuser. Available at: <https://doi.org/10.1515/9783035608656>.

Mitch, D., Harries, K.A. and Sharma, B. (2010) 'Characterization of Splitting Behavior of Bamboo Culms', *Journal of Materials in Civil Engineering*, 22(11), pp. 1195–1199. Available at: [https://doi.org/10.1061/\(ASCE\)MT.1943-5533.0000120](https://doi.org/10.1061/(ASCE)MT.1943-5533.0000120).

Mouka, T., Dimitrakopoulos, E.G. and Lorenzo, R. (2022) 'Insight into the behaviour of bamboo culms subjected to bending', *Journal of The Royal Society Interface*, 19(189), p. 20210913. Available at: <https://doi.org/10.1098/rsif.2021.0913>.

Mujdeci, A., Bompa, D.V. and Elghazouli, A.Y. (2021) 'Confinement effects for rubberised concrete in tubular steel cross-sections under combined loading', *Archives of Civil and Mechanical Engineering*, 21(2), p. 53. Available at: <https://doi.org/10.1007/s43452-021-00204-8>.

*NEBgS Lecture Series #3 with Jörg Stamm – Bamboo in the Future of Design: Long, light and strong* (2024). Available at: <https://www.youtube.com/watch?v=jgQ0vYAVjzM> (Accessed: 1 July 2025).

Nie, Y. et al. (2021) 'Influence of slenderness ratio and sectional geometry on the axial compression behavior of original bamboo columns', *Journal of Wood Science*, 67(1), p. 36. Available at: <https://doi.org/10.1186/s10086-021-01968-6>.

Nogata, F. and Takahashi, H. (1995) 'Intelligent functionally graded material: Bamboo', *Composites Engineering*, 5(7), pp. 743–751. Available at: [https://doi.org/10.1016/0961-9526\(95\)00037-N](https://doi.org/10.1016/0961-9526(95)00037-N).

Osorio, L. et al. (2011) 'Morphological aspects and mechanical properties of single bamboo fibers and flexural characterization of bamboo/ epoxy composites', *Journal of Reinforced Plastics and Composites*, 30(5), pp. 396–408. Available at: <https://doi.org/10.1177/0731684410397683>.

Paraview (2025) 'ParaView - Open-source, multi-platform data analysis and visualization application'. Available at: <https://www.paraview.org/> (Accessed: 23 August 2025).

Rivera-Segura, R. et al. (2024) 'Analysis of the physical-mechanical properties of Dendrocalamus asper (Schult.) versus two Guadua angustifolia (Kunth) varieties, South and Caribe in the Atlantic Region of Costa Rica', *Advances in Bamboo Science*, 6, p. 100057. Available at: <https://doi.org/10.1016/j.bamboo.2024.100057>.

Röck, M. et al. (2020) ‘Embodied GHG emissions of buildings – The hidden challenge for effective climate change mitigation’, *Applied Energy*, 258, p. 114107. Available at: <https://doi.org/10.1016/j.apenergy.2019.114107>.

Sánchez Cruz, M.L. and Morales, L.Y. (2019) ‘Influence of moisture content on the mechanical properties of Guadua Culms’, *INGE CUC*, 15(1), pp. 99–108. Available at: <https://doi.org/10.17981/ingecuc.15.1.2019.09>.

Structural Bamboo (2013) ‘Simón Vélez. Visit to Cambridge’, *Structural Bamboo*, 6 June. Available at: <https://structuralbamboo.wordpress.com/2013/06/06/simon-velez-visit-to-cambridge/> (Accessed: 3 August 2025).

*The Arc: bamboo as low-carbon structural material* (2024). Available at: <https://www.youtube.com/watch?v=Hb5jfdw9WQQ> (Accessed: 1 July 2025).

Tropical Commons (2018) ‘Guadua – the abundant, fast growing, “vegetable steel” used in Simón Vélez’s structures’, *Tropical Commons*, 1 September. Available at: <https://tropicalcommons.co/en/2018/09/01/guadua-the-abundant-fast-growing-vegetable-steel-used-in-simon-velezs-structures/> (Accessed: 3 July 2025).

Trujillo, D. and López, L.F. (2016) ‘Bamboo material characterisation’, in *Nonconventional and Vernacular Construction Materials*. Elsevier, pp. 365–392. Available at: <https://doi.org/10.1016/B978-0-08-100038-0.00013-5>.

UK Bamboo Suppliers Limited (2025) ‘Request for Quotation’.

UNEP (2024) *2023 Global Status Report for Buildings and Construction: Beyond foundations - Mainstreaming sustainable solutions to cut emissions from the buildings sector*. United Nations Environment Programme. Available at: <https://doi.org/10.59117/20.500.11822/45095>.

UN-Habitat (ed.) (2022) *World cities report 2022: envisaging the future of cities*. Nairobi, Kenya: UN-Habitat (World cities report, 2022).

Vivas, L.S. *et al.* (2019) 'Mechanical properties of bamboo: a research synthesis of strength values and the factors influencing them', *American Bamboo Society*, (29), pp. 1–21.

Wang, M. *et al.* (2022) 'Variation of mechanical properties of P. edulis (Moso) bamboo with moisture content', *Construction and Building Materials*, 324, p. 126629. Available at: <https://doi.org/10.1016/j.conbuildmat.2022.126629>.

WGBC (2019) *Bringing embodied carbon upfront: Coordinated action for the building and construction sector to tackle embodied carbon*. London, United Kingdom.

*Working With Bamboo in Architecture - Simón Vélez | 25 Years 25 Hours* (2021). (Prince Claus Fund). Available at: <https://www.youtube.com/watch?v=5IG60cqLBYc> (Accessed: 3 August 2025).

Ximena Londoño *et al.* (2002) 'Characterization of the anatomy of Guadua angustifolia (Poaceae: Bambusoideae) culms', *American Bamboo Society*, 16(1), pp. 18–31.

Xu, Q. *et al.* (2014) 'Mechanical properties of structural bamboo following immersion in water', *Engineering Structures*, 81, pp. 230–239. Available at: <https://doi.org/10.1016/j.engstruct.2014.09.044>.

Yu, H.Q. *et al.* (2008) 'Selected Physical and Mechanical Properties of Moso Bamboo (*Phyllostachys Pubescens*)', *Journal of Tropical Forest Science*, pp. 258–263.

## **Appendix A. Methodology**



*Figure 1. Full experimental setup*

## **Appendix B. DIC analysis**

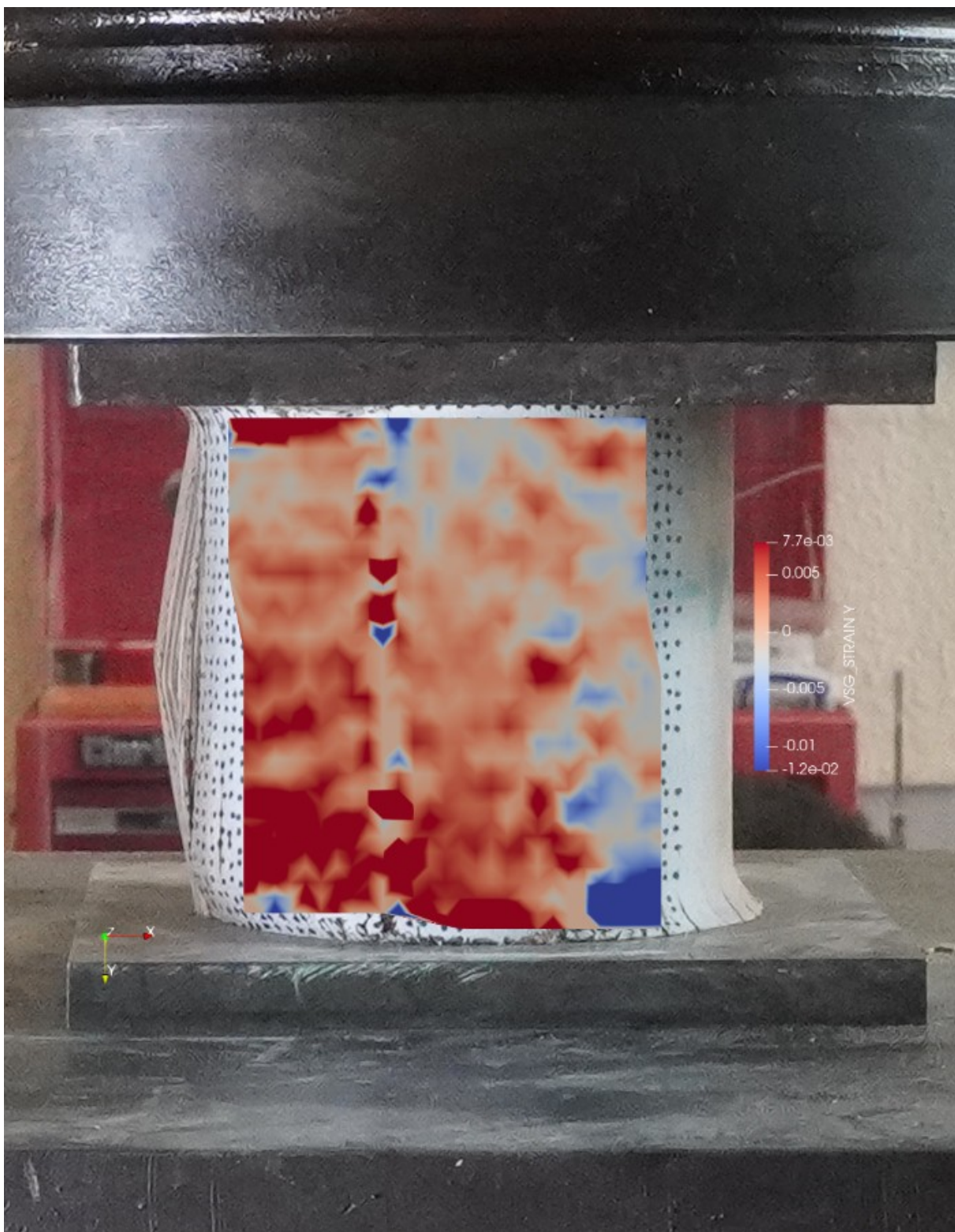


Figure 2. Strains across a specimen undergoing compression

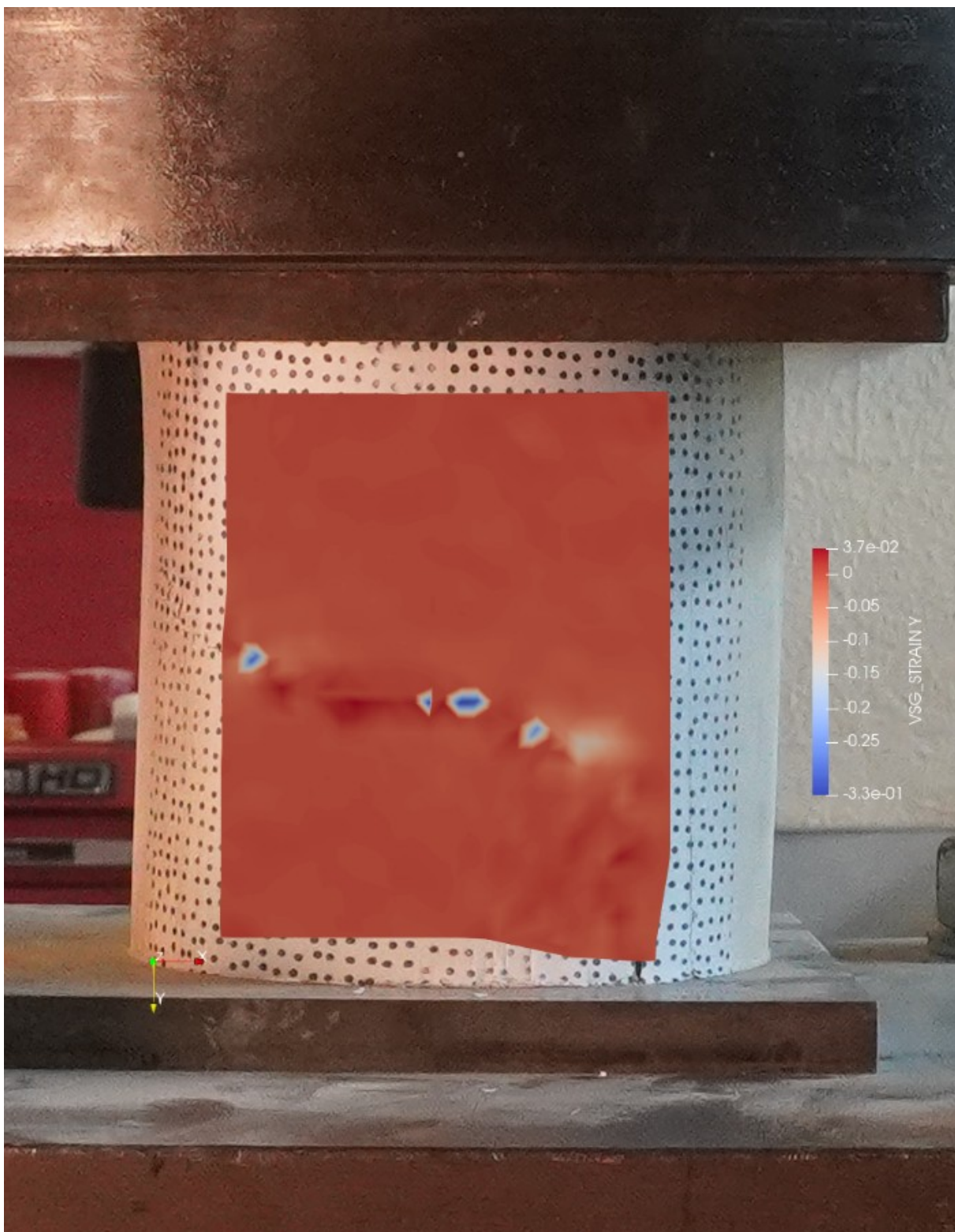


Figure 3. Strains across a specimen undergoing splitting and crushing failure

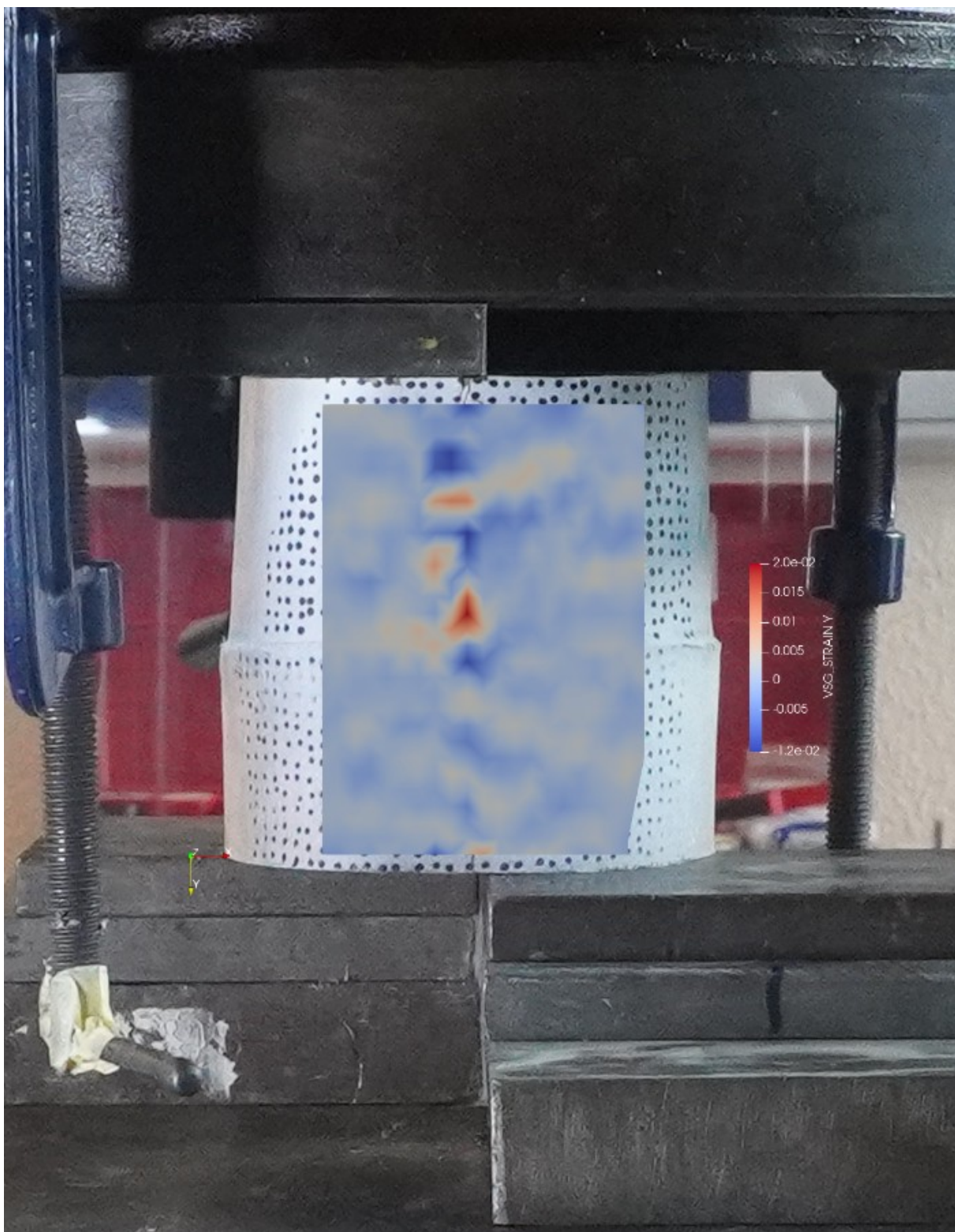


Figure 4. Strains across a specimen undergoing shear failure

**Appendix C. Section analysis (Hutchison and Koepferl, 2024; Bompa, 2025)**

# DM-1-001

August 25, 2025

```
[1]: #pip install openpyxl numpy opencv-python-headless scikit-image matplotlib
    ↪pandas
```

```
[2]: #pip install "numpy<2.0"
```

```
[3]: #import os
#os._exit(00)
```

```
[4]: import numpy as np
import cv2
import matplotlib.pyplot as plt
import pandas as pd
from skimage import measure, morphology
```

```
[5]: # Load the image in grayscale
image_path = 'DM-1-001 preprocessed.jpg' # Replace with your image path
image = cv2.imread(image_path, cv2.IMREAD_GRAYSCALE)

# Check if the image was loaded successfully
if image is None:
    raise ValueError("Image not found. Please check the file path.")

# Enhance contrast using histogram equalization
#equalized_image = cv2.equalizeHist(image)
equalized_image = image

# Display the original grayscale image
#plt.figure(figsize=(12, 6))
#plt.subplot(1, 2, 1)
#plt.imshow(image, cmap='gray')
#plt.title('Original Grayscale Image')
#plt.axis('off')

# Display the contrast-enhanced image
#plt.subplot(1, 2, 2)
plt.imshow(equalized_image, cmap='gray')
plt.title('Contrast-Enhanced Image')
plt.axis('off')
```

```

plt.show()

# Export the image as a JPEG at the highest quality
export_path = image_path.replace('.jpg', '_equalized.jpg')
plt.imsave(export_path, equalized_image, cmap='gray')
print(f"Image saved as {export_path}")

```

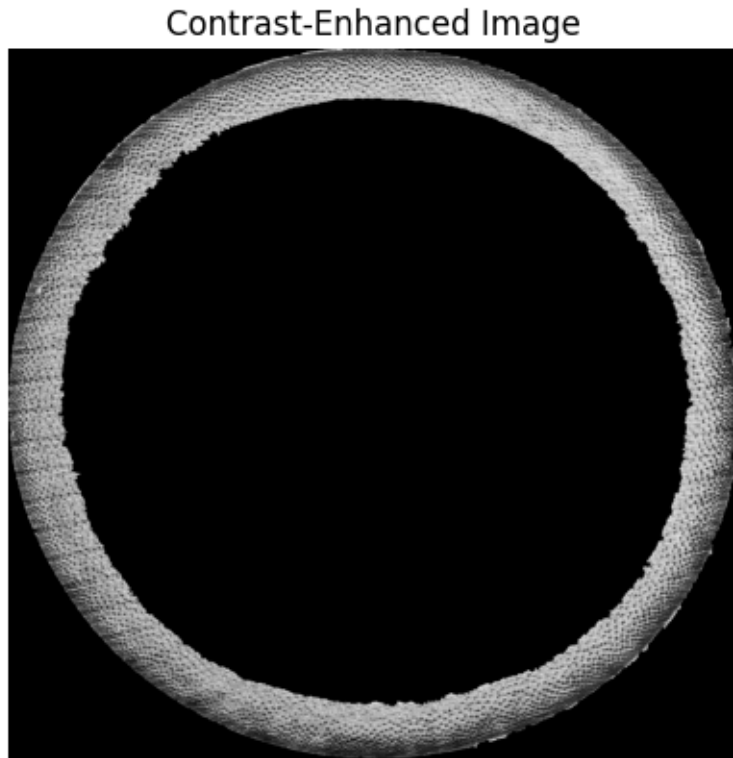


Image saved as DM-1-001 preprocessed\_equalized.jpg

[6]: # Enhance contrast using histogram equalization DONE ABOVE  
*#equalized\_image = cv2.equalizeHist(image)*

##1  
*# Apply Otsu's thresholding*  
~~\_~~, binary\_imageOTSU = cv2.threshold(equalized\_image, 0, 255, cv2.THRESH\_BINARY  
~~\_~~+ cv2.THRESH\_OTSU)

*# Invert the binary image if necessary (fibers should be white)*  
binary\_imageOTSU = cv2.bitwise\_not(binary\_imageOTSU)

*# Display the binary image*

```

plt.imshow(binary_imageOTSU, cmap='gray')
plt.title('Binary Image')
plt.axis('off')
plt.show()

# Export the image as a JPEG at the highest quality
export_path = image_path.replace('.jpg', '_binaryOTSU.jpg')
plt.imsave(export_path, binary_imageOTSU, cmap='gray')
print(f"Image saved as {export_path}")

```

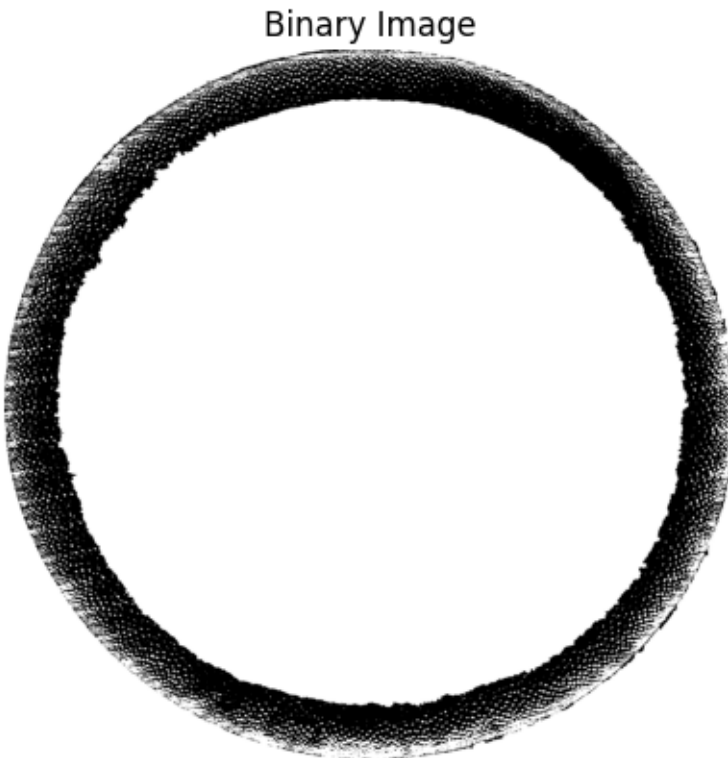


Image saved as DM-1-001 preprocessed\_binaryOTSU.jpg

```

[7]: # Remove small objects (noise) - adjust the min_size parameter as needed
kernel = cv2.getStructuringElement(cv2.MORPH_ELLIPSE, (1, 1))
cleaned_imageOTSU = cv2.morphologyEx(binary_imageOTSU, cv2.MORPH_CLOSE, kernel)
#cleaned_image = cv2.morphologyEx(closed_image, cv2.MORPH_CLOSE, kernel)

#cleaned_image = morphology.remove_small_objects(binary_image.astype(bool), ↴
min_size=50)

# Convert back to uint8 format
cleaned_imageOTSU = (cleaned_imageOTSU * 255).astype(np.uint8)

```

```

# Invert image
cleaned_imageOTSU = cv2.bitwise_not(cleaned_imageOTSU)

# Display the cleaned binary image
plt.imshow(cleaned_imageOTSU, cmap='gray')
plt.title('Cleaned Binary OTSU Image')
plt.axis('off')
plt.show()

# Export the image as a JPEG at the highest quality
export_path = image_path.replace('.jpg', '_cleanedOTSU.jpg')
plt.imsave(export_path, cleaned_imageOTSU, cmap='gray')
print(f"Image saved as {export_path}")

```

Cleaned Binary OTSU Image

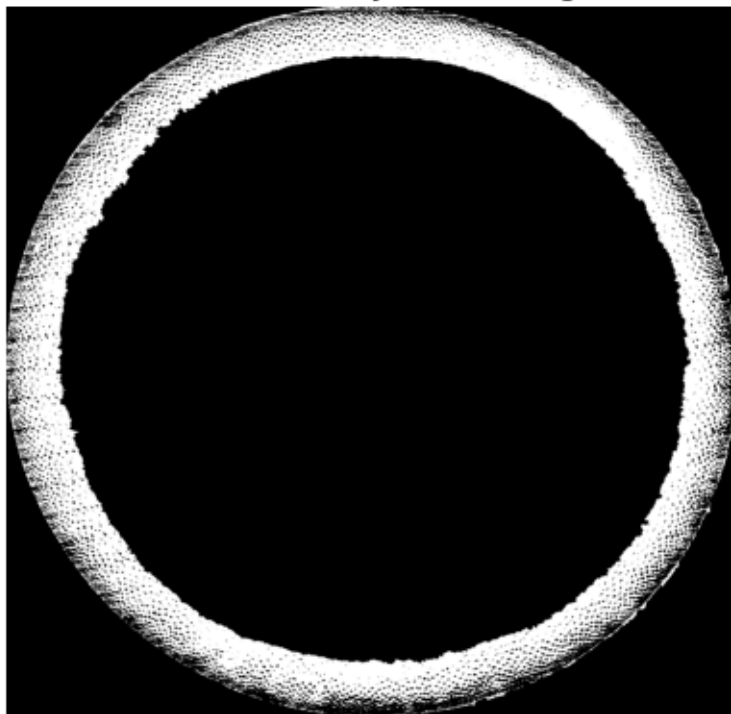


Image saved as DM-1-001 preprocessed\_cleanedOTSU.jpg

```

[8]: import cv2
import numpy as np
import matplotlib.pyplot as plt

# Assuming 'binary_image' is your input binary image

```

```

# Invert the binary image if necessary (objects should be white)
inverted_imageOTSU = cv2.bitwise_not(binary_imageOTSU)

# Remove small objects (noise) - adjust the kernel size as needed
kernel = cv2.getStructuringElement(cv2.MORPH_ELLIPSE, (1,1))
cleaned_imageOTSU = cv2.morphologyEx(inverted_imageOTSU, cv2.MORPH_CLOSE, ↴
    ↪kernel)

# Ensure the image is in uint8 format
if cleaned_imageOTSU.dtype != np.uint8:
    cleaned_imageOTSU = (cleaned_imageOTSU * 255).astype(np.uint8)

# Find contours
contours, hierarchy = cv2.findContours(cleaned_imageOTSU, cv2.RETR_TREE, cv2.
    ↪CHAIN_APPROX_SIMPLE)

# Check if contours are found
if len(contours) == 0:
    raise ValueError("No contours found. Ensure the image has clear boundaries.
        ↪")

# Sort contours by area (largest to smallest)
contours = sorted(contours, key=cv2.contourArea, reverse=True)

# Initialize variables for external and internal contours
external_contour = None
internal_contour = None

# Iterate through contours to find the external and internal ones
for i, contour in enumerate(contours):
    # Check if the contour is large enough to be considered
    if cv2.contourArea(contour) > 100: # Adjust the area threshold as needed
        if external_contour is None:
            external_contour = contour
        elif internal_contour is None:
            internal_contour = contour
        break

# Ensure both contours are found
if external_contour is None or internal_contour is None:
    raise ValueError("Could not find both external and internal contours. Check
        ↪the image preprocessing steps.")

# Draw contours on a copy of the original image for visualization
image_with_contoursOTSU = cv2.cvtColor(binary_imageOTSU, cv2.COLOR_GRAY2BGR) # ↪
    ↪Convert to BGR for color drawing

```

```

cv2.drawContours(image_with_contoursOTSU, [external_contour], -1, (0, 255, 0), 5) # Green for external contour
cv2.drawContours(image_with_contoursOTSU, [internal_contour], -1, (255, 0, 0), 5) # Blue for internal contour

# Display the image with contours
plt.imshow(cv2.cvtColor(image_with_contoursOTSU, cv2.COLOR_BGR2RGB))
plt.title('External and Internal Contours')
plt.axis('off')
plt.show()

# Export the image as a JPEG at the highest quality
export_path = image_path.replace('.jpg', '_contoursOTSU.jpg')
plt.imsave(export_path, image_with_contoursOTSU, cmap='gray')
print(f"Image saved as {export_path}")

```

External and Internal Contours

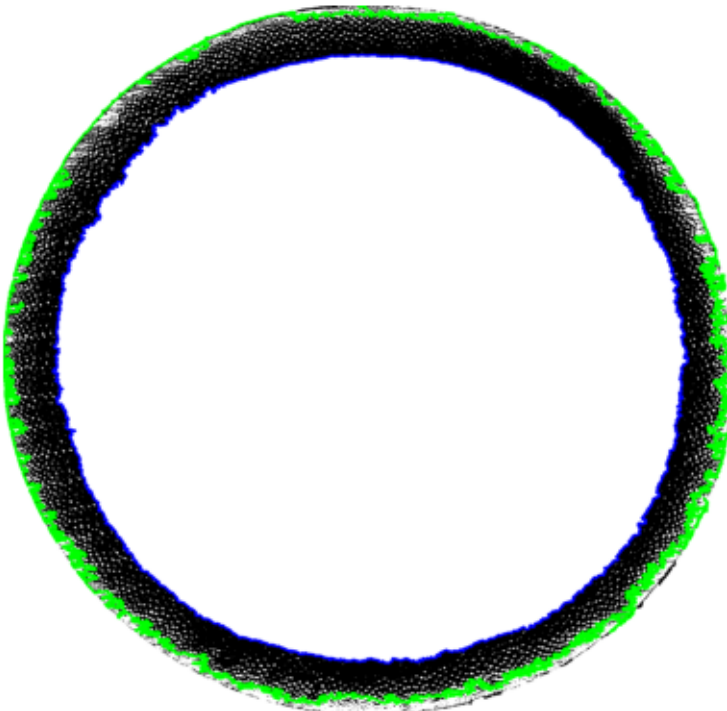


Image saved as DM-1-001 preprocessed\_contoursOTSU.jpg

```
[9]: import cv2
import numpy as np
import matplotlib.pyplot as plt
```

```

# Assuming 'cleaned_image', 'external_contour', and 'internal_contour' are
# already defined

# Fit ellipses to the external and internal contours
ellipse_external = cv2.fitEllipse(external_contour)
ellipse_internal = cv2.fitEllipse(internal_contour)

# External ellipse parameters
(x_ext, y_ext), (major_axis_ext, minor_axis_ext), angle_ext = ellipse_external
external_diameter_major = major_axis_ext
external_diameter_minor = minor_axis_ext

# Internal ellipse parameters
(x_int, y_int), (major_axis_int, minor_axis_int), angle_int = ellipse_internal
internal_diameter_major = major_axis_int
internal_diameter_minor = minor_axis_int

# Print the diameters
print(f"External Major Diameter: {external_diameter_major:.2f} pixels")
print(f"External Minor Diameter: {external_diameter_minor:.2f} pixels")
print(f"Internal Major Diameter: {internal_diameter_major:.2f} pixels")
print(f"Internal Minor Diameter: {internal_diameter_minor:.2f} pixels")

# Calculate the center of the image
image_center_x = cleaned_imageOTSU.shape[1] // 2
image_center_y = cleaned_imageOTSU.shape[0] // 2

# Calculate the offsets of the bamboo cross-section centers relative to the
# image center
offset_x_ext = x_ext - image_center_x
offset_y_ext = y_ext - image_center_y
offset_x_int = x_int - image_center_x
offset_y_int = y_int - image_center_y

# Print the center coordinates and offsets
print(f"External Ellipse Center: ({x_ext:.2f}, {y_ext:.2f}) pixels")
print(f"Internal Ellipse Center: ({x_int:.2f}, {y_int:.2f}) pixels")
print(f"Image Center: ({image_center_x}, {image_center_y}) pixels")
print(f"External Ellipse Offset from Image Center: (\Delta x: {offset_x_ext:.2f} pixels, \Delta y: {offset_y_ext:.2f} pixels)")
print(f"Internal Ellipse Offset from Image Center: (\Delta x: {offset_x_int:.2f} pixels, \Delta y: {offset_y_int:.2f} pixels)")

# Convert cleaned image to BGR for color drawing
image_with_ellipses = cv2.cvtColor(cleaned_imageOTSU, cv2.COLOR_GRAY2BGR)

# Draw the external ellipse in green

```

```

cv2.ellipse(image_with_ellipses, (int(x_ext), int(y_ext)), (int(major_axis_ext / 
    ↵ 2), int(minor_axis_ext / 2)),
    angle_ext, 0, 360, (0, 255, 0), 2)

# Draw the internal ellipse in blue
cv2.ellipse(image_with_ellipses, (int(x_int), int(y_int)), (int(major_axis_int / 
    ↵ 2), int(minor_axis_int / 2)),
    angle_int, 0, 360, (255, 0, 0), 2)

# Draw the external contour in red
cv2.drawContours(image_with_ellipses, [external_contour], -1, (0, 0, 255), 1)

# Draw the internal contour in yellow
cv2.drawContours(image_with_ellipses, [internal_contour], -1, (0, 255, 255), 1)

# Display the image with ellipses and contours
plt.figure(figsize=(10, 10))
plt.imshow(cv2.cvtColor(image_with_ellipses, cv2.COLOR_BGR2RGB))
plt.title('Fitted Ellipses and Detected Contours')
plt.axis('off')
plt.show()

# Export the image as a JPEG at the highest quality
export_path = image_path.replace('.jpg', '_ellipses.jpg')
plt.imsave(export_path, image_with_ellipses, cmap='gray')
print(f"Image saved as {export_path}")

```

External Major Diameter: 1735.69 pixels  
External Minor Diameter: 1802.14 pixels  
Internal Major Diameter: 1525.35 pixels  
Internal Minor Diameter: 1571.86 pixels  
External Ellipse Center: (910.19, 879.53) pixels  
Internal Ellipse Center: (919.23, 880.47) pixels  
Image Center: (914, 888) pixels  
External Ellipse Offset from Image Center: ( $\Delta x$ : -3.81 pixels,  $\Delta y$ : -8.47 pixels)  
Internal Ellipse Offset from Image Center: ( $\Delta x$ : 5.23 pixels,  $\Delta y$ : -7.53 pixels)

Fitted Ellipses and Detected Contours

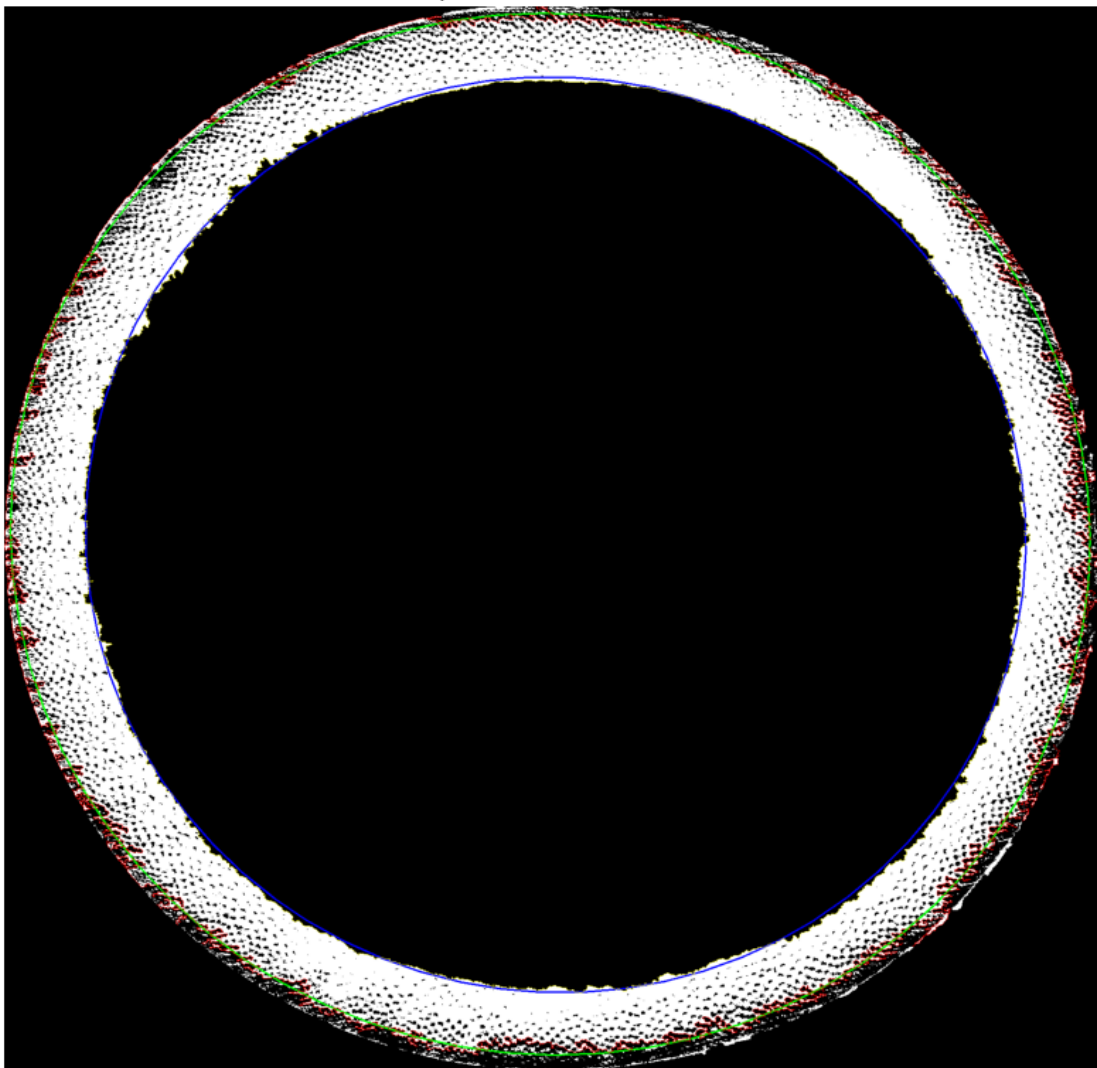


Image saved as DM-1-001 preprocessed\_ellipses.jpg

```
[10]: # Convert cleaned image to BGR for color drawing
#image_with_ellipsesADAPT = cv2.cvtColor(binary_imageADAPT, cv2.COLOR_GRAY2BGR)
image_with_ellipsesADAPT = cv2.cvtColor(cleaned_imageOTSU, cv2.COLOR_GRAY2BGR)

# Draw the external ellipse in green
cv2.ellipse(image_with_ellipsesADAPT, (int(x_ext), int(y_ext)), □
    ↳(int(major_axis_ext / 2), int(minor_axis_ext / 2)),
    angle_ext, 0, 360, (0, 255, 0), 10)

# Draw the internal ellipse in blue
```

```

cv2.ellipse(image_with_ellipsesADAPT, (int(x_int), int(y_int)),  

    ↪(int(major_axis_int / 2), int(minor_axis_int / 2)),  

    angle_int, 0, 360, (255, 0, 0), 10)

# Draw the external contour in red  

cv2.drawContours(image_with_ellipsesADAPT, [external_contour], -1, (0, 0, 255),  

    ↪2)

# Draw the internal contour in yellow  

cv2.drawContours(image_with_ellipsesADAPT, [internal_contour], -1, (0, 255,  

    ↪255), 2)

# Display the image with ellipses and contours  

plt.figure(figsize=(10, 10))  

plt.imshow(cv2.cvtColor(image_with_ellipsesADAPT, cv2.COLOR_BGR2RGB))  

plt.title('Fitted Ellipses and Detected Contours ADAPT')  

plt.axis('off')  

plt.show()

# Export the image as a JPEG at the highest quality  

export_path = image_path.replace('.jpg', '_ellipsesADAPT.jpg')  

plt.imsave(export_path, image_with_ellipsesADAPT, cmap='gray')  

print(f"Image saved as {export_path}")

```

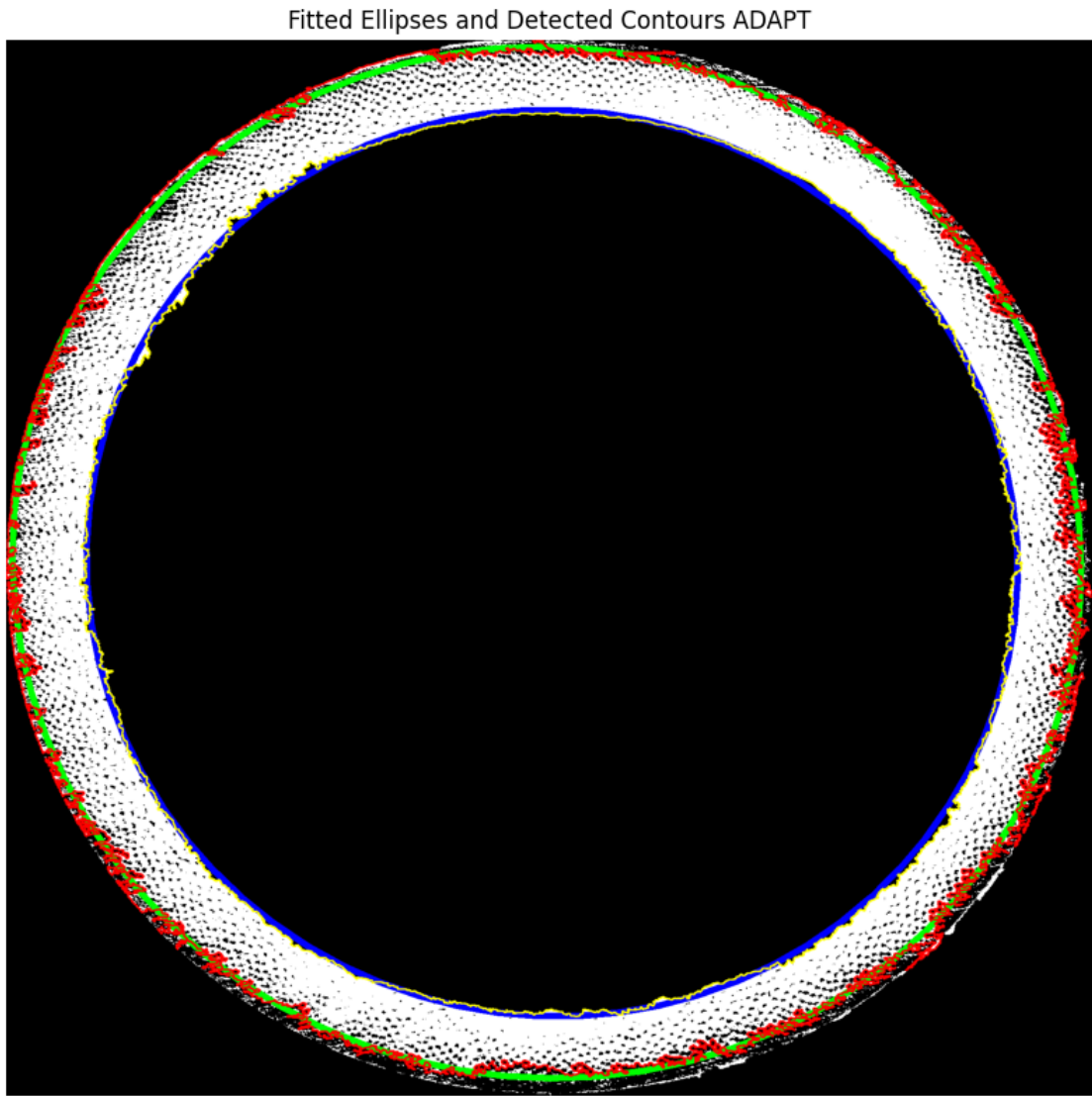


Image saved as DM-1-001 preprocessed\_ellipsesADAPT.jpg

```
[11]: import cv2
import numpy as np
import matplotlib.pyplot as plt

# Assuming 'image_with_ellipses', 'ellipse_external', and 'ellipse_internal' are already defined

# External ellipse parameters
(x_ext, y_ext), (major_axis_ext, minor_axis_ext), angle_ext = ellipse_external

# Internal ellipse parameters
```

```

(x_int, y_int), (major_axis_int, minor_axis_int), angle_int = ellipse_internal

# Number of tangential segments
num_segments = 10

# Calculate the semi-major and semi-minor axes lengths
semi_major_ext = major_axis_ext / 2
semi_minor_ext = minor_axis_ext / 2
semi_major_int = major_axis_int / 2
semi_minor_int = minor_axis_int / 2

# Calculate the incremental change in axes lengths for each segment
delta_major = (semi_major_ext - semi_major_int) / num_segments
delta_minor = (semi_minor_ext - semi_minor_int) / num_segments

# Create a copy of the image to draw on
image_with_segmentsADAPT = image_with_ellipsesADAPT.copy()

# Draw tangential segments
for i in range(num_segments + 1):
    # Calculate the current axes lengths
    current_major = semi_major_ext - i * delta_major
    current_minor = semi_minor_ext - i * delta_minor
    # Draw the ellipse representing the current segment boundary
    cv2.ellipse(image_with_segmentsADAPT, (int(x_ext), int(y_ext)), ▾
    ↵(int(current_major), int(current_minor)),
        angle_ext, 0, 360, (255, 0, 0), 2) # Blue ellipses

# Display the image with tangential segments
plt.figure(figsize=(10, 10))
plt.imshow(cv2.cvtColor(image_with_segmentsADAPT, cv2.COLOR_BGR2RGB))
plt.title('Bamboo Cross-Section with Tangential Segments')
plt.axis('off')
plt.show()

# Export the image as a JPEG at the highest quality
export_path = image_path.replace('.jpg', '_segmentsADAPT.jpg')
plt.imsave(export_path, image_with_segmentsADAPT, cmap='gray')
print(f"Image saved as {export_path}")

```

Bamboo Cross-Section with Tangential Segments

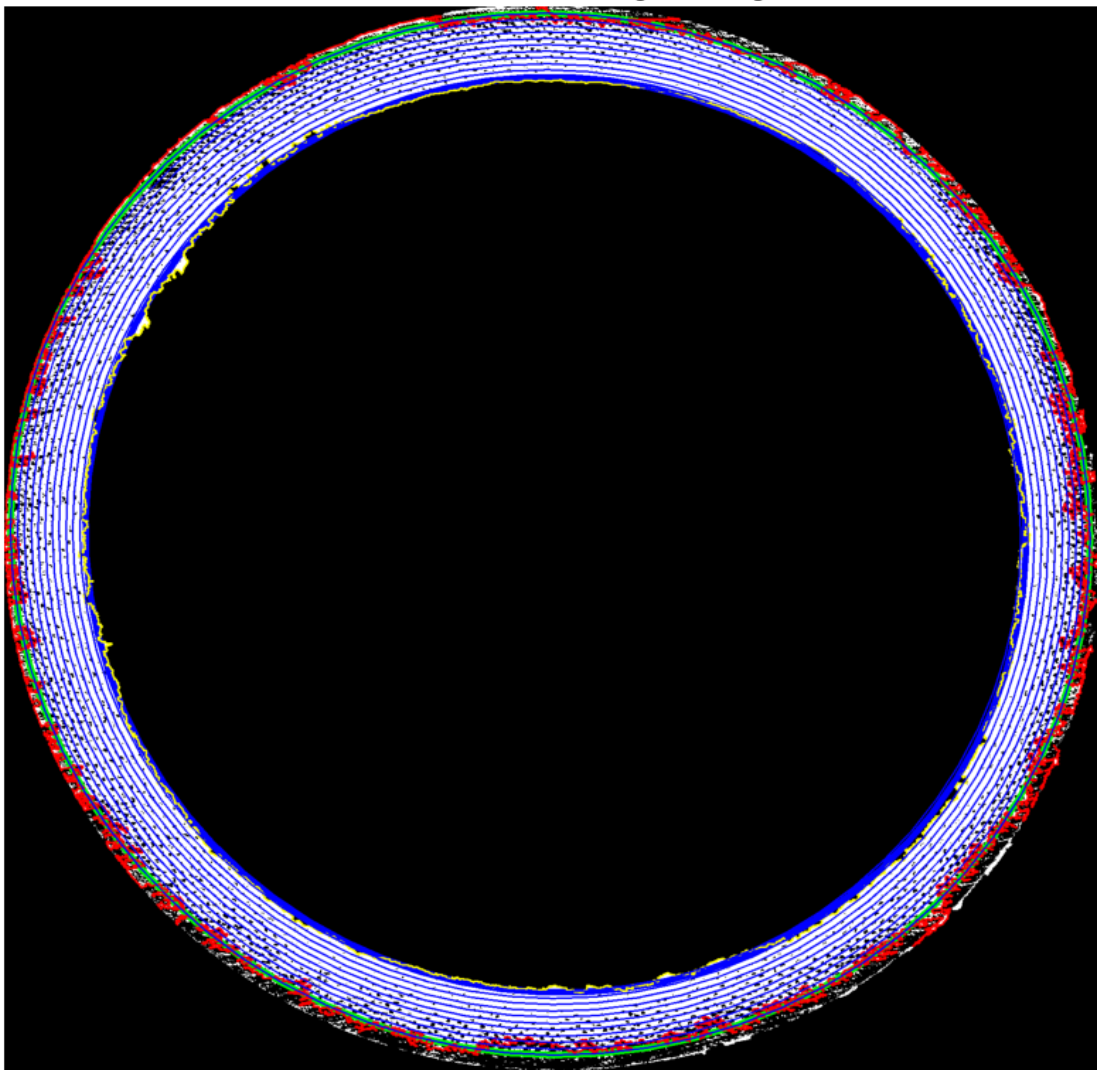


Image saved as DM-1-001 preprocessed\_segmentsADAPT.jpg

```
[12]: import cv2
import numpy as np
import matplotlib.pyplot as plt

# Assuming 'cleaned_imageADAPT', 'ellipse_external', and 'ellipse_internal' are
# already defined

image_for_segmentation=cv2.bitwise_not(cleaned_imageOTSU)

# External ellipse parameters
(x_ext, y_ext), (major_axis_ext, minor_axis_ext), angle_ext = ellipse_external
```

```

# Internal ellipse parameters
(x_int, y_int), (major_axis_int, minor_axis_int), angle_int = ellipse_internal

# Number of tangential segments
num_segments = 10

# Calculate the semi-major and semi-minor axes lengths
semi_major_ext = major_axis_ext / 2
semi_minor_ext = minor_axis_ext / 2
semi_major_int = major_axis_int / 2
semi_minor_int = minor_axis_int / 2

# Calculate the incremental change in axes lengths for each segment
delta_major = (semi_major_ext - semi_major_int) / num_segments
delta_minor = (semi_minor_ext - semi_minor_int) / num_segments

# Initialize lists to store volume fractions
fiber_volume_fractions = []
matrix_volume_fractions = []

# Iterate over each segment
for i in range(num_segments):
    # Define the inner and outer ellipses of the current segment
    inner_major = semi_major_int + i * delta_major
    inner_minor = semi_minor_int + i * delta_minor
    outer_major = semi_major_int + (i + 1) * delta_major
    outer_minor = semi_minor_int + (i + 1) * delta_minor

    # Create masks for the inner and outer ellipses
    inner_mask = np.zeros_like(image_for_segmentation, dtype=np.uint8)
    outer_mask = np.zeros_like(image_for_segmentation, dtype=np.uint8)

    # Draw filled ellipses on the masks
    cv2.ellipse(inner_mask, (int(x_int), int(y_int)), (int(inner_major), int(inner_minor)),
               angle_int, 0, 360, 255, thickness=-1)
    cv2.ellipse(outer_mask, (int(x_int), int(y_int)), (int(outer_major), int(outer_minor)),
               angle_int, 0, 360, 255, thickness=-1)

    # The segment mask is the difference between the outer and inner masks
    segment_mask = cv2.subtract(outer_mask, inner_mask)

    # Apply the segment mask to the cleaned image
    segment_pixels = cv2.bitwise_and(image_for_segmentation, image_for_segmentation, mask=segment_mask)

```

```

# Calculate the number of white (fiber) pixels in the segment
fiber_area_segment = cv2.countNonZero(segment_pixels)

# Calculate the total number of pixels in the segment
total_area_segment = cv2.countNonZero(segment_mask)

# Compute the fiber and matrix volume fractions for the segment
if total_area_segment > 0:
    fiber_fraction = fiber_area_segment / total_area_segment
    matrix_fraction = 1 - fiber_fraction
else:
    fiber_fraction = 0
    matrix_fraction = 0

# Append the fractions to the lists
fiber_volume_fractions.append(fiber_fraction)
matrix_volume_fractions.append(matrix_fraction)

# Print the volume fractions for each segment
for i in range(num_segments):
    print(f"Segment {i + 1}:")
    print(f"  Fiber Volume Fraction: {fiber_volume_fractions[i]:.4f}")
    print(f"  Matrix Volume Fraction: {matrix_volume_fractions[i]:.4f}")

# Optional: Visualize the segments on the image
image_with_segments = cv2.cvtColor(image_for_segmentation, cv2.COLOR_GRAY2BGR)
for i in range(num_segments):
    outer_major = semi_major_int + (i + 1) * delta_major
    outer_minor = semi_minor_int + (i + 1) * delta_minor
    cv2.ellipse(image_with_segments, (int(x_int), int(y_int)), □
    ↵(int(outer_major), int(outer_minor)),
                angle_int, 0, 360, (0, 255, 0), 2) # Green ellipses

# Create DataFrame from the lists
df = pd.DataFrame({
    'SEG': [f"Segment {i+1}" for i in range(num_segments)],
    'VF': fiber_volume_fractions,
    'VM': matrix_volume_fractions
})

# Define the path for saving the Excel file
excel_path = image_path.replace('.jpg', '_volumes.xlsx')

# Save the DataFrame to an Excel file
df.to_excel(excel_path, index=False)

```

```
print(f"Data saved to Excel file at: {excel_path}")
```

Segment 1:  
Fiber Volume Fraction: 0.3016  
Matrix Volume Fraction: 0.6984  
Segment 2:  
Fiber Volume Fraction: 0.1595  
Matrix Volume Fraction: 0.8405  
Segment 3:  
Fiber Volume Fraction: 0.1709  
Matrix Volume Fraction: 0.8291  
Segment 4:  
Fiber Volume Fraction: 0.1850  
Matrix Volume Fraction: 0.8150  
Segment 5:  
Fiber Volume Fraction: 0.1986  
Matrix Volume Fraction: 0.8014  
Segment 6:  
Fiber Volume Fraction: 0.2256  
Matrix Volume Fraction: 0.7744  
Segment 7:  
Fiber Volume Fraction: 0.2631  
Matrix Volume Fraction: 0.7369  
Segment 8:  
Fiber Volume Fraction: 0.3353  
Matrix Volume Fraction: 0.6647  
Segment 9:  
Fiber Volume Fraction: 0.4019  
Matrix Volume Fraction: 0.5981  
Segment 10:  
Fiber Volume Fraction: 0.4936  
Matrix Volume Fraction: 0.5064

Data saved to Excel file at: DM-1-001 preprocessed\_volumes.xlsx

[ ]:

## **Appendix D. Elastic modulus, ISO 22157:2019 (ISO, 2019)**

# G. angustifolia Ambient-dry Compression Stress-strain curves

August 25, 2025

```
[3]: import pandas as pd
import numpy as np
import matplotlib.pyplot as plt
import os
from pathlib import Path

# Configuration and data input functions
def load_spreadsheet_data(file_path):
    """
    Load force-displacement data from spreadsheet
    Assumes columns: 'time', 'force', 'displacement'
    Adjust column names as needed for your data format
    """
    df = pd.read_csv(file_path) # or pd.read_csv(file_path) for CSV files
    return df

def convert_to_stress_strain(df, cross_sectional_area, original_length):
    """
    Convert force-displacement data to stress-strain

    Parameters:
    - df: DataFrame with 'force' and 'displacement' columns
    - cross_sectional_area: cross-sectional area of specimen (mm2)
    - original_length: original gauge length of specimen (mm)

    Returns:
    - DataFrame with 'strain' and 'stress' columns
    """
    # Convert force from kN to N
    force_N = df['Force'] * 1000 # Convert kN to N

    stress = force_N / cross_sectional_area # Force/Area (MPa if force in N, area in mm2)

    # Express strain as percentage
    strain_percentage = (df['Displacement'] / original_length) * 100 # Strain as percentage
```

```

    return pd.DataFrame({
        'strain': strain_percentage,
        'stress': stress
    })

def get_vibrant_colors(num_colors):
    """
    Generate vibrant and highly distinguishable colors for plotting

    Parameters:
    - num_colors: Number of colors needed

    Returns:
    - List of vibrant color hex codes
    """
    # Vibrant and highly distinguishable color palette[1][3][6]
    vibrant_colors = [
        '#FF0000', # Bright Red
        '#0000FF', # Bright Blue
        '#00FF00', # Bright Green
        '#FF00FF', # Magenta
        '#FFA500', # Orange
        '#800080', # Purple
        '#FFFF00', # Yellow
        '#00FFFF', # Cyan
        '#FF1493', # Deep Pink
        '#32CD32', # Lime Green
        '#FF4500', # Red Orange
        '#4169E1', # Royal Blue
        '#DC143C', # Crimson
        '#228B22', # Forest Green
        '#8A2BE2', # Blue Violet
        '#FF6347', # Tomato
        '#20B2AA', # Light Sea Green
        '#DAA520', # Golden Rod
        '#B22222', # Fire Brick
        '#483D8B' # Dark Slate Blue
    ]

    # If we need more colors than available, cycle through the palette
    if num_colors <= len(vibrant_colors):
        return vibrant_colors[:num_colors]
    else:
        # Repeat the palette if needed
        extended_colors = []
        cycles_needed = (num_colors // len(vibrant_colors)) + 1

```

```

    for i in range(cycles_needed):
        extended_colors.extend(vibrant_colors)
    return extended_colors[:num_colors]

def plot_stress_strain_curves(stress_strain_list, specimen_labels=None,
                               title="Stress-Strain Curves for Bamboo Specimens",
                               save_plot=True, filename=None):
    """
    Plot individual stress-strain curves with vibrant, distinguishable colors

    Parameters:
    - stress_strain_list: List of stress-strain DataFrames
    - specimen_labels: List of labels for each specimen
    - title: Plot title
    - save_plot: Boolean to save plot as JPG
    - filename: Custom filename for saved plot
    """
    plt.figure(figsize=(14, 10))

    # Default labels if none provided
    if specimen_labels is None:
        specimen_labels = [f'Specimen {i+1}' for i in
                           range(len(stress_strain_list))]

    # Get vibrant colors for all specimens
    colors = get_vibrant_colors(len(stress_strain_list))

    # Plot individual curves with vibrant colors and increased line width
    for i, (df, label) in enumerate(zip(stress_strain_list, specimen_labels)):
        plt.plot(df['strain'], df['stress'],
                  color=colors[i],
                  linewidth=2.5,
                  label=label,
                  alpha=0.9) # Slightly transparent for better visual appeal

    # Formatting with enhanced visibility
    plt.xlabel('Strain (%)', fontsize=12, fontweight='bold')
    plt.ylabel('Stress (MPa)', fontsize=12, fontweight='bold')
    plt.title(title, fontsize=16, fontweight='bold', pad=20)
    plt.grid(True, alpha=0.3, linestyle='--')

    # Enhanced legend formatting
    plt.legend(bbox_to_anchor=(1.05, 1), loc='upper left',
               fontsize=12, frameon=True, fancybox=True, shadow=True)

    # Improve overall appearance
    plt.tight_layout()

```

```

# Save plot as JPG
if save_plot:
    if filename is None:
        # Create safe filename from title
        safe_title = "".join(c for c in title if c.isalnum() or c in (' ',_,_'))
        filename = f"{safe_title.replace(' ', '_)}.jpg"

    plt.savefig(filename, format='jpg', dpi=300, bbox_inches='tight',
                facecolor='white', edgecolor='none')
    print(f"Plot saved as: {filename}")

plt.show()

def calculate_elastic_modulus_bamboo(data, max_stress):
    """
    Calculate elastic modulus for bamboo using proper methodology

    Parameters:
    - data: DataFrame with 'strain' (%) and 'stress' (MPa) columns, sorted by strain
    - max_stress: Maximum stress value (MPa)

    Returns:
    - elastic_modulus: Elastic modulus in MPa
    """
    try:
        # Step 1: Remove toe region (initial non-linear behavior)
        toe_removal_stress = 0.05 * max_stress
        data_no_toe = data[data['stress'] >= toe_removal_stress].copy()

        if len(data_no_toe) < 10:
            print("Warning: Insufficient data after toe removal")
            return np.nan

        # Step 2: Define linear elastic region (10-40% of ultimate stress)
        lower_bound = 0.10 * max_stress
        upper_bound = 0.40 * max_stress

        linear_region = data_no_toe[
            (data_no_toe['stress'] >= lower_bound) &
            (data_no_toe['stress'] <= upper_bound)
        ].copy()

        if len(linear_region) < 5:
            print("Warning: Insufficient linear region data")
    
```

```

    return np.nan

# Step 3: Calculate slope (convert strain % to decimal)
strain_decimal = linear_region['strain'] / 100
stress_values = linear_region['stress']

coefficients = np.polyfit(strain_decimal, stress_values, 1)
elastic_modulus = coefficients[0]

# Step 4: Quality check using R-squared
predicted_stress = np.polyval(coefficients, strain_decimal)
ss_res = np.sum((stress_values - predicted_stress) ** 2)
ss_tot = np.sum((stress_values - np.mean(stress_values)) ** 2)
r_squared = 1 - (ss_res / ss_tot)

if r_squared < 0.95:
    print(f"Warning: Low R2 ({r_squared:.3f}) in elastic region")

return elastic_modulus

except Exception as e:
    print(f"Error calculating elastic modulus: {str(e)}")
    return np.nan

def calculate_mechanical_properties(stress_strain_data, specimen_labels):
    """
    Calculate key mechanical properties for each specimen with improved elastic
    modulus calculation
    """
    properties = []

    for data, label in zip(stress_strain_data, specimen_labels):
        # Sort data by strain to ensure proper order
        data_sorted = data.sort_values('strain').reset_index(drop=True)

        # Ultimate tensile strength
        max_stress = data_sorted['stress'].max()

        # IMPROVED ELASTIC MODULUS CALCULATION
        elastic_modulus = calculate_elastic_modulus_bamboo(data_sorted, max_stress)

        # Strain at failure
        failure_strain = data_sorted.loc[data_sorted['stress'].idxmax(), 'strain']

        properties.append({
            'label': label,
            'max_stress': max_stress,
            'failure_stress': failure_stress,
            'failure_strain': failure_strain,
            'elastic_modulus': elastic_modulus
        })

```

```

        'Specimen': label,
        'Ultimate_Stress_MPa': max_stress,
        'Elastic_Modulus_MPa': elastic_modulus,
        'Failure_Strain_Percent': failure_strain
    })

    return pd.DataFrame(properties)

# Main analysis workflow
def main_analysis():
    """
    Main function to process all spreadsheets and create stress-strain plots
    """

    # Define your file paths - adjust as needed
    file_directory = "." # Update this path
    file_pattern = "*.csv" # or "*.csv" depending on your file format

    # Alternative: Define file paths manually
    file_paths = [
        "GB-1-001.csv",
        "GB-1-008.csv",
        "GB-2-004.csv",
        "GB-2-011.csv",
        "GM-1-004.csv",
        "GM-1-006.csv",
        "GM-1-012.csv",
        "GM-2-006.csv",
        "GT-1-001.csv",
        "GT-1-009.csv",
        "GT-2-003.5.csv",
        "GT-2-004.csv",
        "GT-2-009.csv",
        "GT-2-010.csv",
        "UNNAMED.csv",
        # Add all 15 file paths here
    ]

    # Define specimen properties - UPDATE THESE VALUES FOR YOUR SPECIMENS
    specimen_properties = [
        {"area": 2892.288069, "length": 197.875, "label": "GB-1-001"}, 
        {"area": 4560.176239, "length": 108.485, "label": "GB-1-008"}, 
        {"area": 3026.802877, "length": 220.5, "label": "GB-2-004"}, 
        {"area": 3860.486605, "length": 110.205, "label": "GB-2-011"}, 
        {"area": 3034.040518, "length": 98.6375, "label": "GM-1-004"}, 
        {"area": 3469.209537, "length": 200.125, "label": "GM-1-006"}, 
        {"area": 3353.311661, "length": 99.6975, "label": "GM-1-012"}, 
    ]

```

```

        {"area": 2630.389358, "length": 99.6975, "label": "GM-2-006"},  

        {"area": 2014.205595, "length": 94.7525, "label": "GT-1-001"},  

        {"area": 2765.324725, "length": 95.1225, "label": "GT-1-009"},  

        {"area": 1900.644232, "length": 93.47, "label": "GT-2-003.5"},  

        {"area": 1901.122616, "length": 190.5, "label": "GT-2-004"},  

        {"area": 2127.732138, "length": 189.25, "label": "GT-2-009"},  

        {"area": 2252.013789, "length": 96.1975, "label": "GT-2-004"},  

        {"area": 2368.501289, "length": 133.59, "label": "UNNAMED"},  

    ]  
  

# Load and process all data  

stress_strain_data = []  

specimen_labels = []  
  

for i, (file_path, properties) in enumerate(zip(file_paths, specimen_properties)):  

    try:  

        # Load raw data  

        raw_data = load_spreadsheet_data(file_path)  
  

        # Convert to stress-strain  

        stress_strain = convert_to_stress_strain(  

            raw_data,  

            properties["area"],  

            properties["length"]  

        )  
  

        stress_strain_data.append(stress_strain)  

        specimen_labels.append(properties["label"])  
  

        print(f"Processed: {properties['label']}")  
  

    except Exception as e:  

        print(f"Error processing {file_path}: {str(e)}")  
  

# Create comprehensive plot with vibrant colors and no average curve  

plot_stress_strain_curves(stress_strain_data, specimen_labels,  

                           "Stress-Strain Curves: Guadua Ambient-dry  

                           Compression",  

                           save_plot=True,  

                           filename="comprehensive_stress_strain_curves.jpg")  
  

return stress_strain_data, specimen_labels  
  

# Optional: Visualization function to verify elastic modulus calculation  

def plot_elastic_modulus_verification(data, elastic_modulus, max_stress, specimen_label):

```

```

"""
Plot to verify elastic modulus calculation visually
"""

plt.figure(figsize=(10, 6))

# Plot full curve
plt.plot(data['strain'], data['stress'], 'b-', linewidth=2, alpha=0.7, label='Full Curve')

# Highlight linear region used for calculation
lower_bound = 0.20 * max_stress
upper_bound = 0.60 * max_stress
linear_region = data[
    (data['stress'] >= lower_bound) &
    (data['stress'] <= upper_bound)
]

plt.plot(linear_region['strain'], linear_region['stress'], 'ro',
         markersize=4, label='Linear Region Used')

# Plot fitted line
if not np.isnan(elastic_modulus):
    strain_fit = np.linspace(linear_region['strain'].min(),
                             linear_region['strain'].max(), 100)
    stress_fit = elastic_modulus * (strain_fit / 100)
    plt.plot(strain_fit, stress_fit, 'r--', linewidth=3,
             label=f'Fitted Line (E = {elastic_modulus:.0f} MPa)')

plt.xlabel('Strain (%)', fontsize=12, fontweight='bold')
plt.ylabel('Stress (MPa)', fontsize=12, fontweight='bold')
plt.title(f'Elastic Modulus Verification: {specimen_label}', fontsize=14,
          fontweight='bold')
plt.legend(fontsize=10)
plt.grid(True, alpha=0.3)
plt.tight_layout()
plt.savefig(f'elastic_modulus_verification_{specimen_label.replace("-", "_")}.jpg',
            dpi=300, bbox_inches='tight', facecolor='white')
plt.show()

# Export individual specimen plots function
def export_individual_plots(stress_strain_data, specimen_labels):
    """Export individual stress-strain plots for each specimen with vibrant colors"""
    colors = get_vibrant_colors(len(stress_strain_data))

    for i, (data, label) in enumerate(zip(stress_strain_data, specimen_labels)):

```

```

plt.figure(figsize=(10, 6))
plt.plot(data['strain'], data['stress'], linewidth=3, color=colors[i])
plt.xlabel('Strain (%)', fontsize=12, fontweight='bold')
plt.ylabel('Stress (MPa)', fontsize=12, fontweight='bold')
plt.title(f'Stress-Strain Curve: {label}', fontsize=14,
    fontweight='bold')
plt.grid(True, alpha=0.3)
plt.tight_layout()

# Save individual plot
filename = f"stress_strain_{label.replace('-', '_')}.jpg"
plt.savefig(filename, format='jpg', dpi=300, bbox_inches='tight',
            facecolor='white', edgecolor='none')
plt.close() # Close to save memory
print(f"Individual plot saved: {filename}")

# Execute the analysis
if __name__ == "__main__":
    # Run main analysis
    stress_strain_data, specimen_labels = main_analysis()

    # Calculate mechanical properties
    mechanical_props = calculate_mechanical_properties(stress_strain_data,
    specimen_labels)
    print("\nMechanical Properties Summary:")
    print(mechanical_props)

    # Save results
    mechanical_props.to_csv("bamboo_mechanical_properties.csv", index=False)
    print("\nResults saved to 'bamboo_mechanical_properties.csv'")

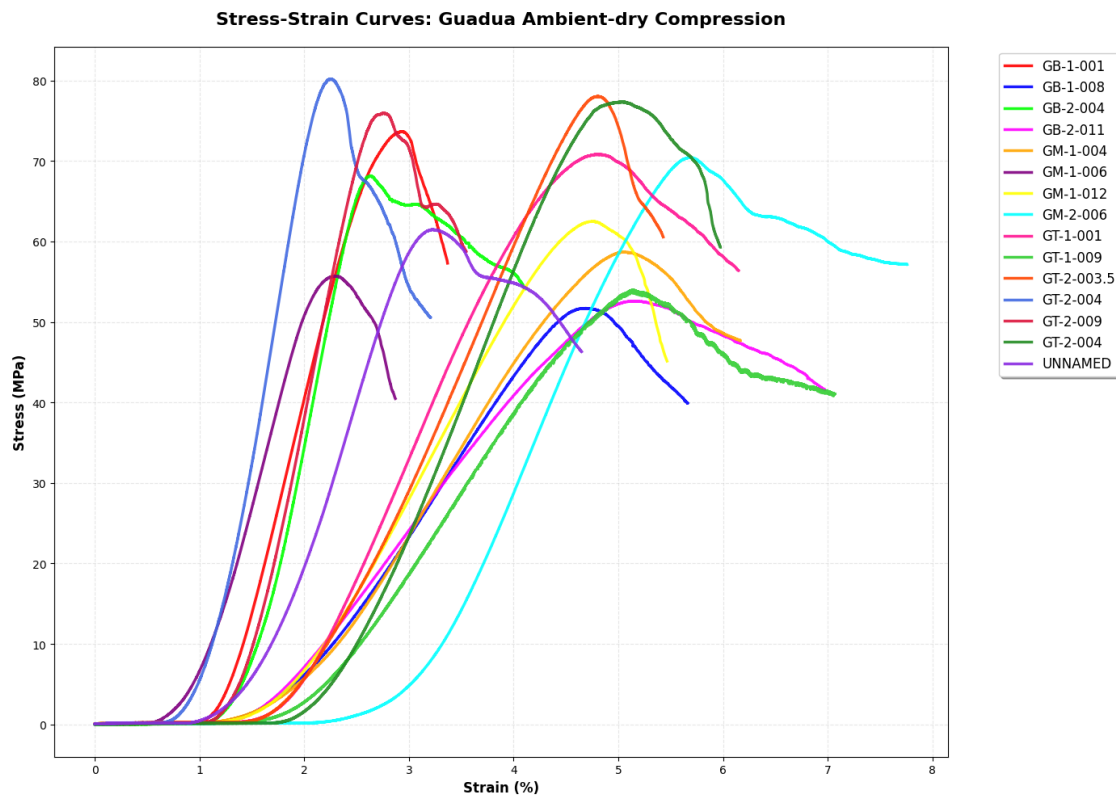
    # Optional: Export individual plots
    # Uncomment the line below if you want individual plots for each specimen
    # export_individual_plots(stress_strain_data, specimen_labels)

    # Optional: Verify elastic modulus calculations for first few specimens
def verify_elastic_modulus_calculation():
    for i, (data, label) in enumerate(zip(stress_strain_data,
    specimen_labels)):
        if i < 3: # Only plot first 3 specimens
            data_sorted = data.sort_values('strain').reset_index(drop=True)
            max_stress = data_sorted['stress'].max()
            elastic_modulus = calculate_elastic_modulus_bamboo(data_sorted,
            max_stress)
            plot_elastic_modulus_verification(data_sorted, elastic_modulus,
            max_stress, label)

```

```
# Uncomment to verify elastic modulus calculations
# verify_elastic_modulus_calculation()
```

Processed: GB-1-001  
 Processed: GB-1-008  
 Processed: GB-2-004  
 Processed: GB-2-011  
 Processed: GM-1-004  
 Processed: GM-1-006  
 Processed: GM-1-012  
 Processed: GM-2-006  
 Processed: GT-1-001  
 Processed: GT-1-009  
 Processed: GT-2-003.5  
 Processed: GT-2-004  
 Processed: GT-2-009  
 Processed: GT-2-004  
 Processed: UNNAMED  
 Plot saved as: comprehensive\_stress\_strain\_curves.jpg



#### Mechanical Properties Summary:

Specimen	Ultimate_Stress_MPa	Elastic_Modulus_MPa	\
GB-1-001	~75	~150	\
GB-1-008	~80	~150	\
GB-2-004	~75	~150	\
GB-2-011	~70	~150	\
GM-1-004	~70	~150	\
GM-1-006	~65	~150	\
GM-1-012	~65	~150	\
GM-2-006	~70	~150	\
GT-1-001	~70	~150	\
GT-1-009	~65	~150	\
GT-2-003.5	~78	~150	\
GT-2-004	~80	~150	\
GT-2-009	~75	~150	\
GT-2-004	~75	~150	\
UNNAMED	~60	~150	\

0	GB-1-001	73.641005	5009.558549
1	GB-1-008	51.698506	1647.909778
2	GB-2-004	68.117122	4756.064388
3	GB-2-011	52.596452	1659.653201
4	GM-1-004	58.720442	1801.981368
5	GM-1-006	55.678476	3746.128377
6	GM-1-012	62.488764	2082.837329
7	GM-2-006	70.442043	2595.192561
8	GT-1-001	70.808859	2770.789128
9	GT-1-009	53.956629	1788.657858
10	GT-2-003.5	78.026438	2416.708593
11	GT-2-004	80.192408	5693.282662
12	GT-2-009	75.941608	5345.710724
13	GT-2-004	77.355654	2771.760159
14	UNNAMED	61.489179	2972.923108

#### Failure\_Strain\_Percent

0	2.924574
1	4.689681
2	2.625215
3	5.121546
4	5.048688
5	2.307308
6	4.761704
7	5.695429
8	4.799768
9	5.139899
10	4.801648
11	2.256378
12	2.758415
13	5.028821
14	3.228385

Results saved to 'bamboo\_mechanical\_properties.csv'

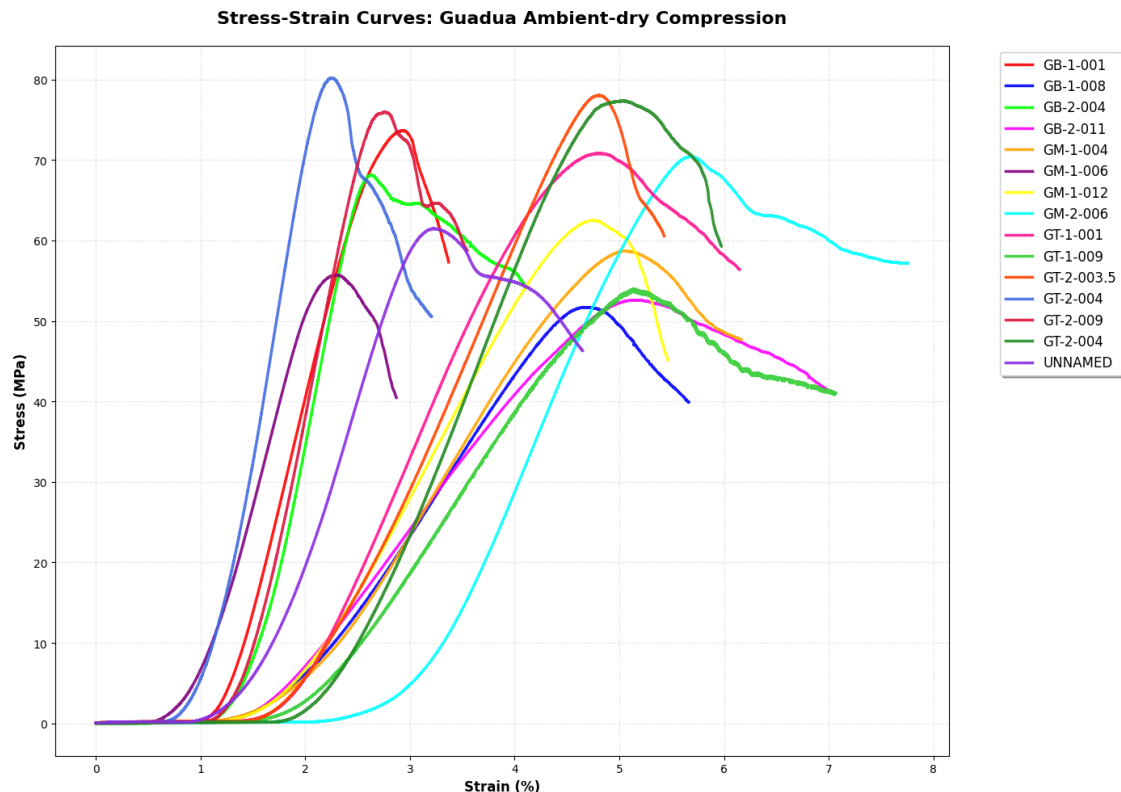
[4]: main\_analysis()

```
Processed: GB-1-001
Processed: GB-1-008
Processed: GB-2-004
Processed: GB-2-011
Processed: GM-1-004
Processed: GM-1-006
Processed: GM-1-012
Processed: GM-2-006
Processed: GT-1-001
Processed: GT-1-009
Processed: GT-2-003.5
```

```

Processed: GT-2-004
Processed: GT-2-009
Processed: GT-2-004
Processed: UNNAMED
Plot saved as: comprehensive_stress_strain_curves.jpg

```



```

[4]: ([
        strain      stress
  0   -0.000101  0.025309
  1    0.000000  0.020399
  2   -0.000152  0.025136
  3   -0.000101  0.032500
  4    0.000051  0.025654
...
  ...
  ...
20003  3.368490  57.327865
20004  3.368642  57.316559
20005  3.368743  57.305011
20006  3.368793  57.300032
20007  3.368793  57.298269

[20008 rows x 2 columns],
        strain      stress
  0   -0.000830  0.019648

```

```
1      -0.000922  0.020021
2      -0.000922  0.026841
3      -0.000830  0.014934
4      -0.000922  0.027718
```

```
...
...
18428  5.661428  39.921571
18429  5.661704  39.907076
18430  5.662073  39.912493
18431  5.662350  39.896090
18432  5.662718  39.901155
```

```
[18433 rows x 2 columns],
      strain      stress
0      -0.000045  0.011729
1      -0.000227  -0.001784
2      -0.000227  0.016849
3      -0.000091  -0.001916
4      0.000408   0.014372
```

```
...
...
27250  4.119864  54.122289
27251  4.120045  54.142244
27252  4.120136  54.119943
27253  4.120272  54.133456
27254  4.120454  54.114062
```

```
[27255 rows x 2 columns],
      strain      stress
0      0.000272  0.040228
1      0.000181  0.036084
2      0.000181  0.032198
3      0.000091  0.031835
4      0.000091  0.034555
```

```
...
...
23052  6.972642  41.586156
23053  6.973096  41.587607
23054  6.973277  41.590819
23055  6.973640  41.594161
23056  6.973731  41.591855
```

```
[23057 rows x 2 columns],
      strain      stress
0      0.000101  0.044001
1      0.000101  0.038266
2      -0.000203  0.032234
3      -0.000101  0.037211
4      0.000101  0.038266
```

```
...
...

```

```
18243  6.164897  47.707932
18244  6.165404  47.707965
18245  6.165708  47.704076
18246  6.165911  47.692507
18247  6.166012  47.691651
```

```
[18248 rows x 2 columns],
      strain      stress
0     -0.000100   0.017641
1     -0.000050   0.023838
2     -0.000100   0.024703
3     -0.000150   0.017468
4     -0.000100   0.019687
...
17230  2.869307  40.492365
17231  2.869557  40.478299
17232  2.869706  40.479538
17233  2.869956  40.480172
17234  2.869956  40.478155
```

```
[17235 rows x 2 columns],
      strain      stress
0     0.000000   0.048281
1     0.000100   0.047595
2     0.000100   0.042346
3     0.000100   0.041839
4     0.000201   0.050398
...
16344  5.464631  45.162131
16345  5.465132  45.161206
16346  5.465232  45.155809
16347  5.465634  45.143970
16348  5.465934  45.132906
```

```
[16349 rows x 2 columns],
      strain      stress
0     0.000000   0.048396
1     0.000301   0.047407
2     0.000201   0.055011
3     0.000401   0.057710
4     0.000702   0.061702
...
23205  7.758168  57.113180
23206  7.758670  57.121315
23207  7.758971  57.124053
23208  7.759272  57.120707
23209  7.759272  57.124623
```

```
[23210 rows x 2 columns],  
      strain      stress  
0      0.000211  0.047910  
1      0.000211  0.054116  
2     -0.000106  0.044832  
3      0.000106  0.053619  
4      0.000211  0.054612
```

```
...       ...      ...  
17478   6.148017  56.376469  
17479   6.148439  56.371356  
17480   6.148650  56.357951  
17481   6.148967  56.350702  
17482   6.149178  56.357703
```

```
[17483 rows x 2 columns],  
      strain      stress  
0     -0.000105  0.043250  
1      0.000000  0.052761  
2      0.000000  0.035294  
3      0.000000  0.046794  
4     -0.000105  0.036741
```

```
...       ...      ...  
40346   7.068149  41.039556  
40347   7.068149  41.050586  
40348   7.068569  41.050875  
40349   7.068464  41.038363  
40350   7.068675  41.053190
```

```
[40351 rows x 2 columns],  
      strain      stress  
0      0.000000  0.065451  
1      0.000000  0.052193  
2      0.000107  0.061663  
3      0.000107  0.066083  
4      0.000107  0.074869
```

```
...       ...      ...  
15224   5.428266  60.608870  
15225   5.428587  60.585720  
15226   5.428908  60.577407  
15227   5.429122  60.564464  
15228   5.429443  60.554941
```

```
[15229 rows x 2 columns],  
      strain      stress  
0      0.000000  0.049707  
1      0.000105  0.051180
```

```
2      0.000157  0.058650
3      0.000052  0.066066
4      0.000052  0.051233
```

```
...
18321  3.205774  50.543294
18322  3.205879  50.527725
18323  3.206142  50.521781
18324  3.206247  50.534983
18325  3.206404  50.531354
```

```
[18326 rows x 2 columns],
      strain      stress
0      0.000000  0.038022
1      0.000053  0.036471
2      0.000053  0.042252
3      0.000053  0.041171
4      0.000053  0.030925
...
20130  3.545522  58.753730
20131  3.545680  58.771167
20132  3.545839  58.762660
20133  3.545892  58.754999
20134  3.546050  58.757114
```

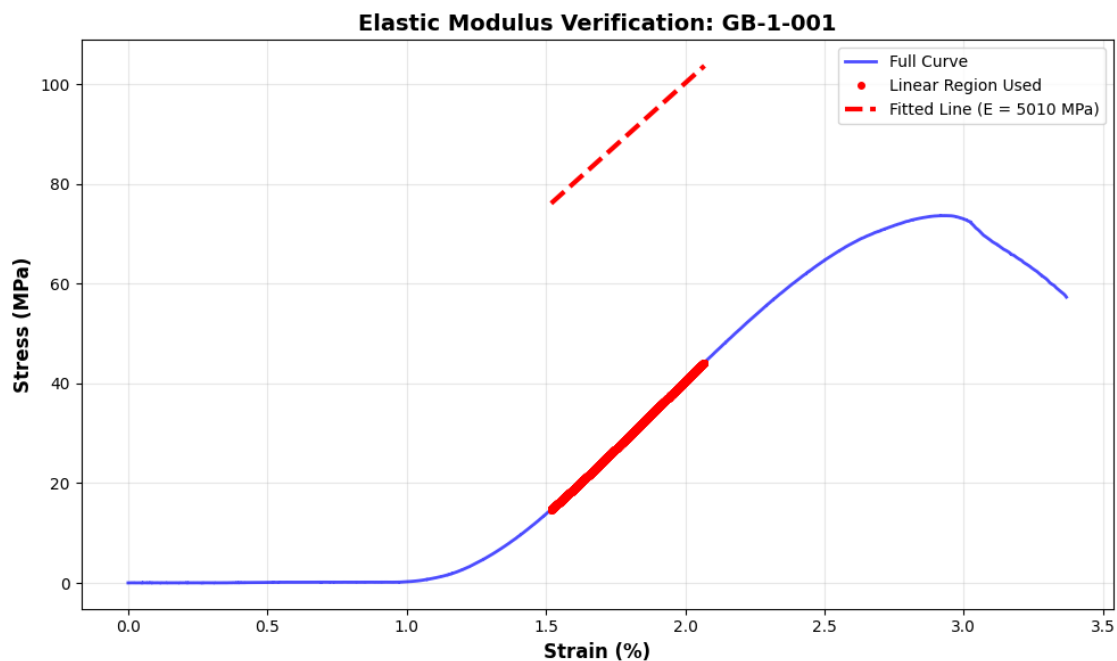
```
[20135 rows x 2 columns],
      strain      stress
0      0.000208  0.052176
1      0.000104  0.049689
2      0.000104  0.055906
3      -0.000104 0.055239
4      0.000000  0.053463
...
17240  5.974168  59.299148
17241  5.974584  59.302612
17242  5.974999  59.294308
17243  5.975103  59.276014
17244  5.975207  59.276147
```

```
[17245 rows x 2 columns],
      strain      stress
0      0.000000  0.040448
1      0.000075  0.038843
2      -0.000075 0.044036
3      0.000225  0.050158
4      0.000524  0.052649
...
18632  4.648776  46.317475
```

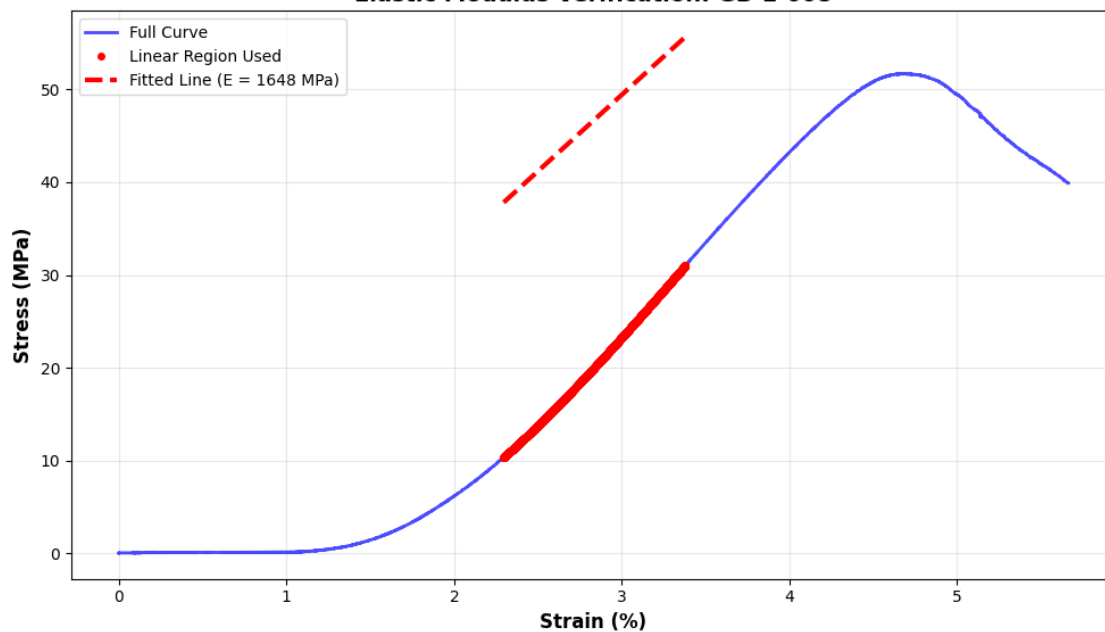
```
18633 4.648926 46.316293
18634 4.649225 46.318826
18635 4.649450 46.320684
18636 4.649749 46.310002
```

```
[18637 rows x 2 columns]],
['GB-1-001',
'GB-1-008',
'GB-2-004',
'GB-2-011',
'GM-1-004',
'GM-1-006',
'GM-1-012',
'GM-2-006',
'GT-1-001',
'GT-1-009',
'GT-2-003.5',
'GT-2-004',
'GT-2-009',
'GT-2-004',
'UNNAMED'])
```

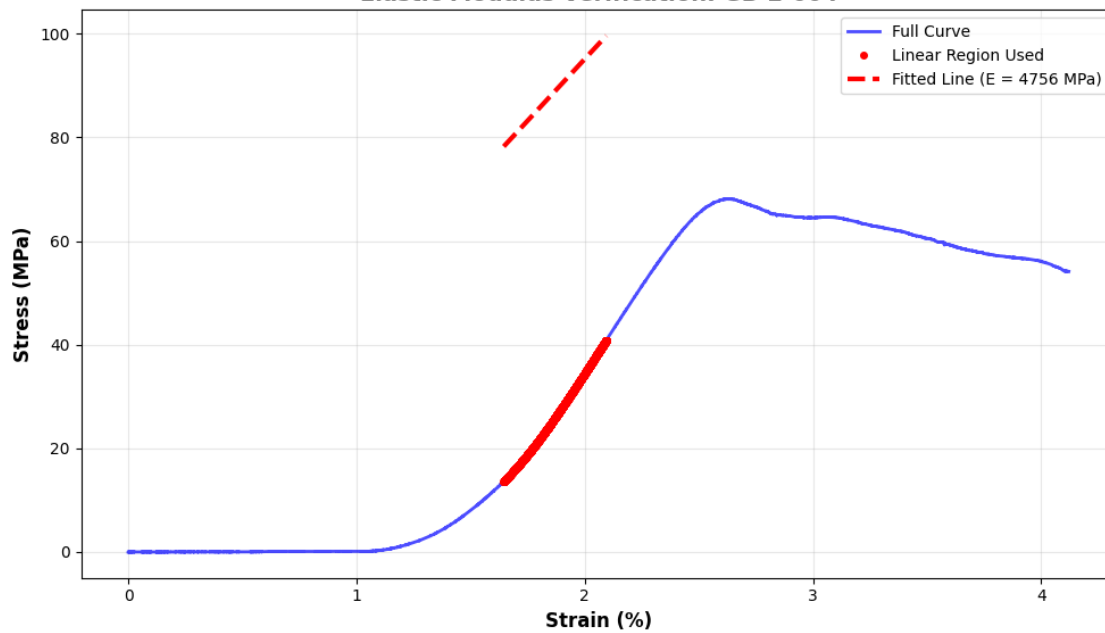
```
[5]: verify_elastic_modulus_calculation()
```



### Elastic Modulus Verification: GB-1-008



### Elastic Modulus Verification: GB-2-004



[ ]: